Directed Evolution of Sortase Activity and Specificity

Directed Evolution of Sortase Activity and Specificity

A dissertation presented

by

Brent Matthew Dorr

to

The Department of Chemistry and Chemical Biology

in partial fulfillment of the requirements
for the degree of
Doctor of Philosophy
in the subject of
Chemistry

Harvard University
Cambridge, Massachusetts

April, 2014

Dissertation Advisor: Professor David R. Liu Brent Matthew Dorr

Directed Evolution of Sortase Activity and Specificity

Abstract

Nature employs complex networks of protein-tailoring enzymes to effect the post-translational modification of proteins *in vivo*. By comparison, modern chemical methods rely upon either nonspecific labeling techniques or upon the genetic incorporation of bioorthogonal handles. To develop truly robust bioconjugates it is necessary to develop methods which possess the exquisite activity and specificity observed in biological catalysts. One attractive strategy to achieve this is the engineering of protein-tailoring enzymes possessing user-defined specificity and high catalytic efficiency.

In Chapter Two, we describe a directed evolution strategy for enzymes that catalyze desired bond-forming reactions. We then employed this system for the directed evolution of *S. aureus* sortase A (SrtA), a bacterial transpeptidase catalyzing the cleavage and re-ligation of a five amino acid peptide (Leu-Pro-Xxx-Thr-Gly) to a three amino acid acceptor sequence (Gly-Gly-Gly). Over the course of three rounds of mutagenesis and screening, we isolated variants of SrtA with up to a 140-fold increase in LPXTG-coupling activity compared with the starting wild-type enzyme.

In Chapters Three and Four, we demonstrated the usefulness of this evolved SrtA variant (eSrtA) by using it to both generate, as well as to strip and regenerate, a surface consisting of the antithrombotic protein Thrombomodulin attached covalently to a synthetic base layer. By

appending a pentaglycine motif to a polyurethane catheter, we demonstrated that eSrtA catalyzed the covalent attachment of a C-terminally LPETG-ylated antithrombotic protein, even in whole blood. We further demonstrated that this protein layer could be removed by subsequent treatment with eSrtA, then washed and recharged with fresh LPETG-tagged protein *in vivo*.

In Chapter Five, we further developed the selection scheme described in Chapter One, and applied it to the evolution of eSrtA variants with dramatically altered substrate specificities. Applying a technique of competitive inhibition led to the evolution of two new eSrtA variants, recognizing LPESG and LAETG but not LPETG with up to a 51,000-fold change in substrate specificity. Finally, we demonstrate that these novel SrtA derivatives enable the synthesis of new classes of materials, the streamlined construction of complex bioconjugates and the direct functionalization of endogenous human proteins without the use of genetic manipulation.

Table of Contents

Acknowledgments

Above everyone else, my family was instrumental in all of the work that I have done. My parents Barry and Denise instilled into me from a young age the value of challenging yourself – to never satisfy for easy victories, to always follow challenging paths and interesting ideas, rather than ones that are safe, or easy. They have supported me in decisions that I know they would have not made for me, helped me through challenges that I could not have overcome alone, and never let me feel as though I was operating alone. Their love and guidance have made me the man that I am today. My sister Kelli is the mirror that I look to in order to judge myself, and her love and respect have helped to push me ever-forward. My fiancee Heather is everything I could ever want in another person – she brings an element of whimsy and joy that does not come naturally to me, but which has helped me make it through my most difficult moments in graduate school not only intact, but with a smile on my face.

In my scientific career, I have been blessed with an abundance of excellent mentors. Three deserve special mention. David Liu has been an outstanding advisor through my graduate studies, and his guidance has proven invaluable in accomplishing so much in so short of a time. He has been supportive through rough times, skeptical through good, and always enthusiastic to advise me, both in my career and in my research. He gave me every opportunity to pursue even the most bizarre of ideas, and was always willing to indulge both my ignorance and my difference of opinion when we found ourselves in disagreement.

Jens Meiler was my undergraduate research advisor, who oversaw my evolution from bright-eyed mathematician into cocky computational biologist. My frequent scientific conversations with him continue to shape my thinking, and his giddy excitement over the art and practice of science continues to be a beacon of inspiration.

Finally, Irwin Chen had the most arduous task of anyone I know – that of teaching me proper bench science. I arrived in the Liu lab trained in the ideas of chemistry and biology, but it was Irwin that helped me to truly grasp the difficulties and the technique of doing careful experiment. His ideas helped to push forward my own, and his depth of experience and knowledge of enzyme evolution is, in my opinion, unsurpassed. I am fortunate to have met him, even more fortunate to have studied under him, and truly blessed to count him as a friend.

The process of going through graduate school is by its nature an isolating experience, and my friends and colleagues have made it far less painful than it could have been. Matthew Edwards is my oldest friend, and we that we both ended up in Boston for graduate school has been a treat. I've known Robin Chisnell for nearly as long as Matt, and our years as roommates were as varied as they were entertaining. Aaron Garner and I met at a sparsely attended ice cream social on the first day of grad school orientation, and though ice cream tastings have changed into cocktail and scotch tastings, his friendship has been unwavering. Joshua Mosberg is a dear friend whose earnest wit and deep passions have made many a weekend night into a lot of fun. We have all endured much in our search for scientific meaning and success, and their continuing friendship means a lot to me.

My fellow labmates, past and present, have made my time working in the Liu lab a lot of fun. Beyond acknowledging all of my coworkers past and present, several deserve special mention. Vikram Pattanayak is a brilliant statistician and talented doctor who was my baymate for three years, and who allowed me more opportunities to talk math than I'd ever expected in an experimental graduate program. He also probably kept me from quitting in my second year after a disastrous sequence of failed experiments, and for that he deserves a lot more recognition than I can give in this small space. David Thompson is one of the most gifted biologists that I know,

and our (often heated) scientific discussions remain some of the high points of my graduate career. John Qu, while not a member of the Liu lab, has proven to be a fantastic friend and colleague. Jacob Carlson is one of the funniest people I've ever met, and an incredibly talented scientist whose passion and refusal to accept anything short of perfect science is both rare and impressive. Sun Chung's passion for football, barbeque and college basketball brought a sense of home to lab. Ahmed Badran is a very gifted scientist, and though I doubt he will ever appreciate my taste in music, our conversations have been a highlight of my time in the Liu lab. Finally, Chihui An has been a far quicker study than I was, and an excellent teammate as we pressed forward towards the more challenging next steps of the sortase evolution program.

Given the nature of my thesis work, I ended up spending a lot of time in the flow cytometry core, and during that time I had the pleasure of meeting Patricia Rogers, Mandy Tam and Brian Tilton, each of whom helped in both teaching me the fine art of instrumentation and in passing the long hours spent collecting yeast. Patricia in particular has been a delight to work with, and I wish her (and her menagerie) all the best going forward.

All three members of my graduate advising committee have contributed in many ways to my development as a scientist, not the least of which being slogging through my in retrospect horribly written project updates. Alan Saghatelian is one of the nicest people that I have met, a fact that makes his success as a chemist all the more remarkable. Elliot Chaikof has been an amazing collaborator, and his enthusiasm and clinical insight has given me a window into a world of medicine that I had only dimly understood. Gregory Verdine was one of the first people to point out some of the problems in an early analysis I made of the SrtA crystal structure that probably saved me a year of failed effort.

For my family

Chapter One

Introduction

Abstract

Gram-positive bacteria possess complex peptidoglycan cell walls contained in a periplasmic space between their inner and outer membranes. Serving multiple functions, the cell wall is in many cases modified with different protein components in order to facilitate its catalytic as well as structural role in bacterial physiology. This dynamic incorporation of cellular proteins is facilitated by the bacterial sortases, a class of enzymes which catalyze the direct cleavage and transpeptidation of peptide sorting sequences onto target anchor substrates, and come in multiple flavors corresponding to their particular substrates and functional roles. Following the discovery that the catalytic domain of *S. aureus* sortase A (SrtA) could catalyze the post-translational conjugation of C-terminal Leu-Pro-Xxx-Thr-Gly (where Xxx=any amino acid) moieties onto N-terminal Gly-Gly-Gly peptides, there has been a flurry of interest in using it for the synthesis of otherwise synthetically intractable protein conjugates. However, its poor kinetics and rigidly defined substrate scope have greatly limited SrtA's applications in the broader research community. In this chapter, we first review the discovery and physiological role of bacterial sortases, then examine prior investigations into the enzymology, structure and inhibition of SrtA. Finally, we briefly review current techniques in bioconjugate chemistry, and applications of SrtA to the synthesis of novel bioconjugates.

The Physiological Role of Sortases

The cell wall of gram-positive bacteria is a complex, extracellular organelle which envelops its maintaining organism and in turn may present a variety of species- and strain-specific factors to its surrounding environment.[1] These factors are important for many host-pathogen interaction[2-6], including bacterial adhesion to eukaryotic cells[3,4] and extracellular

matrix[5,6], and may be additionally involved in the evasion of immune responses[7] by pathogenic bacteria. Given this plurality of functions, it is therefore desirable that the machinery for installation of proteins into the cell wall be robust to extracellular conditions as well as capable of dynamic regulation in order to adjust the milieu of factors presented to the extracellular environment.

S. aureus sortase A was discovered by Mazmanian et al[8] following the isolation of strains defective in the anchoring of cell wall proteins, however the LPXTG sorting signal was known from prior molecular biological[9] and proteolytic[10] characterization of the protein component of the peptidoglycan cell wall. Research into the homologous *S. aureus* sortase B (SrtB) gene suggested its importance in the capture of heme from its local environment, derived from its role in anchoring the ferrichrome transporter IsdC[11,12]. Further analysis of the Isd locus, as well as biochemical characterization of SrtB, revealed it to catalyze the same sorting substrate/lipid II conjugation reaction as SrtA, but with an aberrant, NPQTN sorting specificity.[11] These results collectively suggested the regulatory nature of sortases, with the expression of each enzyme controlling dynamically the composition of the bacterial cell wall.

Subsequent computational analysis suggested the presence of three other families of sortase genes including variants in gram negative bacteria[13,14], with many species employing different sorting motifs from the canonical LPXTG[15]. Simultaneous investigation of gram-positive pilus biochemistry suggested that several of these sortases were responsible for the polymerization of protein precursors to form bacterial pili, ultimately anchored to the cell wall[16]. This, coupled with the presence of sortase genes in every sequenced gram positive bacterial strain to date, suggests that these enzymes are the primary determinants of cell wall covalency in gram positive bacteria.

Figure 1-1 The NMR ensemble structure of substrate-unbound *S. aureus* sortase A

The catalytic cysteine residue is shown in blue, the catalytic histidine is shown in orange. The substrate binding channel is located down the center of the image, with the β6-7 substrate binding loop unstructured, at left.

Structural and Mechanistic Studies of *S. aureus* sortase A

Given their fundamental role in bacterial physiology and their lack of sequence homology to known eukaryotic proteins, sortases have presented a compelling target for structural and mechanistic study. Consequently, the apo-SrtA crystal[17] and NMR[18] structures were determined shortly after its discovery. However, the lack of structure in the LPXTG binding region of the enzyme provided little insight into the binding modes of SrtA (Figure 1-1). Similarly, the distal binding of LPXTG in attempted co-crystal structures of the LPXTG/SrtA structure led to

significant early controversy as to SrtA's detailed chemical mechanism. Conservation across all known sortases suggested the essential roles of the catalytic residues Cys184 and His120, a hypothesis supported by early alanine screening experiments.[19,20]

This observation taken with the close proximity of Arg197 to the enzyme's putative active site and the reactivity of the enzyme to the thiolate-reactive small molecule MTSET suggested a cysteine protease-like mechanism whereby His120 deproto nates Cys184 to generate

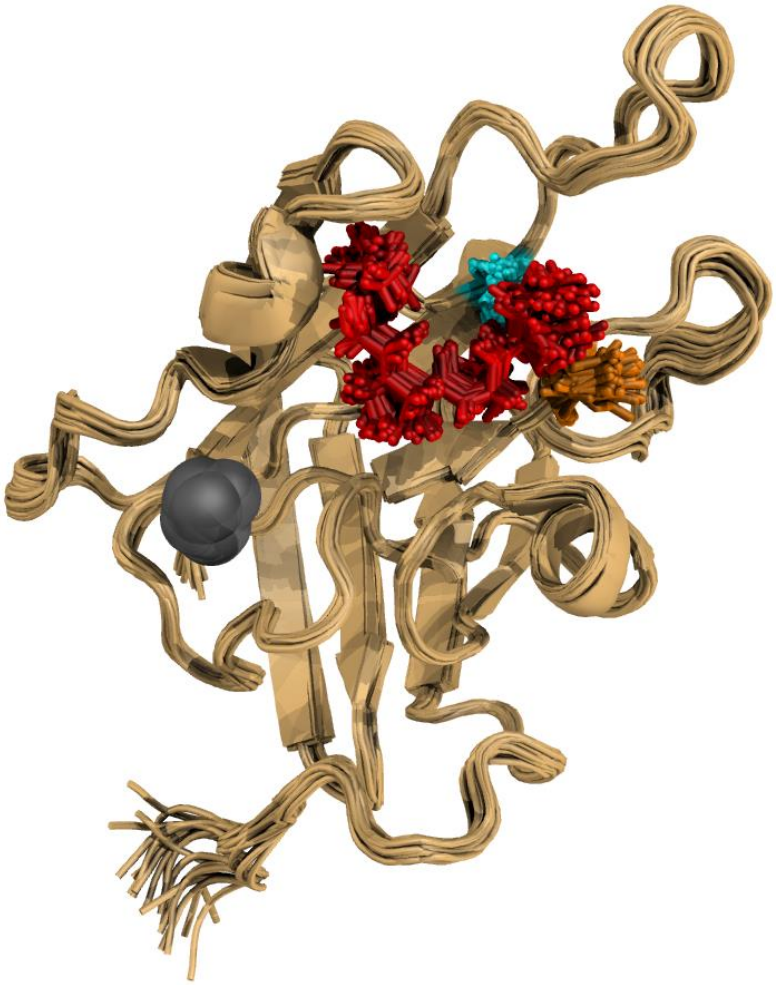

Figure 1-2 The NMR ensemble structure of the LPAT-charged intermediate *S. aureus* sortase A

The catalytic cysteine residue is shown in blue, the catalytic histidine is shown in orange. The LPAT substrate is attached via a disulfide linker to the active site cysteine, and is shown in red. The bound calcium ion is shown as a grey sphere

a thiolate, with Arg197 generating an oxyanion hole to facilitate overall catalysis. This idea was drawn into question when it was found that substituting Arg197 by citrulline, an analog which retains arginine's hydrogen bonding properties but lacks its positive charge. On synthesizing this SrtA variant b y a combination of solid phase peptide synthesis and native chemical ligation, Bentley et al found that it retained nearly all of SrtA's native activity.[21] Together with detailed kinetic measurements and the enzyme's apparent pH independence[22] these data collectively support an alternate mechanism, whereby a rare (ca 0.06% of all enzymes) thiolate-containing SrtA forms an unstable tetrahedral intermediate which is subsequently protonated by the adjacent

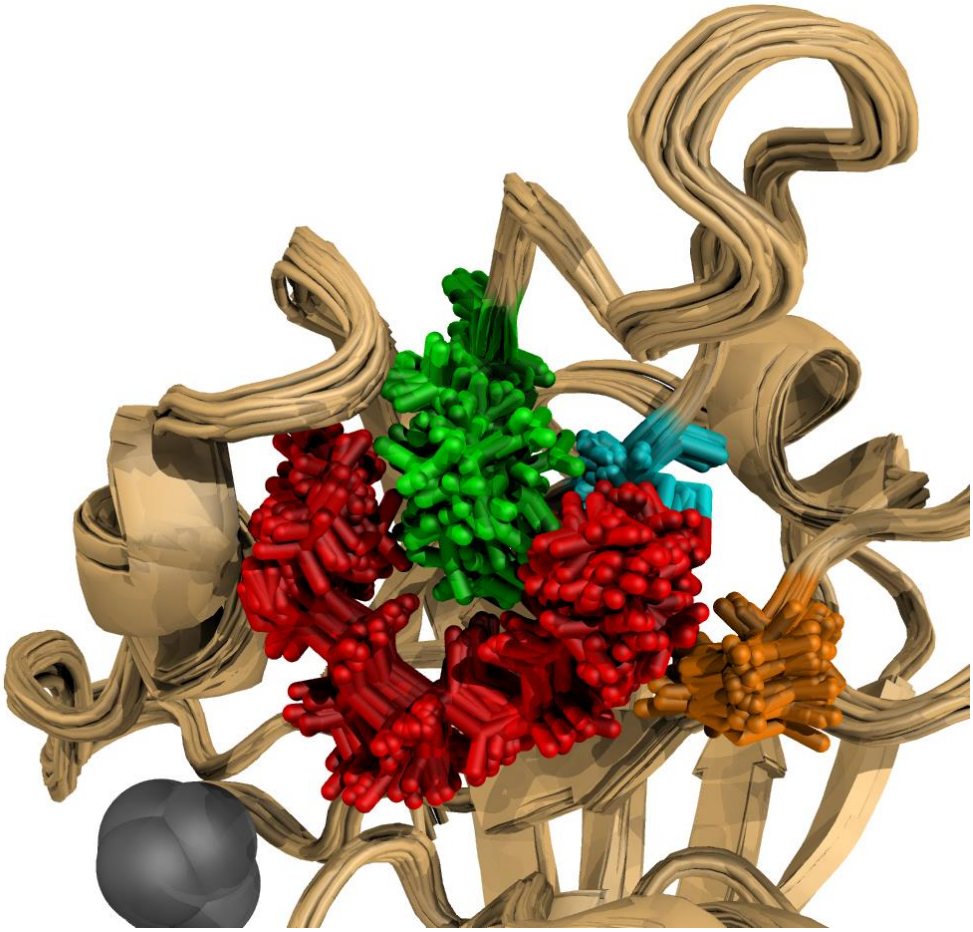

Figure 1-3 The positioning of Arg197 enforces a horseshoe conformation on the bound LPXTG peptide

His120. This leads to the formation of an exceptionally stable thioester intermediate between Cys184 and the threonine residue of the sorting signal, and the ejection of the C-terminal glycine residue of the sorting signal. Subsequent binding of an N-terminal GGG motif leads to the reverse reaction of this taking place, wherein the thioester is attacked by the deprotonated amine terminus of GGG to yield a new conjugate (Figure 1-4).

Unusually, Arg197 appears to function only as a hydrogen bond donor, serving to position the peptide substrate for attack in this reverse protonation mechanism[21]. This hypothesis was essentially confirmed in the holo-NMR structure of SrtA (Figure 1-2), determined with a

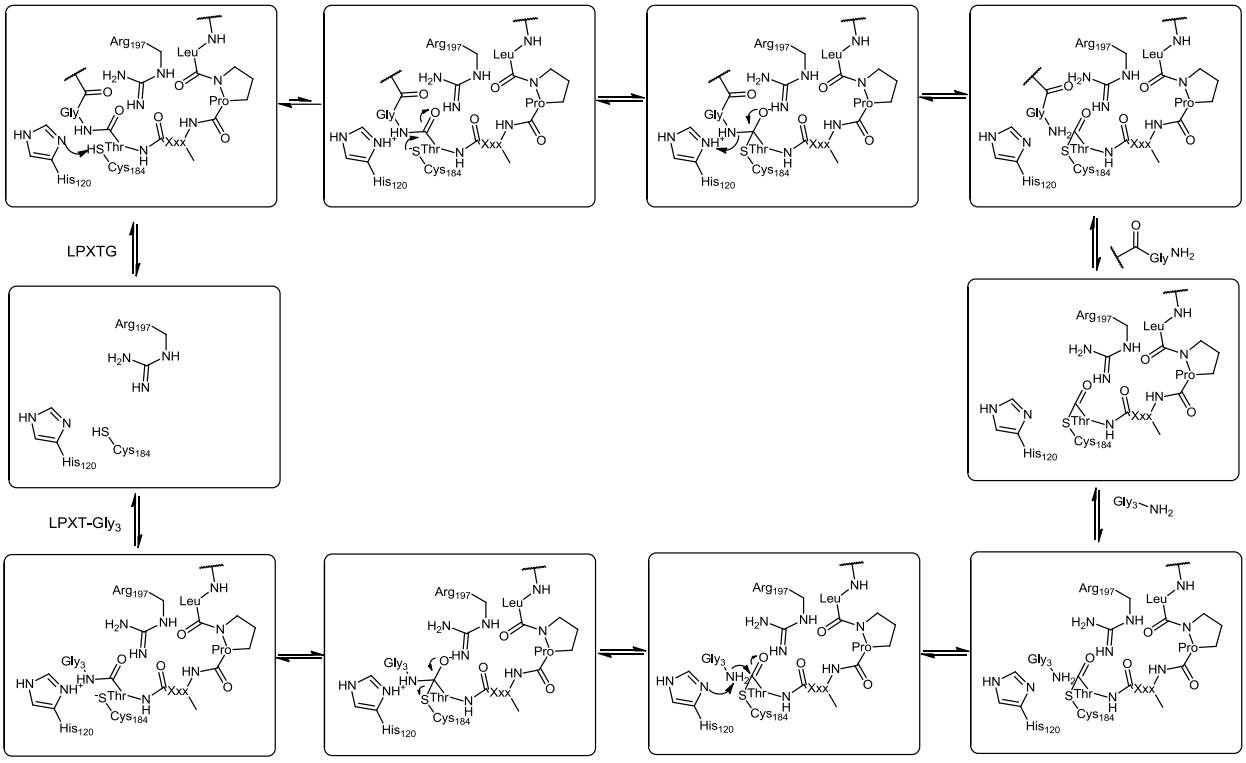

Figure 1-4 The Reverse Protonation Mechanism of *S. aureus* SrtA

The Arg197 residue makes hydrogen bonding contacts with the LPXTG backbone, orienting it for attack by the Cys120 thiolate. Protonation of the leaving glycine moiety by His120 leads to the ejection of the sorting signal's C-terminal glycine moiety and the formation of a stable Cys120 thioester intermediate. The reverse reaction, wherein an N-terminal glycine residue resolves the thioester and forms a new LPXTG peptide, proceeds via the reverse mechanism

covalently linked LPAT moiety to mimic the enzyme's catalytic intermediate, with Arg197 forming hydrogen bonds along a horseshoe-shaped peptide conformation (Figure 1-3). This is further facilitated by the behavior of the β6-7 binding loop in SrtA, which is normally unstructured, but rigidifies on binding of a calcium ion to facilitate binding of the LPXTG sorting signal[23].

In light of their physiological importance, periplasmic expresion and biochemically unique mechanism, then, sortases make for compelling targets for antibiotic discovery. Such notions are well supported by literature precedent, as ΔsrtA and ΔsrtB knockouts of *S. aureus* show abrogated binding to various eukaryotic cellular, ECM and immune components[24] and exhibit considerably diminished virulence in mouse models[24,25]. Indeed, there have been multiple academic discovery efforts aimed at identifying inhibitors of SrtA and related transpeptidases[26-33], and while no reversible inhibitors have risen above micromolar-scale

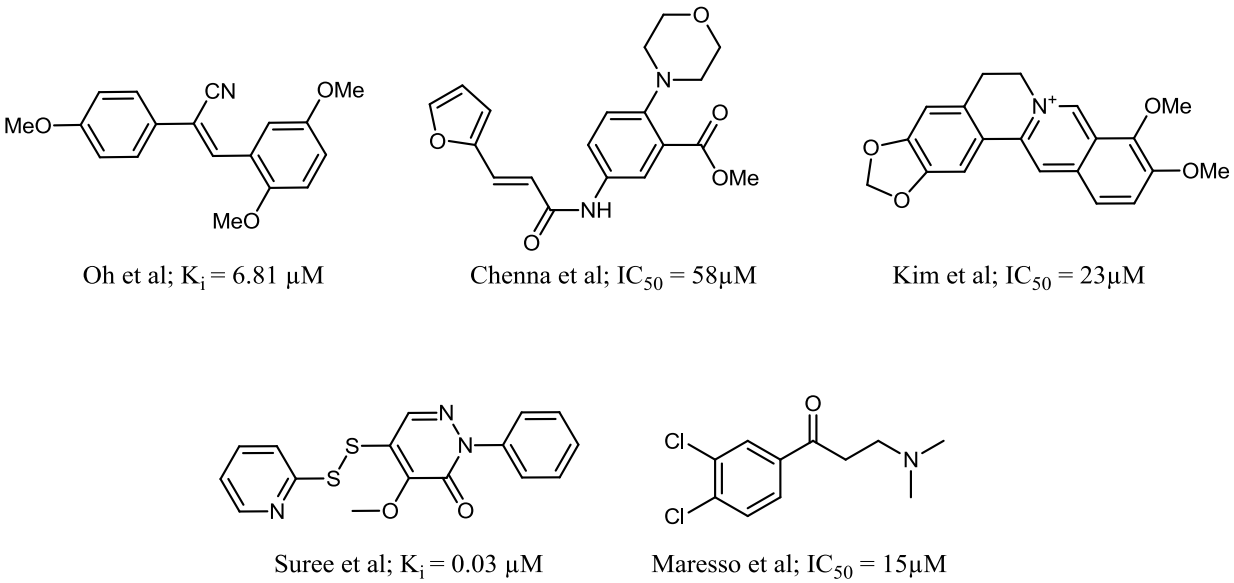

Oh et al; K_i = 6.81 μM

Chenna et al; IC_{50} = 58μM

Kim et al; IC_{50} = 23μM

Suree et al; K_i = 0.03 μM

Maresso et al; IC_{50} = 15μM

Figure 1-5 Selected Inhibitors of SrtA

Top row: Reversible inhibitors, Bottom row: Covalent inhibitors.

inhibition of the enzyme, irreversible covalent modification of the catalytic cysteine in *S. aureus* SrtA has proven effective at the nanomolar scale, both via disulfide-mediated crosslinking[27] as well as by a β-dimethylamino ketone that is converted into an α-β unsaturated ketone by the action of the enzyme[30] (Figure 1-5). That trans-micromolar inhibition has only been achieved by covalent inhibitors is unsurprising in light of SrtA's unique enzymology – the enzyme's dynamically unstructured binding site and small fraction of reaction-competent enzymes collectively makes access by traditional small molecule drug candidates extremely challenging. It also presents the unique situation where inhibition has little effect in cell proliferation assays, as ΔsrtA knockouts show little change in growth phenotype[19] but dramatic changes in virulence[24,25], septic arthritis and biofilm formation[34]. Such subtle phenotypes demand either carefully constructed phenotypic assays or the use of targeted drug discovery efforts.

The use of *S. aureus* SrtA in bioconjugate synthesis

Given SrtA's efficacy *in vivo*, it is unsurprising that it was rapidly co-opted by the biotechnology community for use in protein-peptide ligation[35], protein-PEG[36] and peptide-peptide nucleic acid[37] conjugate synthesis. Though conceptually similar, these initial reports were not widely adopted until the development of streamlined techniques for protein labeling by Popp et al[38] later on. This publication opened the floodgates for using SrtA to append a wide variety of small molecule modifiers onto proteins of interest, including lipidation[39-41], aminoglycoside conjugation[42], photocleavable handle conjugation[38], biotinylation[38,43], fluorophore conjugation[43-45], bioorthogonal handle introduction[46], and protein circularization[47]. Additionally, the *S. pyogenes* SrtA isoform was found to react with tri-alanine probes and the LPXTA tag[48,49], a feature which has been exploited for the separate bifunctionalization of N- and

C-terminal protein tags[50] as well as the introduction of bioorthogonal handles in circularized proteins[51].

Such approaches clearly show the power of sortagging as a ligation scheme, however the technique is historically hampered by several key limitations. The poor enzymatic efficiency of both the *S. aureus* SrtA[52] catalytic domain (k_{cat}/K_m ~ 120 $M^{-1}s^{-1}$) as well as the orthogonal *S. pyogenes* SrtA[48] catalytic domain (k_{cat}/K_m ~ 12 $M^{-1}s^{-1}$) necessitate the use of stoichiometric, rather than catalytic amounts of these reagents. The high stability of the thioester intermediate formed during the SrtA catalytic cycle, therefore, soaked away large fractions of the available substrate pool, leading to reduced yields and greatly increased the complexity of purifying away both excess SrtA and substrate-SrtA intermediates from the final reaction mixture. Additionally, this slow catalysis prevented the use of SrtA in the conjugation of otherwise unstable chemical modifiers, such as thioesters[53].

More generally, the low catalytic activity of SrtA often made it a poor substitute for high-efficiency chemical methods such as the copper-catalyzed click reaction[54-57] (k ~ 10-200 $M^{-1}s^{-1}$) or copper-free click reaction[57-61] (k ~ 10^{-2}-1 $M^{-1}s^{-1}$). In each case, the poor activity of SrtA can often overcome its biocompatibility and easy substrate synthesis, making either of these (in addition to other[57]) reaction chemistries the more attractive option for bioconjugate synthesis *in vivo* and *in vitro*. Additionally, with the advent of genetically encodable click handles, these approaches enjoy very broad applicability, as tags can be incorporated more or less arbitrarily into target protein sequences. These approaches are not without their drawbacks, however, as modern genetic encoding techniques rely upon competition of native protein translation termination factors with engineered tRNA machinery, leading to any cellular expression system producing a mixture of mislabeled, truncated, and correctly charged proteins[61]. Additionally, the

copper-catalyzed version of the click reaction is not, in principle, biocompatible due to the toxicity of the requisite Cu(I) ion, while the copper-free version relies upon the synthesis of complex cyclooctyne moieties that in general very low-yielding. SrtA, with its facile substrate synthesis and biocompatible reaction conditions, would present a very appealing alternative to these approaches, were a more catalytically active variant with programmable specificity to be developed.

To this end, there have been two major published investigations into changing the substrate specificity of *S. aureus* SrtA. In the first, the β6-7 loop of SrtA was replaced by the homologous binding loop from *S. aureus* sortase B, in order to test if the NPQTN substrate specificity of SrtB could be added to SrtA[62]. In this case, it was found that this altered enzyme possessed greatly (>5000-fold) diminished catalytic efficiency, but now accepted NPQTN sequences preferentially over LPETG. While the low activity of this variant made studying its detailed kinetics intractable, let alone using it as a molecular tool, it served as a valuable proof of principle for later efforts, including those reported in this thesis. A more recent study attempted to evolve SrtA variants with altered specificity by randomizing the amino acid sequence of this binding loop, displaying the resulting variants as fusions to protein III in the bacteriophage M13, and then attempting to pull down variants capable of ligating biotinyl-FPETG peptides onto themselves[63]. The variants isolated by this method also showed greatly (>10-fold) diminished catalytic activity relative to SrtA, but nonetheless showed largely ablated specificity at the first residue of the sorting signal. These promiscuous variants nevertheless proved to be effective for the semisynthesis of histone H3 at low efficiency.

References

1 Ghuysen, J.-M. & Hakenbeck, R. *Bacterial cell wall*. (Elsevier, 1994).

2 Foster, T. J. & Höök, M. Surface protein adhesins of< i> Staphylococcus aureus</i>. *Trends in microbiology* **6**, 484-488 (1998).

3 Cabanes, D., Dehoux, P., Dussurget, O., Frangeul, L. & Cossart, P. Surface proteins and the pathogenic potential of< i> Listeria monocytogenes</i>. *Trends in microbiology* **10**, 238-245 (2002).

4 Milohanic, E., Jonquieres, R., Cossart, P., Berche, P. & Gaillard, J. L. The autolysin Ami contributes to the adhesion of Listeria monocytogenes to eukaryotic cells via its cell wall anchor. *Molecular microbiology* **39**, 1212-1224 (2001).

5 Patti, J. M., Allen, B. L., McGavin, M. J. & Hook, M. MSCRAMM-mediated adherence of microorganisms to host tissues. *Annual Reviews in Microbiology* **48**, 585-617 (1994).

6 Coconnier, M. H., Klaenhammer, T., Kerneis, S., Bernet, M. & Servin, A. Protein-mediated adhesion of Lactobacillus acidophilus BG2FO4 on human enterocyte and mucus-secreting cell lines in culture. *Applied and Environmental Microbiology* **58**, 2034-2039 (1992).

7 Foster, T. J. Immune evasion by staphylococci. *Nature Reviews Microbiology* **3**, 948-958 (2005).

8 Mazmanian, S. K., Liu, G., Ton-That, H. & Schneewind, O. Staphylococcus aureus Sortase, an Enzyme that Anchors Surface Proteins to the Cell Wall. *Science* **285**, 760-763, doi:10.1126/science.285.5428.760 (1999).

9 Schneewind, O., Mihaylova-Petkov, D. & Model, P. Cell wall sorting signals in surface proteins of gram-positive bacteria. *The EMBO journal* **12**, 4803 (1993).

10 Schneewind, O., Fowler, A. & Faull, K. Structure of the cell wall anchor of surface proteins in Staphylococcus aureus. *Science* **268**, 103-106, doi:10.1126/science.7701329 (1995).

11 Mazmanian, S. K., Ton-That, H., Su, K. & Schneewind, O. An iron-regulated sortase anchors a class of surface protein during Staphylococcus aureus pathogenesis. *Proceedings of the National Academy of Sciences* **99**, 2293-2298, doi:10.1073/pnas.032523999 (2002).

12 Mazmanian, S. K. *et al.* Passage of Heme-Iron Across the Envelope of Staphylococcus aureus. *Science* **299**, 906-909, doi:10.1126/science.1081147 (2003).

13 Pallen, M. J., Lam, A. C., Antonio, M. & Dunbar, K. An embarrassment of sortases – a richness of substrates? *Trends in microbiology* **9**, 97-101, doi:http://dx.doi.org/10.1016/S0966-842X(01)01956-4 (2001).

14 Comfort, D. & Clubb, R. T. A Comparative Genome Analysis Identifies Distinct Sorting Pathways in Gram-Positive Bacteria. *Infection and Immunity* **72**, 2710-2722, doi:10.1128/iai.72.5.2710-2722.2004 (2004).

15 Boekhorst, J., de Been, M. W. H. J., Kleerebezem, M. & Siezen, R. J. Genome-Wide Detection and Analysis of Cell Wall-Bound Proteins with LPxTG-Like Sorting Motifs. *Journal of Bacteriology* **187**, 4928-4934, doi:10.1128/jb.187.14.4928-4934.2005 (2005).

16 Ton-That, H. & Schneewind, O. Assembly of pili in Gram-positive bacteria. *Trends in microbiology* **12**, 228-234, doi:http://dx.doi.org/10.1016/j.tim.2004.03.004 (2004).

17 Zong, Y., Bice, T. W., Ton-That, H., Schneewind, O. & Narayana, S. V. Crystal structures of Staphylococcus aureus sortase A and its substrate complex. *Journal of Biological Chemistry* **279**, 31383-31389 (2004).

18 Ilangovan, U., Ton-That, H., Iwahara, J., Schneewind, O. & Clubb, R. T. Structure of sortase, the transpeptidase that anchors proteins to the cell wall of Staphylococcus aureus. *Proceedings of the National Academy of Sciences* **98**, 6056-6061, doi:10.1073/pnas.101064198 (2001).

19 Ton-That, H., Liu, G., Mazmanian, S. K., Faull, K. F. & Schneewind, O. Purification and characterization of sortase, the transpeptidase that cleaves surface proteins of Staphylococcus aureus at the LPXTG motif. *Proceedings of the National Academy of Sciences* **96**, 12424-12429 (1999).

20 Ton-That, H., Mazmanian, S. K., Alksne, L. & Schneewind, O. Anchoring of surface proteins to the cell wall of Staphylococcus aureus Cysteine 184 and histidine 120 of sortase form a thiolate-imidazolium ion pair for catalysis. *Journal of Biological Chemistry* **277**, 7447-7452 (2002).

21 Bentley, M. L., Lamb, E. C. & McCafferty, D. G. Mutagenesis studies of substrate recognition and catalysis in the sortase A transpeptidase from Staphylococcus aureus. *Journal of Biological Chemistry* **283**, 14762-14771 (2008).

22 Frankel, B. A., Kruger, R. G., Robinson, D. E., Kelleher, N. L. & McCafferty, D. G. Staphylococcus aureus sortase transpeptidase SrtA: insight into the kinetic mechanism and evidence for a reverse protonation catalytic mechanism. *Biochemistry* **44**, 11188-11200 (2005).

23 Naik, M. T. *et al.* Staphylococcus aureus Sortase A Transpeptidase: CALCIUM PROMOTES SORTING SIGNAL BINDING BY ALTERING THE MOBILITY AND

STRUCTURE OF AN ACTIVE SITE LOOP. *Journal of Biological Chemistry* **281**, 1817-1826, doi:10.1074/jbc.M506123200 (2006).

24 Mazmanian, S. K., Liu, G., Jensen, E. R., Lenoy, E. & Schneewind, O. Staphylococcus aureus sortase mutants defective in the display of surface proteins and in the pathogenesis of animal infections. *Proceedings of the National Academy of Sciences* **97**, 5510-5515, doi:10.1073/pnas.080520697 (2000).

25 Weiss, W. J. *et al.* Effect of srtA and srtB gene expression on the virulence of Staphylococcus aureus in animal models of infection. *Journal of Antimicrobial Chemotherapy* **53**, 480-486, doi:10.1093/jac/dkh078 (2004).

26 Oh, K.-B. *et al.* Discovery of diarylacrylonitriles as a novel series of small molecule sortase A inhibitors. *Journal of medicinal chemistry* **47**, 2418-2421 (2004).

27 Suree, N. *et al.* Discovery and structure–activity relationship analysis of< i> Staphylococcus aureus</i> sortase A inhibitors. *Bioorganic & medicinal chemistry* **17**, 7174-7185 (2009).

28 Kim, S.-H. *et al.* Inhibition of the bacterial surface protein anchoring transpeptidase sortase by isoquinoline alkaloids. *Bioscience, biotechnology, and biochemistry* **68**, 421-424 (2004).

29 Chenna, B. C. *et al.* Identification of novel inhibitors of bacterial surface enzyme< i> Staphylococcus aureus</i> Sortase A. *Bioorganic & medicinal chemistry letters* **18**, 380-385 (2008).

30 Maresso, A. W. *et al.* Activation of inhibitors by sortase triggers irreversible modification of the active site. *Journal of Biological Chemistry* **282**, 23129-23139 (2007).

31 Kruger, R. G., Barkallah, S., Frankel, B. A. & McCafferty, D. G. Inhibition of the Staphylococcus aureus sortase transpeptidase SrtA by phosphinic peptidomimetics. *Bioorganic & medicinal chemistry* **12**, 3723-3729, doi:http://dx.doi.org/10.1016/j.bmc.2004.03.066 (2004).

32 Kahlon, A. K. *et al.* Identification of 1-chloro-2-formyl indenes and tetralenes as novel antistaphylococcal agents exhibiting sortase A inhibition. *Applied microbiology and biotechnology*, 1-11 (2013).

33 Chan, A. H. *et al.* Discovery of Staphylococcus aureus Sortase A Inhibitors Using Virtual Screening and the Relaxed Complex Scheme. *Chemical biology & drug design* **82**, 418-428 (2013).

34 Trotonda, M. P., Tamber, S., Memmi, G. & Cheung, A. L. MgrA Represses Biofilm Formation in Staphylococcus aureus. *Infection and Immunity* **76**, 5645-5654, doi:10.1128/iai.00735-08 (2008).

35 Mao, H., Hart, S. A., Schink, A. & Pollok, B. A. Sortase-Mediated Protein Ligation: A New Method for Protein Engineering. *Journal of the American Chemical Society* **126**, 2670-2671, doi:10.1021/ja039915e (2004).

36 Parthasarathy, R., Subramanian, S. & Boder, E. T. Sortase A as a novel molecular "stapler" for sequence-specific protein conjugation. *Bioconjugate chemistry* **18**, 469-476 (2007).

37 Pritz, S. *et al.* Synthesis of biologically active peptide nucleic acid-peptide conjugates by sortase-mediated ligation. *The Journal of organic chemistry* **72**, 3909-3912 (2007).

38 Popp, M. W., Antos, J. M., Grotenbreg, G. M., Spooner, E. & Ploegh, H. L. Sortagging: a versatile method for protein labeling. *Nat Chem Biol* **3**, 707-708, doi:http://www.nature.com/nchembio/journal/v3/n11/suppinfo/nchembio.2007.31_S1.html (2007).

39 Antos, J. M., Miller, G. M., Grotenbreg, G. M. & Ploegh, H. L. Lipid Modification of Proteins through Sortase-Catalyzed Transpeptidation. *Journal of the American Chemical Society* **130**, 16338-16343, doi:10.1021/ja806779e (2008).

40 Wu, Z., Guo, X., Wang, Q., Swarts, B. M. & Guo, Z. Sortase A-Catalyzed Transpeptidation of Glycosylphosphatidylinositol Derivatives for Chemoenzymatic Synthesis of GPI-Anchored Proteins. *Journal of the American Chemical Society* **132**, 1567-1571, doi:10.1021/ja906611x (2010).

41 Guo, X., Wang, Q., Swarts, B. M. & Guo, Z. Sortase-Catalyzed Peptide−Glycosylphosphatidylinositol Analogue Ligation. *Journal of the American Chemical Society* **131**, 9878-9879, doi:10.1021/ja903231v (2009).

42 Samantaray, S., Marathe, U., Dasgupta, S., Nandicoori, V. K. & Roy, R. P. Peptide−Sugar Ligation Catalyzed by Transpeptidase Sortase: A Facile Approach to Neoglycoconjugate Synthesis. *Journal of the American Chemical Society* **130**, 2132-2133, doi:10.1021/ja077358g (2008).

43 Tanaka, T., Yamamoto, T., Tsukiji, S. & Nagamune, T. Site-Specific Protein Modification on Living Cells Catalyzed by Sortase. *ChemBioChem* **9**, 802-807, doi:10.1002/cbic.200700614 (2008).

44 Yamamoto, T. & Nagamune, T. Expansion of the sortase-mediated labeling method for site-specific N-terminal labeling of cell surfaceproteins on living cells. *Chemical Communications*, 1022-1024, doi:10.1039/b818792d (2009).

45 Hirota, N. *et al.* Amino Acid Residues Critical for Endoplasmic Reticulum Export and Trafficking of Platelet-activating Factor Receptor. *Journal of Biological Chemistry* **285**, 5931-5940, doi:10.1074/jbc.M109.066282 (2010).

46 Nelson, J. W. *et al.* A Biosynthetic Strategy for Re-engineering the Staphylococcus aureus Cell Wall with Non-native Small Molecules. *ACS Chemical Biology* **5**, 1147-1155, doi:10.1021/cb100195d (2010).

47 Antos, J. M. *et al.* A straight path to circular proteins. *Journal of Biological Chemistry* **284**, 16028-16036 (2009).

48 Race, P. R. *et al.* Crystal structure of Streptococcus pyogenes Sortase A implications for sortase mechanism. *Journal of Biological Chemistry* **284**, 6924-6933 (2009).

49 Marraffini, L. A., DeDent, A. C. & Schneewind, O. Sortases and the art of anchoring proteins to the envelopes of gram-positive bacteria. *Microbiology and Molecular Biology Reviews* **70**, 192-221 (2006).

50 Antos, J. M. *et al.* Site-Specific N- and C-Terminal Labeling of a Single Polypeptide Using Sortases of Different Specificity. *Journal of the American Chemical Society* **131**, 10800-10801, doi:10.1021/ja902681k (2009).

51 Popp, M. W., Dougan, S. K., Chuang, T.-Y., Spooner, E. & Ploegh, H. L. Sortase-catalyzed transformations that improve the properties of cytokines. *Proceedings of the National Academy of Sciences* **108**, 3169-3174 (2011).

52 Kruger, R. G., Dostal, P. & McCafferty, D. G. Development of a high-performance liquid chromatography assay and revision of kinetic parameters for the Staphylococcus aureus sortase transpeptidase SrtA. *Analytical Biochemistry* **326**, 42-48, doi:http://dx.doi.org/10.1016/j.ab.2003.10.023 (2004).

53 Ling, J. J., Policarpo, R. L., Rabideau, A. E., Liao, X. & Pentelute, B. L. Protein Thioester Synthesis Enabled by Sortase. *Journal of the American Chemical Society* **134**, 10749-10752, doi:10.1021/ja302354v (2012).

54 Wang, Q. *et al.* Bioconjugation by copper (I)-catalyzed azide-alkyne [3+ 2] cycloaddition. *Journal of the American Chemical Society* **125**, 3192-3193 (2003).

55 Nguyen, D. P. *et al.* Genetic encoding and labeling of aliphatic azides and alkynes in recombinant proteins via a pyrrolysyl-tRNA synthetase/tRNACUA pair and click chemistry. *Journal of the American Chemical Society* **131**, 8720-8721 (2009).

56 Presolski, S. I., Hong, V., Cho, S.-H. & Finn, M. Tailored ligand acceleration of the Cu-catalyzed azide− alkyne cycloaddition reaction: Practical and mechanistic implications. *Journal of the American Chemical Society* **132**, 14570-14576 (2010).

57 Lang, K. & Chin, J. W. Bioorthogonal Reactions for Labeling Proteins. *ACS Chemical Biology* **9**, 16-20, doi:10.1021/cb4009292 (2014).

58 Agard, N. J., Prescher, J. A. & Bertozzi, C. R. A strain-promoted [3+ 2] azide-alkyne cycloaddition for covalent modification of biomolecules in living systems. *Journal of the American Chemical Society* **126**, 15046-15047 (2004).

59 Baskin, J. M. *et al.* Copper-free click chemistry for dynamic in vivo imaging. *Proceedings of the National Academy of Sciences* **104**, 16793-16797 (2007).

60 Ning, X., Guo, J., Wolfert, M. A. & Boons, G. J. Visualizing metabolically labeled glycoconjugates of living cells by copper-free and fast Huisgen cycloadditions. *Angewandte Chemie International Edition* **47**, 2253-2255 (2008).

61 Plass, T., Milles, S., Koehler, C., Schultz, C. & Lemke, E. A. Genetically Encoded Copper-Free Click Chemistry. *Angewandte Chemie International Edition* **50**, 3878-3881 (2011).

62 Bentley, M. L., Gaweska, H., Kielec, J. M. & McCafferty, D. G. Engineering the Substrate Specificity of Staphylococcus aureus Sortase A THE β6/β7 LOOP FROM SrtB CONFERS NPQTN RECOGNITION TO SrtA. *Journal of Biological Chemistry* **282**, 6571-6581 (2007).

63 Piotukh, K. *et al.* Directed Evolution of Sortase A Mutants with Altered Substrate Selectivity Profiles. *Journal of the American Chemical Society* **133**, 17536-17539, doi:10.1021/ja205630g (2011).

Chapter Two

A General Strategy for the Evolution of Bond-Forming Enzymes Using Yeast Display

Irwin Chen, Brent M. Dorr and David R. Liu

Irwin Chen conceptualized and developed the modified yeast display system reported in this work, validated SrtA in the system and synthesized the round 1 and 2 libraries. I synthesized the round 3 library, characterized eSrtA and its intermediates and performed several of the sorts. Irwin and I collaboratively performed the remaining experiments and analysis.

Some of the text in this chapter appears in the *Proceedings of the National Academy of Sciences*, **2011**, 108 (28), pp 11399-11404.

Abstract

The ability to routinely generate efficient protein catalysts of bond-forming reactions chosen by researchers, rather than nature, is a longstanding goal of the molecular life sciences. Here we describe a directed evolution strategy for enzymes that catalyze, in principle, any bond-forming reaction. The system integrates yeast display, enzyme-catalyzed bioconjugation, and fluorescence-activated cell sorting to isolate cells expressing proteins that catalyze the coupling of two substrates chosen by the researcher. We validated the system using model screens for *Staphylococcus aureus* sortase A-catalyzed transpeptidation activity, resulting in enrichment factors of 6,000-fold after a single round of screening. We applied the system to evolve sortase A for improved catalytic activity. After eight rounds of screening, we isolated variants of sortase A with up to a 140-fold increase in LPETG-coupling activity compared with the starting wild-type enzyme. An evolved sortase variant enabled much more efficient labeling of LPETG-tagged human CD154 expressed on the surface of HeLa cells compared with wild-type sortase. As the method developed here does not rely on any particular screenable or selectable property of the substrates or product, it represents a powerful alternative to existing enzyme evolution methods.

Introduction

Despite the many attractive features of protein enzymes as catalysts for organic synthesis[2], as research tools[3-5], and as an important class of human therapeutics[6,7], the extent and diversity of their applications remain limited by the difficulty of finding in nature or creating in the laboratory highly active proteins that catalyze chemical reactions of interest. A significant fraction of protein catalysts currently used for research and industrial applications was obtained through the directed evolution of natural enzymes[8]. Current methods for the directed evolution of enzymes have resulted in some remarkable successes[9,10], but generally suffer from limitations in

reaction scope. For example, screening enzyme libraries in a multi-well format has proven to be effective for enzymes that process chromogenic or fluorogenic substrates, and is typically limited to library sizes of ~10^2-10^6 members, depending on the nature of the screen and on available infrastructure[11]. Selections of cell-based libraries that couple product formation with auxotrophy complementation[12] or transcription of a reporter gene[13] enable larger library sizes to be processed, but also suffer from limited generality because they rely on specific properties of the substrate or product. Likewise, *in vitro* compartmentalization is a powerful genotype-phenotype co-localization platform that has been used to evolve protein enzymes with improved turnover, but also requires corresponding screening or selection methods that thus far have been substrate- or product-specific[14].

Directed evolution strategies that are general for any bond-forming reaction would complement current methods that rely on screenable reactions or selectable properties of the substrate or product. In principle, chemical complementation using an adapted yeast three-hybrid assay is reaction-independent[15], but requires membrane-permeable substrates and offers limited control over reaction conditions because the bond-forming event must take place intracellularly. Phage-display and mRNA-display systems that are general for any bond-forming reaction have been used to evolve enzymes including DNA polymerases[16] and RNA ligases[17]. These approaches also offer advantages of larger library sizes and significant control over reaction conditions because the enzymes are displayed extracellularly or expressed in the absence of a host cell.

Cell surface display [18-21] is an attractive alternative to phage and mRNA display. In contrast with other display methods, the use of bacterial or yeast cells enables up to 100,000 copies of a library member to be linked to one copy of the gene, increasing sensitivity during

screening or selection steps. In addition, cell surface-displayed libraries are compatible with powerful fluorescence-activated cell sorting (FACS) that enable very large libraries to be screened efficiently (>10^7 cells per hour) with precise, quantitative control over screening stringency. The multicolor capabilities of FACS also enable normalization for enzyme display level during screening and simultaneous positive and negative screens, capabilities that are difficult to implement in phage and mRNA display.

In this work we integrated yeast display, enzyme-catalyzed small molecule-protein conjugation, and FACS into a general strategy for the evolution of proteins that catalyze bond-forming (coupling) reactions. We applied the system to evolve the bacterial transpeptidase sortase A for improved catalytic activity, resulting in sortase variants with up to 140-fold improvement in activity. In contrast with wild-type sortase, an evolved sortase enabled highly efficient cell-surface labeling of recombinant human CD154 expressed on the surface of live HeLa cells with a biotinylated peptide.

Results

Design and Implementation of a General System for the Evolution of Bond-Forming Enzymes

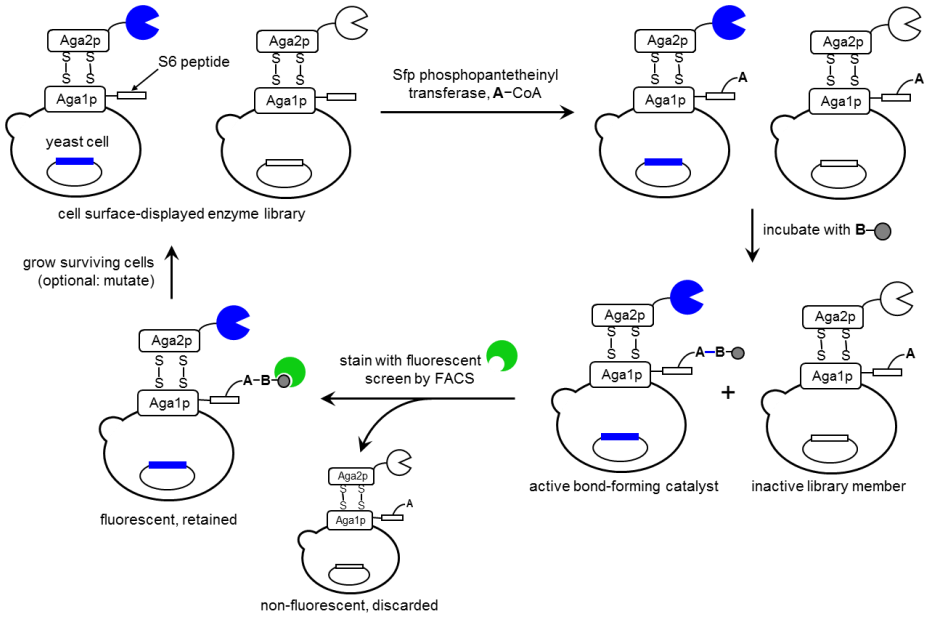

Figure 2-1 A general strategy for the evolution of bond-forming catalysts using yeast display.

The enzyme evolution system is overviewed in Figure 2-1. Yeast cells display the enzyme library extracellularly as a fusion to the Aga2p cell surface mating factor, which is covalently bound to the Aga1p mating factor with a reactive handle that enables covalent attachment of substrate A to cells. We chose the S6 peptide[4] as the reactive handle to link substrate A to cells using Sfp phosphopantetheinyl transferase from *Bacillus subtilis*. Substrate B linked to an affinity handle (e.g. biotin, represented by the gray circle in Figure 2-1) is added to the substrate A-conjugated yeast display enzyme library. Due to the high effective molarity of substrate A with respect to each cell's displayed library member, both of which are immobilized on the cell surface, active library members will predominantly catalyze the pseudo-intramolecular A–B bond formation between affinity handle-linked substrate B and substrate A molecules on their own host cell. The intermolecular coupling of substrate B with substrate A

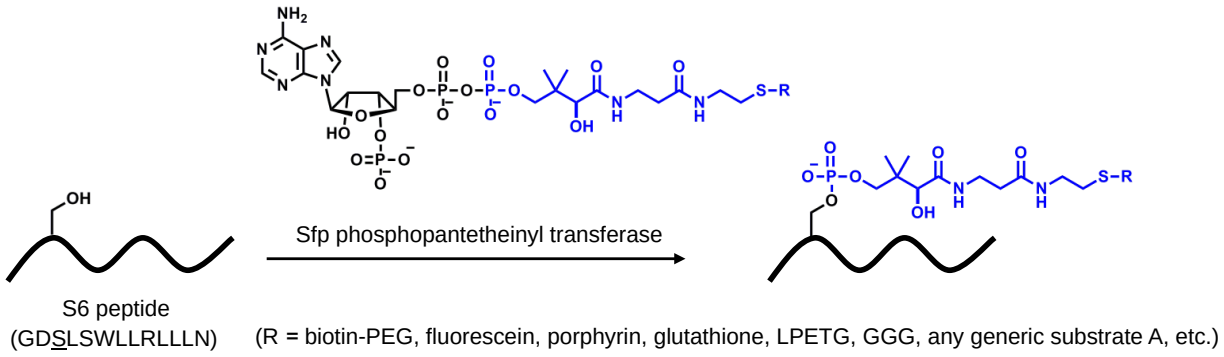

Figure 2-2 Sfp-catalyzed transfer of phosphopantetheinyl derivatives (blue) onto a specific serine residue (underlined) within the S6 peptide sequence.

molecules attached to other cells is entropically much less favorable, and therefore yeast cells displaying inactive enzymes should remain predominantly uncoupled to the affinity handle.

Following incubation with substrate B for the desired reaction time, cells are stained with a fluorescent molecule that binds the affinity handle (e.g., streptavidin-phycoerythrin (streptavidin-PE)). The most fluorescent cells, which encode the most active catalysts, are isolated by FACS. Up to 10^8 cells can be sorted in a two-hour period using modern FACS equipment. After sorting and growth amplification, the recovered cells can be enriched through additional FACS steps, or DNA encoding active library members can be harvested and subjected to point mutagenesis or recombination before entering the next round of evolution.

We used a chemoenzymatic approach to link substrate A to cells rather than a non-specific chemical conjugation strategy to more reproducibly array the substrate on the cell surface and to avoid reagents that might alter the activity of library members. The *B. subtilis* Sfp phosphopantetheinyl transferase catalyzes the transfer of phosphopantetheine from coenzyme A (CoA) onto a specific serine side chain within an acyl carrier protein or peptide carrier protein. We chose Sfp to mediate substrate attachment because of its broad small-molecule substrate

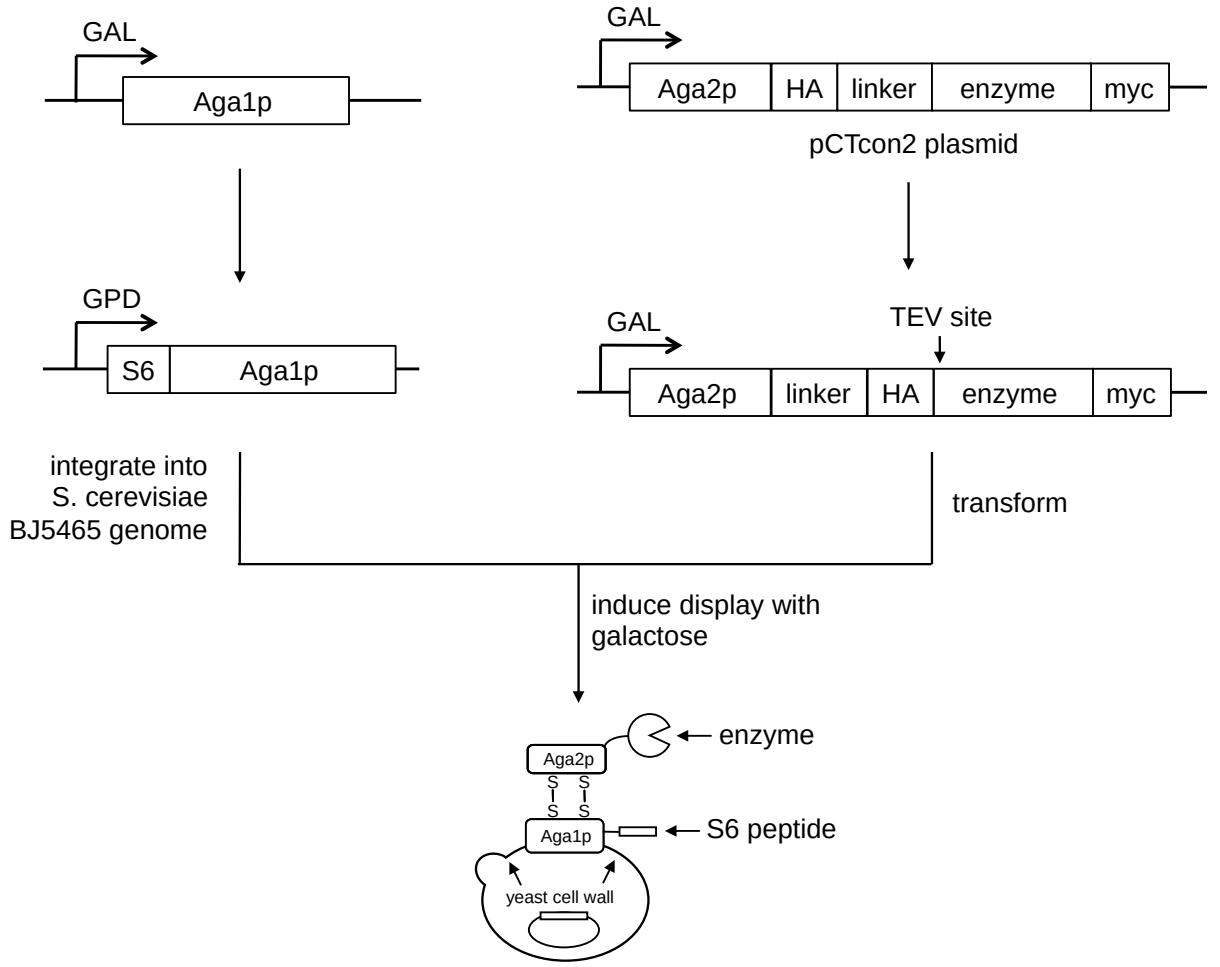

Figure 2-3 Engineering a *Saccharomyces cerevisiae* strain that simultaneously displays the S6 peptide sequence and the sortase enzyme library on its cell surface

The S6-Aga1p construct is cloned under the control of the constitutive glyceraldehyde-3-phosphate dehydrogenase (GPD) promoter and integrated into the genome of *S. cerevisiae* BJ5465 to yield strain ICY200. Through several cloning steps, a TEV recognition site is inserted between the HA tag and enzyme gene of the Aga2p fusion construct. Yeast display of sortases is induced upon the addition of galactose to the media.

tolerance[4,22] and its ability to efficiently conjugate phosphopantetheine derivatives to the 12-residue S6 peptide[23] (Figure 2-2). We speculated that the small size of the S6 peptide would allow it to be well-tolerated in the context of the Aga1p mating factor. Functionalized CoA derivatives can be readily prepared by reacting the free thiol of commercially available CoA[4,22] with a commercially available maleimide-containing bifunctional crosslinker, followed by substrate A bearing a compatible functional group.

To integrate Sfp-catalyzed bioconjugation with yeast display required engineering a new yeast display vector and yeast strain (Figure 2-3). To create a handle for substrate attachment at the cell surface, we fused the S6 peptide onto the N-terminus of Aga1p and integrated this construct under the control of the strong, constitutive GPD promoter in the genome of *Saccharomyces cerevisiae* strain BJ5465[20]. We modified the Aga2p expression construct by inserting the recognition site for tobacco etch virus (TEV) protease between the hemagglutinin (HA) tag and the coding sequence of the protein of interest. Following incubation of the

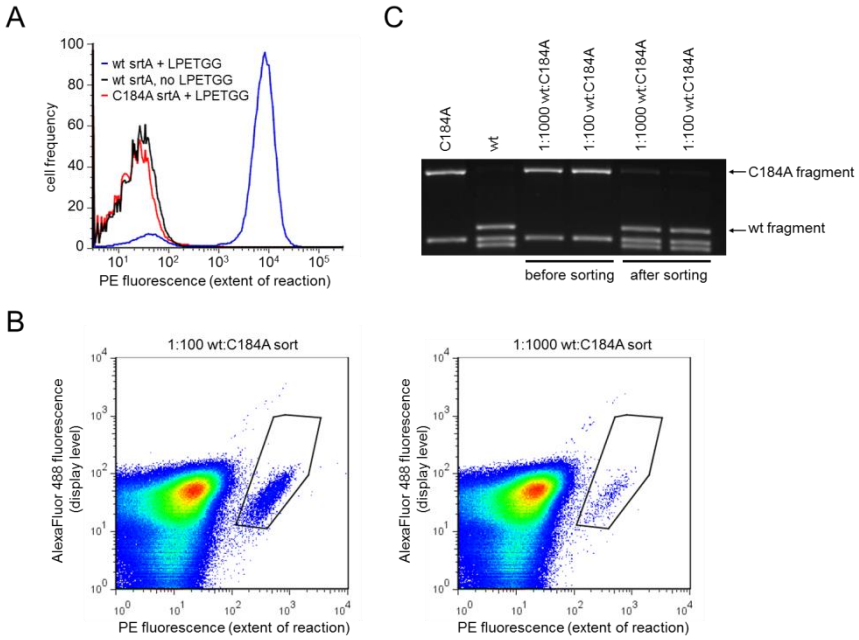

Figure 2-4 Validation of the enzyme evolution strategy.

(A) FACS histogram of the reaction between cell surface-conjugated LPETGG and free GGGYK-biotin catalyzed by yeast-displayed wild-type *S. aureus* sortase A (wt srtA). Cells were stained with streptavidin-PE and an AlexaFluor488-anti-HA antibody. Negative control reactions with either the inactive C184A srtA mutant or without LPETGG are shown. (B) Dot plots comparing PE fluorescence (extent of reaction) vs. AlexaFluor488 fluorescence (display level) for two model screens. Mixtures of cells displaying either wt srtA or the inactive C184A srtA (1:1000 and 1:100 wt:C184A) were processed as in (A), then analyzed by FACS. Cells within the specified gate (black polygon) were collected. (C) Model screening results. Gene compositions before and after sorting were compared following *Hind*III digestion, revealing strong enrichment for active sortase.

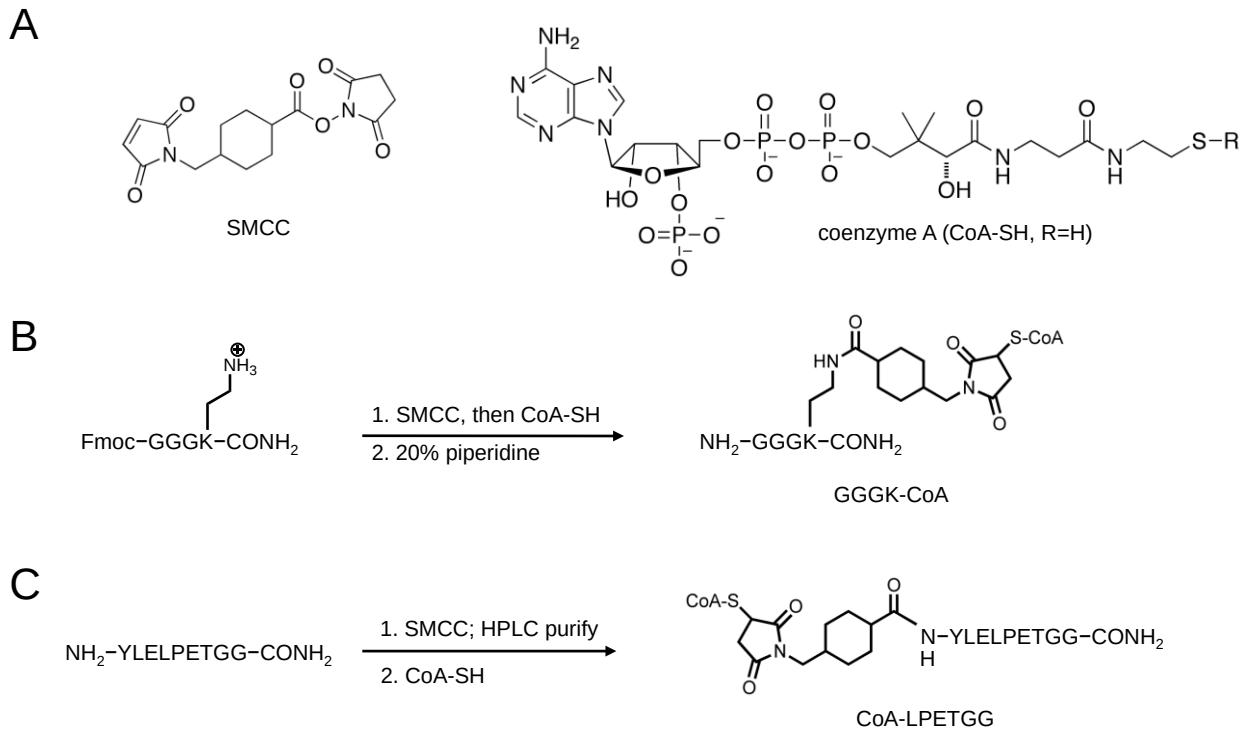

Figure 2-5 Synthesis of coenzyme A-conjugated sortase substrates.

(A) Chemical structures of the SMCC crosslinker and coenzyme A (CoA). (B) Synthesis strategy for GGGK-CoA. (C) Synthesis strategy for CoA-LPETGG.

substrate-A-conjugated yeast library with substrate B, TEV protease digestion removes all library members from the surface, including any undesired enzymes that bind or react directly with substrate B, but do not catalyze A–B bond formation, thus removing a potential source of undesired background. The HA tag remains on the cell surface and enables staining for enzyme display level using an anti-HA antibody. The ability to efficiently cleave enzymes from the yeast cell surface also facilitates enzyme characterization in a cell-free context.

Validation of the Yeast Display System

Sortase A (srtA) is a sequence-specific transpeptidase found in *Staphylococcus aureus* and other Gram positive bacteria. The *S. aureus* enzyme recognizes a LPXTG site (X = any amino acid), cleaves the scissile amide bond between threonine and glycine using a nucleophilic cysteine (C184), and resolves the resulting acyl-enzyme intermediate with oligoglycine-linked molecules to generate the fusion of the LPXT- and oligoglycine-linked peptides or proteins. Sortase A-catalyzed transpeptidation has emerged as a powerful tool for bioconjugation because of the enzyme's high specificity for the LPXTG motif and its extremely broad substrate tolerance outside of the recognition elements described above. Because the LPXTG and oligoglycine motifs can be flanked by virtually any biomolecule, sortase has been used to label proteins, generate nucleic acid-protein conjugates, and immobilize proteins onto solid supports[24]. A significant limitation of srtA is the large quantities of the enzyme or long reaction times that are needed to overcome its poor reaction kinetics ($k_{cat}/K_{m\ LPETG}$ = 200 M^{-1} s^{-1} , Table 1). The evolution of a more active *S. aureus* srtA would therefore significantly enhance the utility and scope of this bond-forming reaction.

We first examined if yeast-displayed sortase enzymes in our system could catalyze the reaction between surface-immobilized LPETGG and exogenous biotinylated trigycine peptide (GGGYK-biotin). To conjugate cells to the LPETGG substrate, we incubated yeast displaying wild-type srtA and the S6 peptide with Sfp and coenzyme A-linked LPETGG (CoA-LPETGG, Figure 2-5). The sortase-catalyzed reactions were initiated with the addition of GGGYK-biotin and 5 mM $CaCl_2$. After washing, the cells were stained with streptavidin-PE and an AlexaFluor488-conjugated anti-HA antibody to analyze the extent of reaction and enzyme display level, respectively, by flow cytometry. When yeast cells displaying wild-type sortase A (wt srtA-yeast) were analyzed, the majority of the cells exhibited high levels of PE fluorescence,

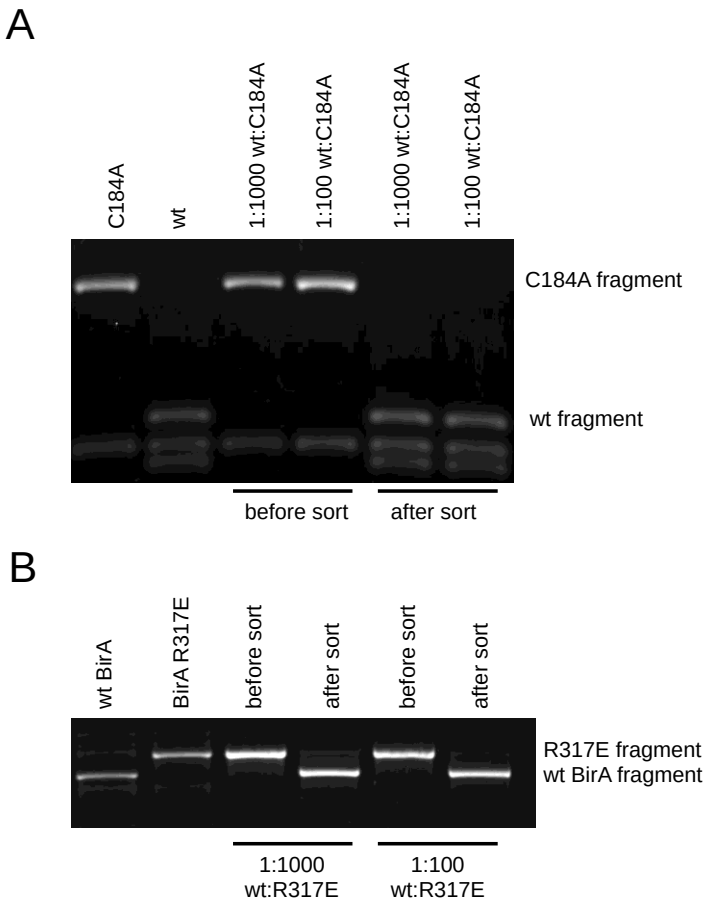

Figure 2-6 Additional model screening results.

(A) The indicated wt:C184A srtA-yeast mixtures were modified with GGGK-CoA, incubated with 50 μM biotin-LPETGG for 15 minutes, and sorted as described in Figure 2. Analysis of the gene compositions before and after sorting by *Hind*III digestions reveals an enrichment factor of ~3,500-15,500 after a single round of sorting. (B) Yeast simultaneously displaying the AviTag sequence and wild-type *E. coli* biotin ligase (BirA) or its less active R317E mutant[1] were mixed in 1:1000 and 1:100 BirA:R317E ratios. The mixtures were incubated with unmodified streptavidin to silence the biotinylation signal that arises from BirA-catalyzed biotinylation of the AviTag within the yeast secretory pathway during induction. The cells were treated with 1 μM biotin, 5 mM $MgCl_2$, and 0.2 mM ATP at room temperature for one hour. Following streptavidin-PE staining, the cells were subjected to FACS and the cells that exhibit the top 0.07% and 0.55% PE fluorescence intensities for the 1:1000 and 1:100 screens, respectively, were collected. Analysis of gene compositions before and after sorting by *Hind*III digestions reveals an enrichment factor of ~3,500-15,500 after one single round of sorting.

indicating substantial conjugation with GGGYK-biotin (Figure 2-4A). In contrast, wt srtA-yeast not conjugated to LPETGG, or LPETGG-conjugated yeast cells displaying the inactive C184A sortase mutant, exhibited only background levels of PE fluorescence after incubation with

GGGYK-biotin, confirming that biotinylation was dependent both on sortase activity and on the presence of both substrates (Figure 2-4A).

To verify that enzymes displayed on the yeast cell surface catalyze pseudo-intramolecular reactions with substrate molecules immobilized on the same cell, we performed one round of model screening on mixtures of wt srtA-yeast and srtA C184A-yeast. Yeast cells were mixed in 1:100 and 1:1000 ratios of wt:C184A sortases. Each mixture of cells was coupled with CoA-LPETGG using Sfp, then incubated with 50 μM GGGYK-biotin for 15 minutes. Because srtA binds weakly to GGG (K_m = 140 μM, Table 1), washing with non-biotinylated GGG was sufficient to remove any background signal and TEV digestion was not performed after the reaction. After fluorophore staining, cells exhibiting both AlexaFluor488 and PE fluorescence were isolated by FACS (Figure 2-4B) and amplified by culturing to saturation. The plasmid DNA encoding survivors was harvested, and the compositions of the recovered genes were analyzed by restriction digestion with *Hind*III following PCR amplification. The wt srtA gene is distinguishable from C184A by the presence of an additional *Hind*III site (Figure 2-4C). In both model FACS sort experiments, we observed ≥ 6,000-fold enrichment of the wild-type gene from both mixtures that were predominantly the inactive C184A mutant (Figure 2-4C). Similarly high enrichment factors were also observed in model sortase screens in which GGG-modified cells were reacted with biotinylated LPETGG peptide, and in model biotin ligase (BirA) screens in which cells displaying a biotinylation substrate peptide and wild-type BirA were enriched in the presence of a large excess of cells displaying a less active BirA mutant (Figure 2-6). These results collectively suggest that this system can strongly enrich yeast displaying active bond-forming enzymes from mixtures containing predominantly yeast displaying inactive or less active enzyme variants.

Directed Evolution of Sortase A Enzymes with Improved Catalytic Activity

Next we sought to evolve *S. aureus* srtA for improved activity using the enzyme evolution strategy validated above. We focused on improving the poor LPXTG substrate recognition of srtA (K_m = 7.6 mM, Table 1), which limits the usefulness of sortase-catalyzed bioconjugation by requiring the use of high concentrations of enzyme (> 30 μM) or long reaction times to compensate for poor reaction kinetics at the micromolar concentrations of LPXTG substrate that are typically used. To direct evolutionary pressure to improve LPXTG recognition, we formatted the screen such that the triglycine substrate is immobilized on the cell surface along with the enzyme library, and the biotinylated LPETG peptide is added exogenously. This

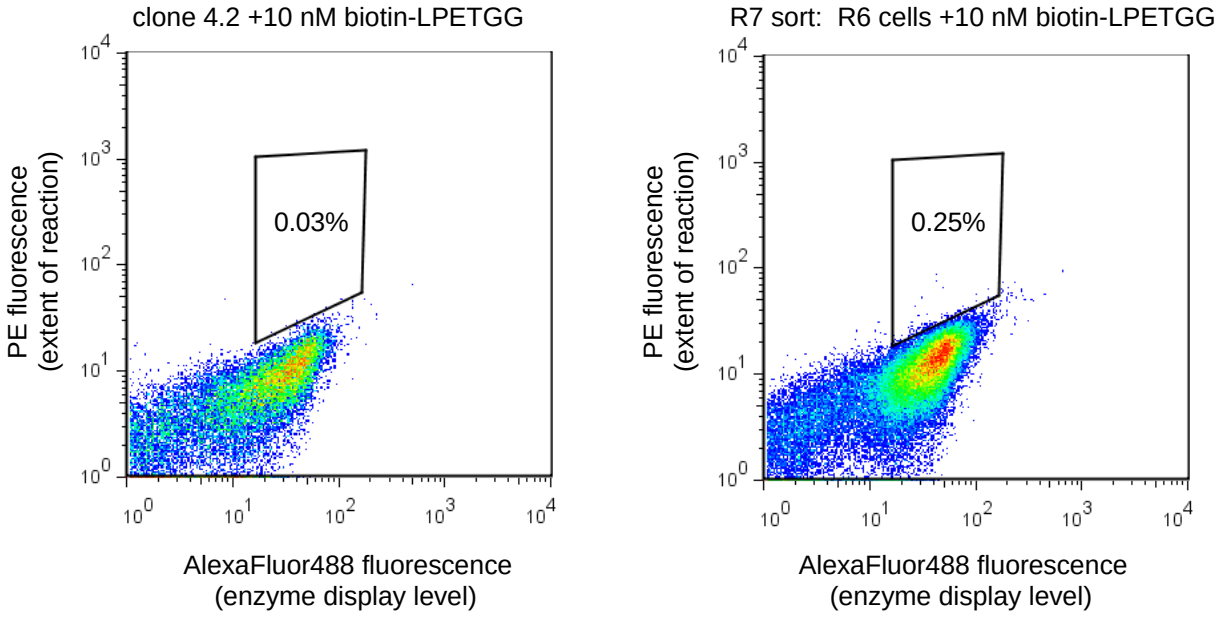

Figure 2-7 FACS enables precise definition of sort gates using parallel control samples

In this example, yeast cells displaying clone 4.2 were subjected to identical reaction conditions and FACS analysis protocols as the cells recovered after R6, enabling the creation of a sort gate (black polygon) that isolates mutants with higher specific activity than clone 4.2 in the R7 sort. The percentage of cells residing within the sort gate is shown.

format enables evolutionary pressure for improved LPETG recognition to be increased simply by lowering the concentration of LPETG peptide provided during the sortase-catalyzed bond-forming reaction.

	substrate A-CoA	biotin-substrate B, concentration	reaction time	cells sorted	cells recovered
R0 (diversity: $7.8x10^7$)					
R1	GGGK-CoA	Biotin-LPETGS, 100 μM	60 min	$6.0x10^8$	$8.5x10^6$
R2	GGGK-CoA	Biotin-LPETGG, 10 μM	60 min	$1.2x10^8$	$1.2x10^6$
R3	GGGK-CoA	Biotin-LPETGS, 1 μM	60 min	$2.5x10^7$	$1.3x10^5$
R4	GGGK-CoA	Biotin-LPETGG, 100 nM	15 min	$1.3x10^7$	$2.0x10^4$
R4Shuf (diversity: $6.9x10^7$)					
R5	GGGK-CoA	Biotin-LPETGG, 100 nM	45 min	$4.0x10^8$	$6.0x10^6$
R6	GGGK-CoA	Biotin-LPETGS, 100 nM	30 min	$1.2x10^8$	$4.7x10^5$
R7	GGGK-CoA	Biotin-LPETGG, 10 nM	15 min	$2.5x10^7$	$6.9x10^5$
R8	GGGK-CoA	Biotin-LPETGG, 10 nM	5 min	$1.0x10^7$	$2.0x10^4$
R9	CoA-LPETGG	GGGYK-biotin, 100 nM	5 min	$7.5x10^6$	$6.0x10^3$
R8mut (diversity: $5x10^7$)					
R9mut	CoA-LPETGG	GGGYK-biotin, 1 μM	15 min	$6.7x10^7$	$9.7x10^4$
R10mut	CoA-LPETGG	GGGYK-biotin, 100 nM	10 min	$1.25x10^7$	$2.8x10^4$

Figure 2-8 Reaction conditions and sorting parameters used to evolve sortase enzymes with improved catalytic activity.

We randomly mutated the wt *S. aureus* srtA gene using PCR with mutagenic dNTP analogs[25] and cloned the resulting genes into the modified yeast display vector using gap repair homologous recombination to yield a library of ~10^8 transformants (round 0, R0). Each library member contained an average of two non-silent mutations. The library was subjected to four rounds of enrichment for sortase activity without any additional diversification between rounds. In each round we subjected control samples— cells displaying wt srtA, or the cells isolated from the previous round— to identical reaction conditions and screening protocols to precisely define

FACS gates that captured cells with PE fluorescence corresponding to improved sortase activity (Figure 2-7). We applied increasing evolutionary pressure for improved LPETG recognition by decreasing the concentration of biotinylated LPETG substrate 10-fold with each successive round, starting from 100 μM in the first round and ending with 100 nM in the fourth round (Figure 2-8). We also increased evolutionary pressure for overall catalytic activity by accepting a smaller percentage of the most PE-fluorescent cells with each successive round, ranging from 1.4% in R1 to 0.15% in R4, and by shortening the reaction time in R4 from 60 to 15 minutes.

To preclude the evolution of specificity for a particular LPETG-containing sequence, we alternated using biotin-LPETGS (R1 and R3) and biotin-LPETGG (R2 and R4) peptides. After

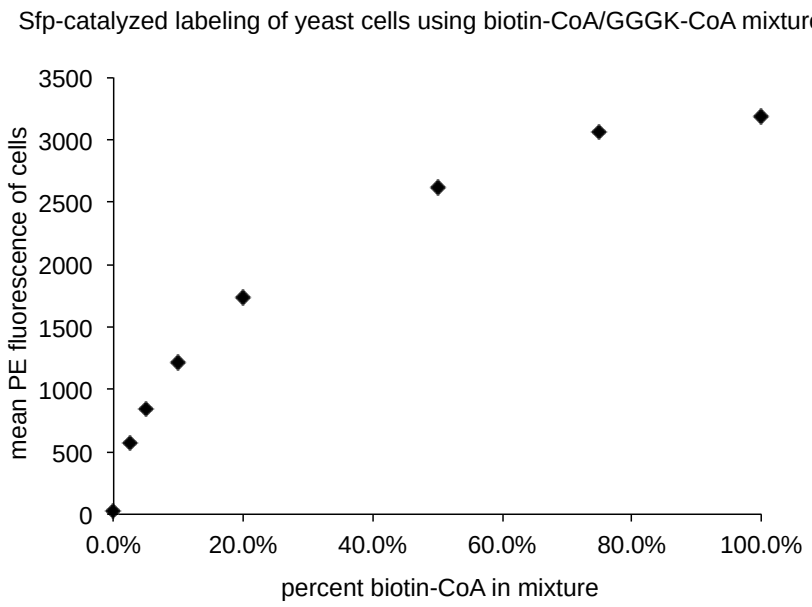

Figure 2-9

The relative amount of biotinylated CoA adduct in the supernatant is reflected by cell-surface fluorescence after Sfp-catalyzed conjugation to yeast cells and streptavidin-PE staining. Biotin-CoA was mixed with GGGK-CoA in various molar ratios. A suspension of ICY200 cells at a density of 2.5×10^7 cells/mL was incubated with 6 μM Sfp and 5 μM total concentration of CoA conjugate. The fluorescence of the cells after streptavidin staining was measured using flow cytometry.

the fourth round of enrichment, surviving genes were subjected to *in vitro* homologous recombination using the NExT procedure[26] and re-cloned into yeast to yield a recombined and diversified library of ~10^8 transformants. The shuffled library (R4Shuf) was subjected to four additional rounds of sorting (resulting in R5, R6, R7, and R8), with the concentration of biotinylated LPETG peptide dropping from 100 nM to 10 nM in the final round (Figure 2-8).

We developed an assay to rapidly compare the activity of yeast-displayed sortase mutants. Yeast ce lls were incubated with TEV protease to release the enzymes from the cell surface into the surrounding supernatant. The reaction in the supernatant was initiated by the addition of the two peptide substrates, CoA-LPETGG and GGGYK-biotin. After 30 minutes of reaction, Sfp was added to the same reaction mixture to attach the biotinylated adduct and unreacted CoA-LPETGG onto the cell surface. We verified that the level of cell-surface fluorescence after streptavidin-PE staining is a direct reflection of the relative amount of

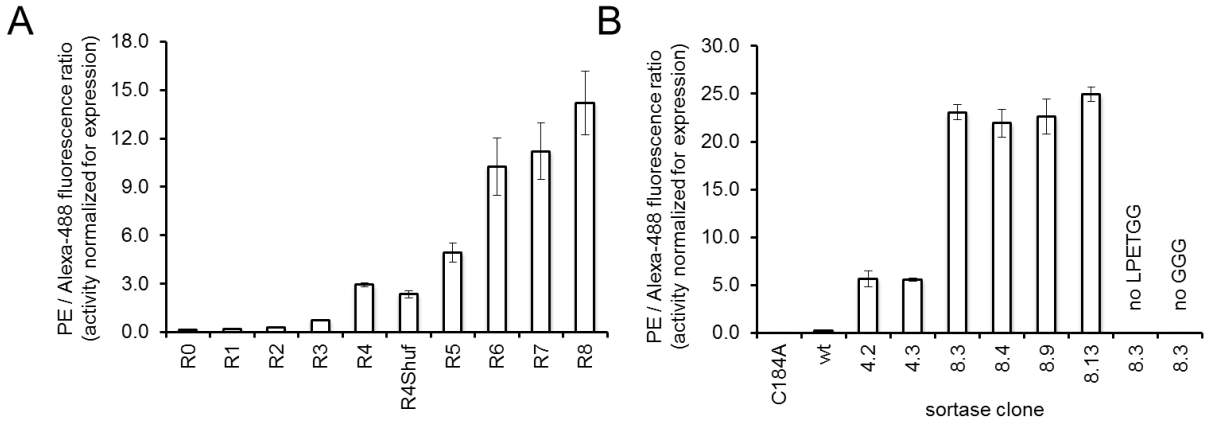

Figure 2-10. Activity assays of mutant sortases.

(A) Yeast pools recovered from the sorts were treated with TEV protease, and the cleaved enzymes were assayed for their ability to catalyze coupling between 5 μM CoA-LPETGG and 25 μM GGGYK-biotin. (B) Yeast cells expressing select individual clones were treated as described above. Error bars represent the standard deviation of three independent experiments.

biotinylated product in so lution (Figure 2-9).

We evaluated the mean activity of the yeast pools recovered after each round of sorting using this assay. Over the course of the selections, we observed a steady increase in the extent of product formation catalyzed by the recovered sortase mutants. By the last round (R8) the activity signal was ~130-fold greater than that of the initial, unselected library (R0), and ~40-fold greater than that of wt srtA (Figure 2-10A, B). These observations suggested that the system had evolved sortase variants with substantially improved activities.

Characterization of Evolved Sortase Mutants

We used the above assay to evaluate the activity of individual clones from R4 and R8 together with wt srtA and the inactive C184A mutant (Figure 2-10B). All tested mutants from R4

A

clone \ amino acid position	94	106	122	154	160	165	174	190	196
wt	P	E	F	K	D	D	G	K	K
4.2	P	E	F	K	N	D	G	E	T
4.3	S	E	F	K	D	A	G	K	K
8.3	S	E	F	K	N	A	S	K	T
8.4	S	E	F	K	N	A	G	E	T
8.9	S	E	F	R	N	A	G	K	T
8.13	S	G	Y	K	N	A	G	K	T

B

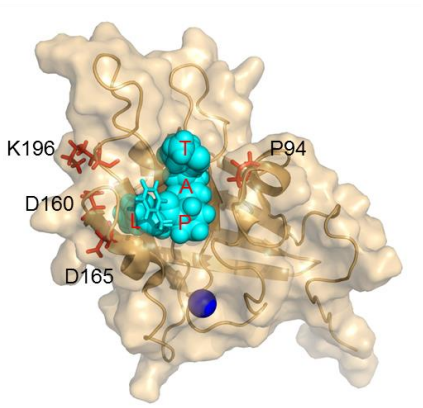

Figure 2-11. Mutations in evolved sortases.

(A) Highly enriched mutations are highlighted in black; other mutations are shown in blue. (B) Mapping evolved mutations on the solution structure of wild-type *S. aureus* sortase A covalently bound to its Cbz-LPAT substrate. The calcium ion is shown in blue, the LPAT peptide is colored cyan with red labels, and the side chains of amino acids that are mutated are in orange. The N-terminal Cbz group is shown in stick form in cyan.

exhibited improved activity relative to wild-type, with the two most active mutants, 4.2 and 4.3, showing ~20-fold more activity than wt srtA. Mutants isolated from R8 exhibited even greater gains in activity, including four mutants that were ≥ 100-fold more active than wild-type srtA under the assay conditions (Figure 2-10B).

Sequences of evol ved sortase genes revealed the predominance of P94S or P94R, D160N, D165A, and K196T m utations among R8 clones (Figure 2-11A). Of the 16 unique sequences

Table 2-1 Kinetic characterization of mutant sortases.

Kinetic parameters k_{cat} and K_m were obtained from fitting initial reaction rates at 22.5 °C to the Michaelis-Menten equation. Errors represent the standard deviation of three independent experiments.

	k_{cat} (s^{-1})	$K_{m\ LPETG}$ (mM)	$k_{cat}/K_{m\ LPETG}$ ($M^{-1}\ s^{-1}$)	$K_{m\ GGG\text{-}COOH}$ (μM)
wild-type	1.5 ± 0.2	7.6 ± 0.5	200 ± 30	140 ± 30
D160N/K190E/K196T (clone 4.2)	3.7 ± 0.6	1.6 ± 0.4	2400 ± 700	1200 ± 200
P94S/D165A (clone 4.3)	2.9 ± 0.0	1.1 ± 0.1	2600 ± 100	1700 ± 400
P94S/D160N/D165A/K196T	4.8 ± 0.8	0.17 ± 0.03	28,000 ± 7000	4800 ± 700
P94S/D160N/K196T	4.8 ± 0.6	0.56 ± 0.07	8600 ± 1500	1830 ± 330
P94S/D160N/D165A	3.8 ± 0.2	0.51 ± 0.38	7500 ± 300	1750 ± 250
P94R/D160N/D165A/K190E/K196T	5.4 ± 0.4	0.23 ± 0.02	23,000 ± 3000	2900 ± 200
P94S	1.6 ± 0.1	2.5 ± 0.6	600 ± 200	650 ± 150
D160N	2.3 ± 0.2	3.7 ± 0.5	600 ± 100	330 ± 20
D165A	2.4 ± 0.3	3.6 ± 1.0	700 ± 200	1000 ± 480
K196T	1.2 ± 0.1	3.3 ± 0.8	400 ± 100	200 ± 70

we isolated from R8, nine contained all four mutations. Thirteen of the 16 unique sequences contained at least three of the mutations, and all sequences contained at least two of the four mutations. All of these mutations also appeared in clones isolated from R4, but no clone from R4 contained more than two of the mutations, suggesting that recombination following R4 enabled combinations of mutations that persisted in rounds 4-8. Indeed, the highly enriched tetramutant combination appears to have arisen from recombination of two mutations each from clones 4.2 and 4.3, the two most active mutants isolated from R4. Gene shuffling was therefore an important component of th e evolutionary strategy to generate genes encoding the most active sortase enzymes tested.

None of these four mutations have been reported in previous mutational studies studying the sortase active site and the molecular basis of LPETG substrate recognition[27,28]. To gain insight into how these mutations improve catalysis, we expressed and purified each sortase single

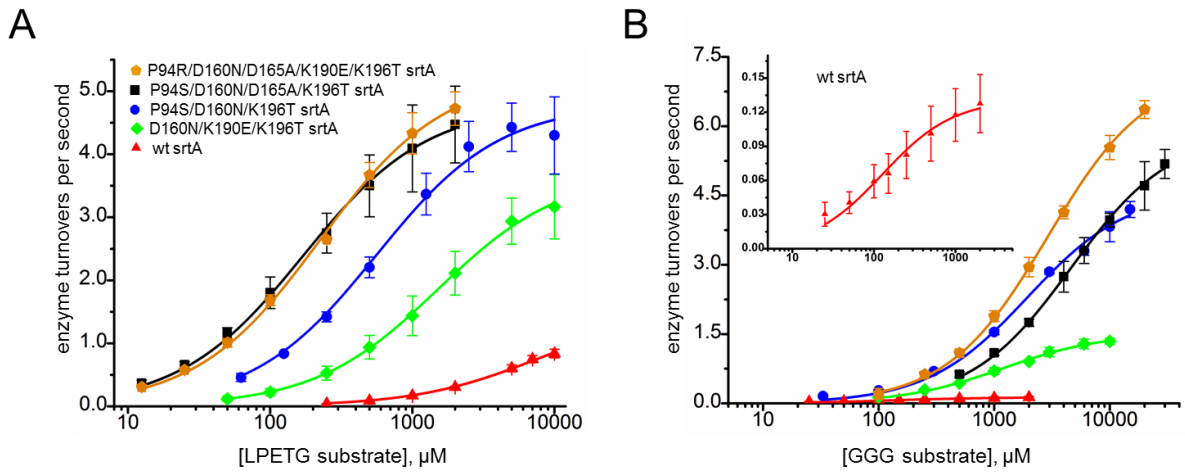

Figure 2-12 Comparison of the kinetic parameters of four evolved sortases.

(A) Plots of reaction velocity (turnovers per second) vs. LPETG peptide substrate concentration, with [GGG] fixed at 9 mM. (B) Plots of reaction velocity vs. GGG concentration, with [LPETG peptide] fixed at 1 mM. Due to its poor kinetics under the assay conditions, the plot for wt srtA is shown in the inset.

mutant, clones 4.2 and 4.3, and the tetramutant from *E. coli*, and we measured the saturation kinetics of wt srtA and the mutants using an established HPLC as say[29]. The observed kinetic parameters for the wild-type enzyme closely match those previously reported[27,29]. Each single mutation in is olation contributed a small beneficial effect on turnover (k_{cat}) and more significant beneficial effects on LPETG substrate recognition, lowering the $K_{m\ LPETG}$ up to three-fold (Table 2-1). The effects of the mutations in combination were largely additive. Compared to wild-type, 4.2 and 4.3 exhibited a 2.0-2.6 -fold improvement in k_{cat} and a 5-7-fold reduction in $K_{m\ LPETG}$, resulting in a ~15-fold enhancement in catalytic efficiency at using the LPETG substrate (Table 2-1). Combining all four mutations yielded a sortase enzyme with a 140-fold improvement in its ability to convert LPETG ($k_{cat}/K_{m\ LPETG}$). This large gain in catalytic efficiency is achieved primarily through 45-fold improved LPETG recognition accompanied by a 3-fold gain in k_{cat} (Table 2-1, Figure 2-12).

The effects of the individual mutations on LPETG substrate recognition can be rationalized in light of the rep orted solution structure of wt *S. aureus* srtA covalently bound to an LPAT peptide substrate[30]. The mutated residues are all located at the surface of the enzyme, near the LPAT-binding groove (Figure 2-11B). P94 lies at the N-terminus of helix 1, and K196 lies at the C-terminus of the β7/β8 loop. Both D160 and D165 lie in the region connecting β6 and β7 that participates in LPETG substrate binding. D165 lies at the N-terminus of a 3_{10} helix that is formed only upon LPAT binding and makes contacts with the leucine residue of LPAT. The localization of the mutations within loops that line the LPAT binding groove suggests that they may be improving binding by altering the conformation of these important loops.

The evolved sortase mutants exhibit decreased GGG substrate binding (Table 2-1, Figure 2-12). Compared to wild-type, we measured a 30-fold increase in $K_{m\ GGG}$ for the sortase A

tetramutant. P94S and D 165A had larger detrimental effects on $K_{m\ GGG}$ than D160N and K196T. These results are consistent with mapping of the GGG-binding region proposed by NMR amide backbone chemical shift data. The chemical shifts of the visible amide hydrogen resonances for residues 92-97 and 165 were among the most perturbed upon binding of a Gly_3 peptide[30]. Due to the absence of a high-resolution structure of the srtA- Gly_3 complex at this time, it is difficult to rationalize in more detail the basis of altered $K_{m\ GGG}$ among evolved mutants.

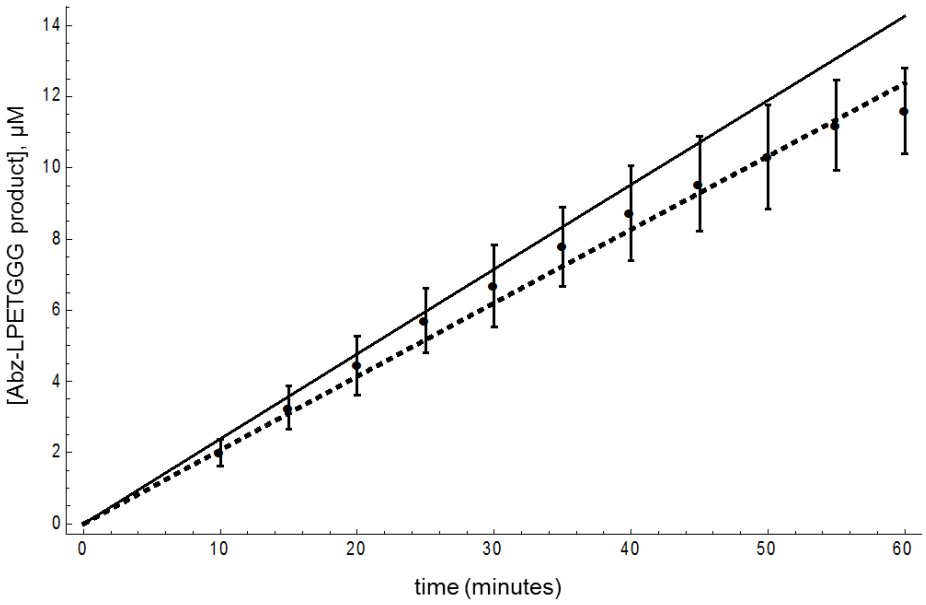

Figure 2-13 Time course of turnovers by the evolved P94R/D160N/D165A/K190E/K196T sortase.

P94R/D160N/D165A/K190E/K196T srtA (914 pM) was incubated with 9 mM GGG and 1 mM Abz-LPETGK(Dnp) substrate in 500 µL of reaction buffer. At 5-minute intervals, 40-µL aliquots were removed, quenched, and analyzed by HPLC as described in the Supporting Information. Each µM of product generated over the course of this experiment corresponds to approximately 1,092 turnover events. Averaged data and standard deviation from triplicate experiments are shown as open squares and bars, respectively. Fit lines were generated by Mathematica according to the integrated Michaelis Menten equation, [Product] = $[Substrate]_0$ - K_m ProductLog[Exp[($[Substrate]_0$ – k_{cat}*time*[Enzyme])/K_m] * $[Substrate]_0/K_m$], where $[Substrate]_0$ = 1 mM and [Enzyme]=914 pM. The expected product concentration from previously determined kinetic parameters is shown (black line) while a fit line to the data is shown (dashed). These data show an r^2 correlation of 0.983 with kinetic parameters k_{cat} = 4.7 ± 0.6 s^{-1} and $K_{m\ LPETG}$ = 245 ± 5 µM, compared with the parameters of k_{cat} = 5.4 ± 0.4 s^{-1} and $K_{m\ LPETG}$ = 230 ± 20 µM determined by endpoint analysis (Table 1, Figures S11, S12). The difference in observed k_{cat} is not statistically significant by Students' t test to p>0.95.

To recover some of the ability to bind the GGG substrate, we reverted A165 of the tetramutant back to the original aspartic acid residue found in wild-type because our results indicated that the D165A mutation was most detrimental for GGG recognition. Compared to the tetramutant, this P94S/D160N/K196T triple mutant exhibited a 2.6-fold improvement in $K_{m\ GGG}$, accompanied by a three-fold increase in $K_{m\ LPETG}$ and no change in k_{cat} (Table 2-1, Figure 2-12). We also subjected the R8 yeast pool to one additional round of screening (R9), immobilizing LPETGG on the cell surface before reaction with 100 nM GGGYK-biotin. The P94S/D160N/K196T reversion mutant was recovered in two out of the 24 sequenced clones from R9, but a different triple mutant (P94S/D160N/D165A) dominated the R9 population after screening, representing 14/24 sequenced clones. Compared to the tetramutant, the $K_{m\ GGG}$ of this mutant improved by 2.7-fold, whereas the k_{cat} and $K_{M\ LPETG}$ were not altered by more than a factor of 3-fold (Table 2-1).

We also performed muta genesis and enrichment to identify additional mutations that improve GGG recognition in the tetramutant context. We combined four R8 clones as templates for additional diversification by PCR, and subjected the resulting yeast library (R8mut) to two rounds of screening, immobilizing LPETGG on the cell surface before reaction with 100-1000 nM GGGYK-biotin. After two rounds of enrichment, the K190E mutation originally observed in clone 4.2 was found in 56% of the unique sequenced clones in R10mut, and 33% of the clones possessed P94R in place of P94S. The other three mutations of the tetramutant motif were found intact in 89% of the unique R10mut clones. We constructed the P94R/D160N/D165A/K190E/K196T pentamutant and assayed its activity. Compared to the tetramutant, the $K_{m\ GGG}$ of this mutant improved by 1.8-fold, whereas the k_{cat} and $K_{M\ LPETG}$ were not altered by more than a factor of 1.3-fold. Compared with wt srtA, this pentamutant has a 120-

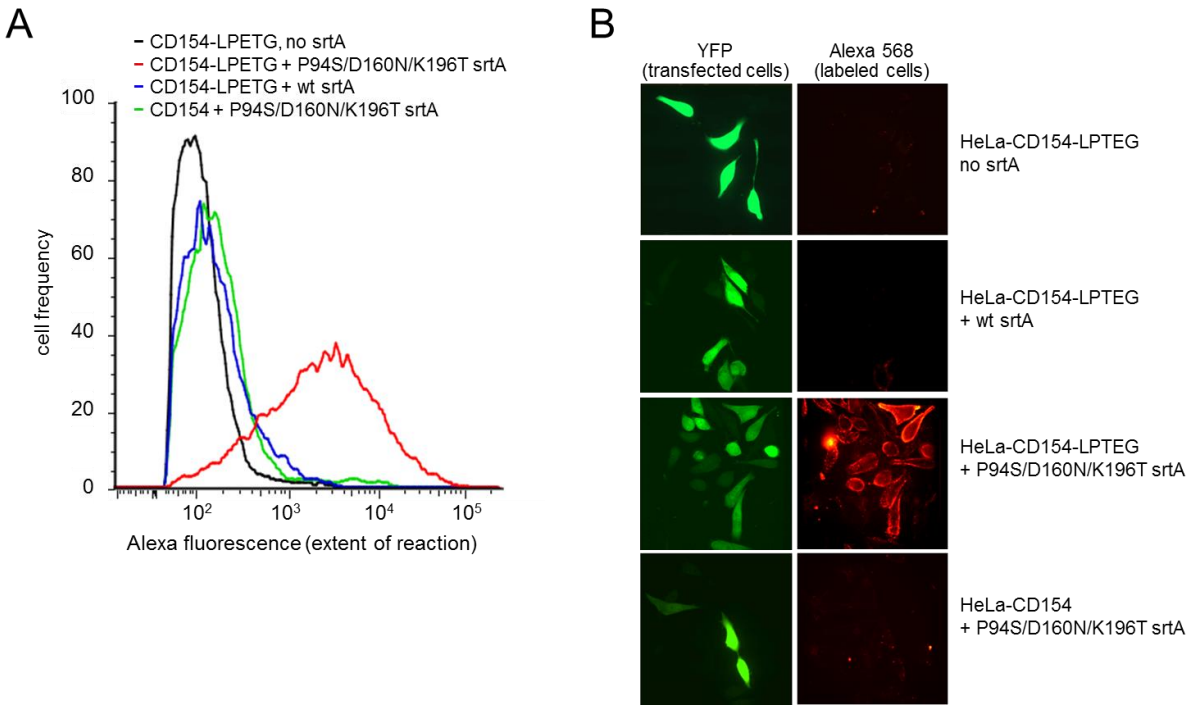

Figure 2-14 Cell-surface labeling with wild-type and mutant sortases.

Live HeLa cells expressing human CD154 conjugated at its extracellular C-terminus to LPETG were incubated with 1 mM GGGYK-biotin and no sortase A (srtA), 100 μM wild-type srtA, or 100 μM P94S/D160N/K196T srtA. The cells were stained with AlexaFluor-conjugated streptavidin. (A) Flow cytometry analysis comparing cell labeling with wild-type sortase (blue) and the mutant sortase (red). Negative control reactions omitting sortase (black) or LPETG (green) are shown. (B) Live-cell confocal fluorescence microscopy images of cells. The YFP (transfection marker) and Alexa (cell labeling) channels are shown.

fold higher $k_{cat}/K_{m\ LPETG}$ an d a 20-fold higher $K_{m\ GGG}$ (Table 2-1, Figure 2-12). To validate our enzyme kinetics measurements, we followed product formation over one hour and observed turnover numbers of greater than 10,000 per hour. The resulting data (Figure 2-13) yielded k_{cat} and $K_{M\ LPETG}$ values that closely agr ee with our kinetics measurements (Table 2-1). Collectively, these results indicate that relatives of the evolved tetramutant can exhibit partially restored GGG binding and therefore provide alternative enzymes for applications in which the GGG-linked substrate is available only in limited quantities.

Cell-Surface Labeling With an Evolved Sortase

The improved activities of the evolved sortase enzymes may enhance their utility in bioconjugation applicati ons such as the site-specific labeling of LPETG-tagged proteins expressed on the surface of living cells. In these a pplications, the effective concentration of the LPETG peptide is typically limit ed to micromolar or lower levels by endogenous expression levels, and therefore the high $K_{M\ LPETG}$ of wt srtA ($K_{M\ LPETG}$ = 7.6 mM, Table 1) necessitates the use of a large excess of coupling partner and enzyme to drive the reaction to a reasonable yield. As it is typically straightforward to synthesize milligram quantities of short oligoglycine-linked probes using solid-phase peptide chemistry, we hypothesized that the much higher $k_{cat}/K_{m\ LPETG}$

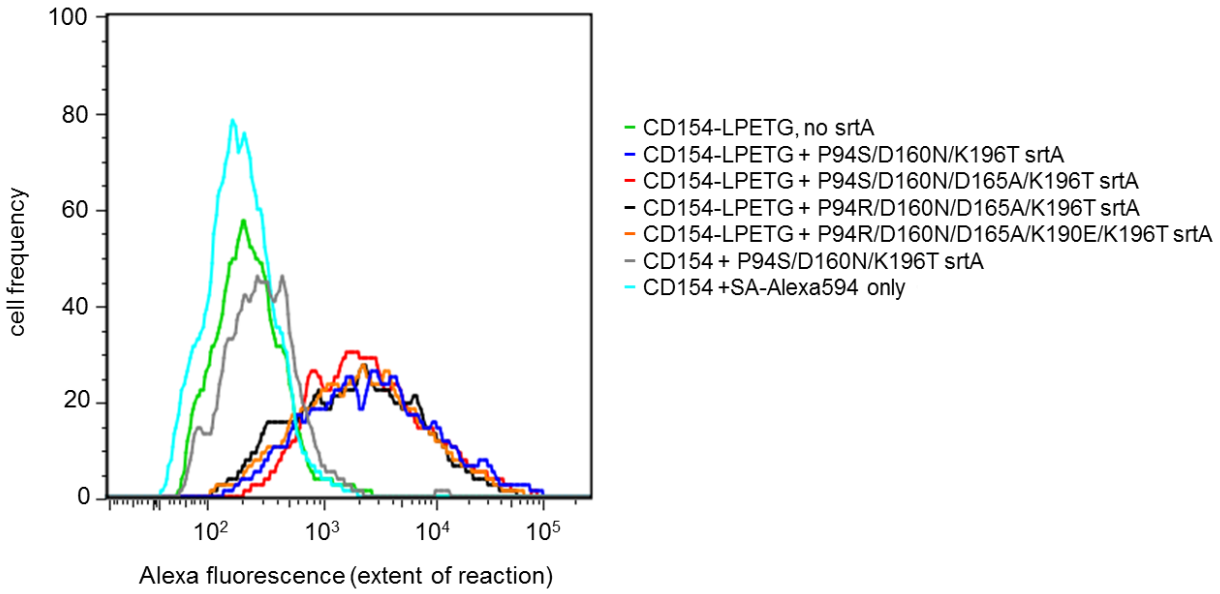

Figure 2-15 Cell-surface labeling with four evolved sortases.

Live HeLa cells expressing human CD154 conjugated at its extracellular C-terminus to LPETG were incubated with 0.5 mM GGGYK-biotin and no sortase A (no srtA) or 100 µM of the mutant sortase A shown in the legend. The cells were stained with AlexaFluor594-conjugated streptavidin (SA-Alexa594) before flow cytometry analysis. Negative control reactions omitting sortase (green) or LPETG (gray) are shown. Untreated cells stained with SA-594 (cyan) are also shown.

of the evolved sortase enzymes might enable them to mediate cell-surfacing reactions that would be inefficient using the wild-type enzyme.

We expressed human CD154 tagged with the LPETG sequence at its C-terminus on the surface of HeLa cells an d compared the labeling of the live cells with GGGYK-biotin using wt srtA and the evolved P94S/D160N/K196T mutant. After staining with a streptavidin-AlexaFluor594 conjugate, flow cytometry analysis revealed that the evolved sortase yielded ≥ 30-fold higher median fluorescence than the wild-type enzyme (Figure 2-14A). Although we used condition s similar to those used to label HEK293 cells using wt srtA for fluorescence microscopy[5], over four independent replicates, the wild-type enzyme did not result in fluorescence more than 2.8-fold higher than the background fluorescence of cells incubated in the absence of enzyme (Figure 2-14A). Consistent with the flow cytometry data, live-cell fluorescence microscopy confirmed very weak labeling by wt srtA and much more efficient labeling by the evolved sortase mutant (Figure 2-14B). Cells expressing CD154 without the LPETG tag were not labeled to a significant extent by the evolved sortase, indicating that the site-specificity of the enzyme has not been significantly compromised. Under the conditions tested, the evolved sortase triple, tetra-, and pentamutants all exhibit comparable and efficient cell-surface labeling, despite their differences in $K_{m\ GGG}$ (Figure 2-15). Collectively, our results suggest that the sortase variants evolved using the enzyme evolution system developed in this work are substantially more effective than the wild-type enzyme at labeling LPETG-tagged proteins on the surface of live mammalian cells.

Discussion

We integrated yeast display, Sfp-catalyzed bioconjugation, and cell sorting into a general directed evolution strategy for enzymes that catalyze bond-forming reactions. We validated the system through model selections enriching for *S. aureus* sortase A-catalyzed transpeptidation activity, attaining enrichment factors greater than 6,000 after a single round of sorting. We applied this system to evolve sortase A for improved catalytic activity. After eight rounds of sorting with one intermediate gene shuffling step, we isolated variants of sortase A that contained four mutations that together resulted in a 140-fold increase in LPETG-coupling activity compared with the wild-type enzyme. An evolved sortase enabled much more efficient labeling of LPETG-tagged human CD154 expressed on the surface of HeLa cells compared with wild-type sortase.

The kinetic properties of the mutant sortases accurately reflect our screening strategy. The 50-fold decrease in $K_{m\ LPETG}$ of the tetramutant compared to wild-type is consistent with lowering the concentration of free biotinylated LPETG peptide during the reaction in successive rounds. Meanwhile, this screening format ensured that a high effective molarity of GGG was presented to each enzyme candidate over eight rounds of enrichment, which we estimated to be ~950 μM (Figure 2-16). It is therefore unsurprising that GGG recognition among evolved sortases drifted during evolution. Likewise, the three-fold increase in k_{cat} of the tetramutant compared to that of the wild-type enzyme may have resulted from screening pressures arising from shortening the reaction time in later rounds. Larger increases in k_{cat} may require modified selection or screening strategies that explicitly couple survival with multiple turnover kinetics, perhaps by integrating our system with *in vitro* compartmentalization.

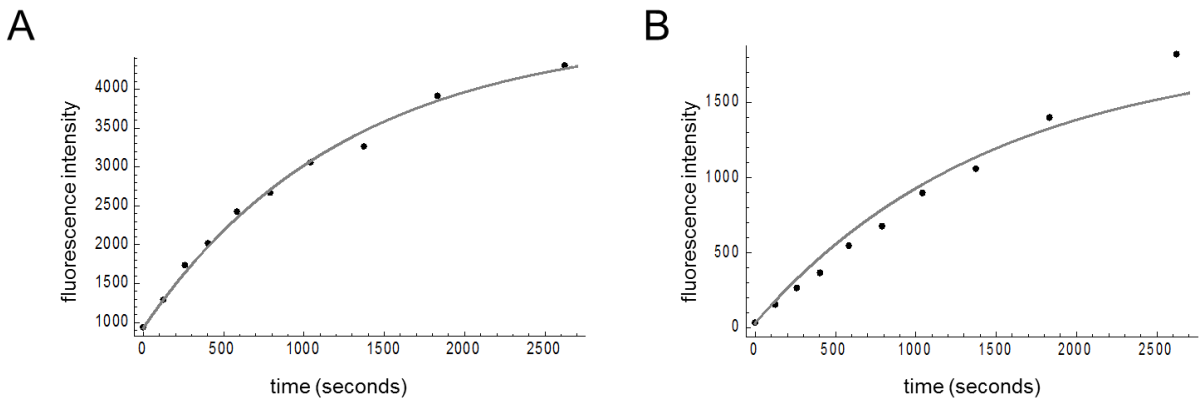

Figure 2-16 Cell-surface reaction time courses to estimate substrate effective molarity.

Yeast displaying clones 4.2 and 4.3 were first labeled with GGGK-CoA and then reacted with 1 μM biotin-LPETGG as described. Representative reaction progress curves for clone 4.2 (A) and 4.3 (B). The data was fit according to the equation described in the Supporting Information. In this case, the 4.2 data show an r^2 correlation of 0.999 with a cell surface GGG effective molarity estimate of 1.007 mM and a theta estimate of 156 s, while the 4.3 data show an r^2 correlation of 0.982 with a GGG effective molarity estimate of 0.967 mM and a theta estimate of 0 s .

Despite the widespread use of yeast display in the evolution of binding interactions[19], to the best of our knowledge, sortase A is only the third enzyme to be evolved using yeast display, in addition to horseradish peroxidase[31,32] and an esterase catalytic antibody[33]. Our results highlight the attractive features of yeast display that offer significant advantages for enzyme evolution, including quality control mechanisms within the secretory pathway that ensure display of properly folded proteins and compatibility with FACS[19]. For these reasons, we used yeast as the vehicle for display instead of an M13 phage simultaneously displaying an Sfp peptide substrate and an enzyme library[34]. As the method developed here does not rely on any particular screenable or selectable property of the substrates or product, it is in principle compatible with any bond-forming enzyme that can be expressed in yeast, including glycosylated proteins that are likely incompatible with phage and mRNA display, provided that linkage of the substrates to CoA and to the affinity handle is possible and tolerated by the enzyme or its evolved variants. In

cases in which the enzyme accepts only one of these modifications, product-specific antibodies in principle could be used to detect bond formation. Furthermore, we note that integrating our yeast display system with the multicolor capabilities of FACS should enable the evolution of enzyme substrate specificity.

Beyond improving existing activities of natural proteins for research, industrial, and medicinal use, we speculate that the enzyme evolution strategy presented here will be valuable in the engineering of artificial proteins with new, tailor-made catalytic activities. The reactions catalyzed by natural enzymes are only a small subset of the diverse array of reactions known in organic chemistry, and a promising route to generating artificial enzymes is the computational design of a protein catalyst with arbitrary activity followed by optimization of its catalytic activity through directed evolution. Indeed, recent advances in computational protein design have created *de novo* catalysts for the retroaldol[35], Kemp elimination[36], and Diels-Alder reactions[37], and these successes demonstrate the feasibility of designing weakly active proteins that are ideal starting points for directed evolution. The integration of computational design and a general enzyme evolution scheme such as the one presented here represents a promising strategy for creating highly active proteins with tailor-made catalytic activities.

Materials and Methods

Sortase evolution. A library of 7.8×10^7 mutant sortase genes containing an average of 2.0 amino acid changes per gene was introduced into yeast cells using gap repair homologous recombination (see the Supporting Information for details on library construction). In Round 1, 6×10^8 sortase library-expressing cells were conjugated to GGGK-CoA, incubated with 100 μM

biotin-LPETGS for 60 minutes, and stained with streptavidin-PE and an AlexaFluor488-conjugated anti-HA antibody (Invitrogen). The top 1.4% of the PE/AlexaFluor488 double-positive population were isolated and grown to saturation. At least a ten-fold excess of cells relative to the number of cells recovered from sorting were removed, pelleted, and induced to display enzymes at the cell surface with galactose before entering the subsequent round of sorting. See Figure S6 for details on screening stringency. Following round 4, the surviving sortase genes were amplified by PCR and shuffled using the NeXT method[26] (see Supporting Information for details). The diversified gene library was introduced into yeast to generate a library of 6.9×10^7 transformants (see Supporting Information for details). Four additional rounds of enrichment were performed with GGG immobilized on the surface and biotinylated LPETG peptide provided exogenously. For rounds 9, 9mut, and 10mut, the cells from the previous round were modified with CoA-LPETGG in TBS-B with 5 mM $MgCl_2$ and 5 mM $CaCl_2$ for 30 minutes to facilitate formation of the acyl-enzyme intermediate, before washing and initiating the reaction with 0.1-1.0 μM GGGYK-biotin.

Mammalian cell labeling. HeLa cells were cultured at 37 °C in DMEM supplemented with 10% fetal bovine serum and 1% penicillin-streptomycin under an atmosphere containing 5% CO_2. The cells were transfected with a 9:1 ratio of plasmid pCDNA3-CD154-LPETG:cytoplasmic YFP expression plasmid (as a transfection marker). After 24 hours, the transfected cells were trypsinized, re-plated onto glass coverslips, and incubated overnight at 37 °C. Each coverslip was washed twice with Hank's balanced salt solution (HBSS) and immersed into HBSS supplemented with 1 mM GGGYK-biotin, 5 mM $CaCl_2$, and 100 μM enzyme. After 5 to 10 minutes, the coverslips were washed twice with PBS supplemented with 1% bovine serum

albumin (BSA), 1 mM unmodified GGG, and 5 mM $MgSO_4$ before immersion into a solution of streptavidin-AlexaFluor594 (1:200, Invitrogen) in PBS with 1% BSA and 5 mM $MgSO_4$. For flow cytometry analysis, the coverslips were washed twice with PBS before incubation in PBS on ice for 30 minutes. Cells were resuspended and analyzed using a BD Fortessa flow cytometer. The AlexaFluor594 fluorescence of the top 16-25% most YFP-positive cells was recorded. For imaging, the coverslips were washed twice with PBS containing 5 mM $MgSO_4$ before analysis on a Perkin Elmer spinning disk confocal microscope (Harvard Center for Biological Imaging). Images were recorded using the DIC, YFP, and Alexa channels.

Methods for Sortase Reactions on Yeast Cells and Model Screens.

Sortase Reactions on Yeast with Biotinylated GGG Peptide. S*accharomyces cerevisiae* cells displaying *Staphylococcus aureus* sortase A and the S6 peptide (see below for details on induction of yeast display) were resuspended to a cell density of 2.5×10^8 cells/mL in Tris-buffered saline (pH 7.5) with 1 mg/mL bovine serum albumin (TBS-B) and 5 mM $MgCl_2$ and incubated with 6 μM Sfp and 5 μM CoA-LPETGG (see below for synthesis details) for 15 minutes. Cells were pelleted and washed with TBS-B before resuspension to a cell density of 3×10^6 to 1×10^7 cells/mL in TBS-B with 5 mM $CaCl_2$ and 10 nM to 100 μM GGGYK-biotin peptide. After 15 to 60 minutes, the reactions were stopped by pelleting the cells and washing with ice-cold phosphate-buffered saline with 1 mg/mL bovine serum albumin (PBS-B). The cells were washed with ice-cold PBS-B containing 500 μM AAEK2 (Astatech), an inhibitor of sortase enzymes[38], and 100 μM unmodified GGG (Sigma) before incubation with streptavidin-phycoerythrin (streptavidin-PE) (Fluka) and AlexaFluor488-conjugated anti-hemagglutinin antibody (Invitrogen) to detect the extent of the sortase-catalyzed reaction and the enzyme

display level, respectively. Cells were washed once more with PBS-B before flow cytometry analysis or FACS.

Sortase Reactions on Yeast with Biotinylated LPETG Peptide. Yeast cells were conjugated to GGGK-CoA (see below for synthesis details) and reacted with the biotinylated LPETG peptide as described above. After stopping the reaction by centrifuging and washing, the cells were resuspended in TBS-B containing 5 μM TEV S219V protease[39] and incubated for 15-30 minutes to remove the background signal from the formation of any covalent acyl biotin-LPETG-enzyme intermediate. After washing with cold PBS-B, the cells were stained with fluorophore-conjugated proteins as described above.

Model Screens. Yeast displaying wild-type sortase or the inactive C184A mutant were mixed in ratios of 1:1000 and 1:100 wt:C184A and treated as described above. After incubation with fluorophore-conjugated proteins, 10^7 cells from each mixture were sorted in a MoFlo cell sorter (DakoCytomation). The top 0.06% and top 0.7% of the PE/AlexaFluor488 double positive population for the 1:1000 and 1:100 experiments, respectively, were collected. Collected cells were cultured until saturation in growth media (see below) with 50 μg/mL carbenicillin, 25 μg/mL kanamycin, and 50 μg/mL streptomycin. Plasmid DNA was harvested using the Zymoprep kit (Zymo Research), and the recovered sortase genes were amplified using the primers 5'-CCCATAAACACACAGTATGTT and 5'-AATTGAAATATGGCAGGCAGC and digested with *Hin*dIII to determine the relative recovery of wild-type and C184A genes.

Sortase Assay Methods.

Flow Cytometry Activity Assay For Yeast Pools or Individual Yeast Clones. A total of 1.25×10^7 yeast cells were resuspended in 50 μL of TBS-B containing 5 μM TEV S219V

protease, 5 mM $MgCl_2$, and 5 mM $CaCl_2$. After incubation for 30 minutes at room temperature, the CoA-LPETGG and GGGYK-biotin peptides were added to the cell suspension to final concentrations of 5 μM and 25 μM, respectively. The cells were incubated at room temperature for an additional 30 minutes before Sfp was added to a final concentration of 6 μM. The cells were incubated at room temperature for 7 minutes, pelleted by centrifugation, and washed with ice-cold PBS-B. The cells were stained with fluorophore-conjugated proteins as described above, washed, and analyzed by flow cytometry.

In Vitro *Sortase Kinetics Assays.* See below for details on sortase expression and purification, and on the synthesis of Abz-LPETGK(Dnp)-$CONH_2$. Assays to determine k_{cat} and $K_{m\ LPETG}$ were performed in 300 mM Tris pH 7.5, 150 mM NaCl, 5 mM $CaCl_2$, 5% v/v DMSO, and 9 mM Gly-Gly-Gly-COOH (GGG). The concentration of the LPETG peptide substrate ranged from 12.5 μM to 10 mM, and enzyme concentrations ranged from 25 nM to 1000 nM. Assays for determination of $K_{m\ GGG}$ were performed under the same conditions, except the LPETG peptide concentration was fixed at 1 mM, the enzyme concentration was fixed at 41.5 nM, and the concentration of GGG was varied from 33 μM to 30 mM, depending on the enzyme. Reactions were initiated with the addition of enzyme and incubated at 22.5 °C for 3 to 20 minutes before quenching with 0.5 volumes of 1 M HCl. Five to ten nmol of peptide from the quenched reactions were injected onto an analytical reverse-phase Eclipse XDB-C18 HPLC column (4.6×150 mm, 5 μm, Agilent Technologies) and chromatographed using a gradient of 10 to 65% acetonitrile with 0.1% TFA in 0.1% aqueous TFA over 13 minutes. Retention times under these conditions for the Abz-LPETGK(Dnp)-$CONH_2$ substrate, the released GKDnp peptide, and the Abz-LPETGGG-COOH product were 12.8, 10.4, and 9.1 min, respectively. To

calculate the percent conversion, the ratio of the integrated areas of the Abz-LPETGGG-COOH and Abz-LPETGK(Dnp)-$CONH_2$ peptide Abs_{220} peaks was compared to a standard curve generated by mixing the product and starting peptide in known ratios. To determine k_{cat} and K_m, reaction rates were fit to the Michaelis-Menten equation using OriginPro 7.0 software. All kinetics values reported represent the average of at least three measurements.

Substrate Synthesis Methods.

Biotin-LC-LELPETGG-$CONH_2$, Fmoc-GGGK-$CONH_2$, and NH_2-YLELPETGG-$CONH_2$ were purchased from Genscript and used without further purification. NH_2-GGGYK(biotin)-$CONH_2$ was purchased from Genscript and purified using reverse-phase HPLC on a C18 column. Biotin-LC-YGLPETGS-$CONH_2$ was purchased from New England Peptide and used without further purification.

Synthesis of GGGK-CoA. Fmoc-GGGK-$CONH_2$ was dissolved in DMSO to a final concentration of 100 mM, and 1.5 equivalents of sulfo-SMCC (Thermo-Fisher) and 2 equivalents of DIPEA (Sigma) in DMSO were added. The reaction was incubated for 1 hr at room temperature, then added to 1.5 equivalents of coenzyme A trilithium hydrate (Sigma) in DMSO to a final peptide concentration of 25 mM and mixed at room temperature overnight. If appropriate, the Fmoc protecting group was removed with 20% vol/vol piperidine and incubation for 20 minutes. The reaction was quenched by the addition of 1 equivalent of TFA, and the product was purified on a preparative Kromasil 100-5-C18 column (21.2×250 mm, Peeke Scientific) by reverse phase HPLC (flow rate: 9.5 mL/min; gradient: 10% to 70% acetonitrile with 0.1% TFA in 0.1% aqueous TFA gradient over 30 minutes; retention time: 17.1 minutes). ESI-MS (found): $[M-H]^-$ *m/z* = 1300.1. Calculated for $C_{45}H_{72}N_{14}O_{23}P_3S^-$: *m/z* = 1301.4. The

concentration of GGGK-CoA peptide was determined from the measured A_{259} using the known molar extinction coefficient of coenzyme A, 15,000 M^{-1} cm^{-1} [40].

Synthesis of CoA-LPETGG. NH_2-YLELPETGG-$CONH_2$ (0.0084 mmol) was incubated with sulfo-SMCC (0.021 mmol, 2.5 eq.) in 142 μL of DMSO and 3 μL DIPEA (0.017 mmol, 2.0 equivalents) for 2 hours at room temperature. The maleimide adduct was purified using reverse-phase HPLC on a preparative C18 column (flow rate: 9.5 mL/min; gradient: 10% to 60% acetonitrile with 0.1% TFA in 0.1% aqueous TFA over 30 minutes; retention time: 22.0 minutes). After lyophilization of the collected peak, the white solid was dissolved in 0.1 M phosphate buffer pH 7.0 with 45% acetonitrile. Coenzyme A trilithium hydrate (11.2 mg) was added, and the reaction was incubated at one hour at room temperature. The desired product was obtained after purification on a C18 column (flow rate: 9.5 mL/min flow rate; 0% to 50% acetonitrile in 0.1 M triethylammonium acetate over 30 minutes; retention time: 21.9 minutes). ESI-MS (found): $[M-H]^-$ *m/z* = 1961.8. Calculated for $C_{77}H_{116}N_{18}O_{34}P_3S^-$: *m/z* =1961.7. The concentration of CoA-LPETGG peptide was determined as described above for GGGK-CoA.

Abz-LPETGK(Dnp)-$CONH_2$ Substrate for HPLC Assays. This compound was synthesized at 200 μmol scale using an Applied Biosystems 433A peptide synthesizer. 200 μmol-equivalents of NovaPEG Rink Amide resin (EMD biosciences) were loaded onto the machine and coupled using 5 equivalents of each Fmoc-protected amino acid building block with standard acid labile side-chain protecting groups (Thr(OtBu), Glu(OtBu)) and using Fmoc Lysine(Dnp) (Chem-Impex). Terminal coupling with Boc 2-Aminobenzoic Acid (Chem-Impex) yielded the fully protected peptide, which was cleaved by three 1-hour treatments with 20 mL of 95% TFA + 2.5% water + 2.5% triisopropylsilane (Sigma). The cleavage mixtures were pooled and concentrated by rotary evaporation, and the peptide was precipitated by the addition of 9

volumes of ice-cold diethyl ether. The samples were purified by reverse phase HPLC as described above for GGGK-CoA (retention time: 28 minutes), pooled and concentrated by lyophilization. The concentration of the peptide was determined by the known molar extinction coefficient of the Dnp group, ε_{355nm} = 17,400 M^{-1} cm^{-1} [41].

Cloning Methods Including Library Generation.

Primers Used in the Procedures Below

prime	sequence
1F	5’-
1R	5’-CAGAAATAAGCTTTTGTTCGGATCCTTTGACTTCTGTAGCTACAAAG
2F	5’-CCCATAAACACACAGTATGTT
2R	5’-ACCTTGAAAGTACAAGTTCTCAGATCCTGCATAGTCTGGAACGTCGT
3F	5’-AAAGATAAACAATTAACATTAATTACTGCTGATGATTACAATGAA
3R	5’-ATCTCGAGCTATTACAAGTCCTCTTCAGAAATAAGCTTTTGTTCGGA
4F	5’-GTGGAGGAGGCTCTGGTGGAGGCGGTAGCGGAGGCGGAGGGT
4R	5’-AGTAATTAATGTTAATTGTTTATCTTT
5F	5’-TGGGAATTCCATATGCAAGCTAAACCTCAAATTCCG
5R	5’-TTTTTTCTCGAGTTTGACTTCTGTAGCTACAAAG
6R	5’-AATTGAAATATGGCAGGCAGC
7F	5'-CCAGGACCAGCAACAAGYGAACAATTAAATAGA
8F	5'-ATGACAAGTATAAGAAAYGTTAAGCCAACAGCKGTAGAAGTTCTAGAT
9F	5’-TTAATTACTTGTGATGGKTACAATGAAAAGACA

Y = C,T; K=G,T; underlined nucleotides represent mixtures of 70% the indicated nucleotide and 10% each of the remaining three nucleotides

YIPlac211-GPD-S6-Aga1p and Integration Into the Yeast Genome. The YIPlac211-GPD-Avitag-Aga1p plasmid, constructed by ligation of the Avitag-Aga1p gene into YIPlac211 (ATCC) at *BamH*I / *Sac*I and ligation of the glyceraldehyde-3-phosphate dehydrogenase (GPD) promoter sequence at *Xba*I / *BamH*I, served as the starting point. The S6 peptide sequence was inserted after the signal sequence and before Ile30 of Aga1p by overlap extension PCR. The extended PCR product was digested with *BamH*I and *BsiW*I and ligated into similarly digested

YIPlac211-GPD-Avitag-Aga1p plasmid, resulting in the yeast integrating plasmid YIPlac211-GPD-S6-Aga1p.

To integrate the plasmid into the genome, YIPlac211-GPD-S6-Aga1p was linearized by digestion with *BsiWI* and transformed into *S. cerevisiae* strain BJ5465 with lithium acetate, selecting for transformants harboring the integrated plasmid on solid media lacking uracil. A yeast colony with the S6-Aga1p construct correctly inserted was designated ICY200 and displays the S6 peptide sequence constitutively on the cell surface as a fusion to the N-terminus of Aga1p.

pCTCon2CTEV-wt srtA and pCTCon2CTEV-srtA C184A (−HindIII). The pCTCon2CTEV-wt srtA plasmid was constructed inside yeast through a three-part, gap repair homologous recombination process[42]. The pCTCon2B-BirA plasmid, which was constructed from pCTCon2 and expresses the Aga2p-linker-HA-*E. coli* biotin ligase-myc construct, served as the starting point. *S. aureus* genomic DNA was amplified with primers 1F and 1R, and pCTCon2B-BirA with primers 2F and 2R. These two products were transformed together with *Pst*I / *BamH*I-digested pCTCon2B-BirA into *S. cerevisiae* strain ICY200 to yield the pCTCon2CTEV-wt srtA plasmid. The cloned sortase A gene lacks the N-terminal 59 amino acids, which do not impact catalytic activity[43], but these amino acids are still included in the numbering for the mutations.

To introduce the C184A mutation, pCTCon2CTEV-wt srtA was separately amplified with primer pairs 3F/3R and 4F/4R, and the two gene fragments were transformed into ICY200 together with *Nhe*I / *BamH*I-digested pCTCon2CTEV-wt srtA. The *Hind*III site within the myc coding sequence was then removed using an analogous process, allowing the wt and C184A plasmids to be distinguished by a *Hind*III restriction digest.

pET29 Sortase Expression Plasmids. Sortase genes were subcloned into pET29 at *Nde*I and *Xho*I using the primers 5F and 5R. Plasmids encoding sortase single mutants were constructed using the Quikchange method. All expressed sortases lack the N-terminal 59 amino acids.

Sortase A Library R0. The round zero (R0) sortase A library was cloned into *S. cerevisiae* ICY200 using gap repair homologous recombination. The wild-type sortase A gene, lacking the N-terminal 59 amino acids, was mutagenized in PCR reactions containing 5 μM 8-oxo-2'deoxyguanosine (8-oxo-dGTP), 5 μM 6-(2-deoxy-b-D-ribofuranosyl)-3,4-dihydro-8H-pyrimido-[4,5-C][1,2]oxazin-7-one (dPTP), 200 μM each dNTP, and 0.4 μM each of primers 1F and 1R. Reactions were thermocycled ten times and the mutagenized genes were further amplified in PCR reactions without mutagenic dNTP analogs using primers 1F and 3R. Gel-purified genes and *Nhe*I / *BamH*I-digested pCTCon2CTEV-wt srtA were combined in a 1:3 mass ratio, concentrated by ethanol precipitation, and electroporated into competent ICY200 as described, resulting in a library of $7.8x10^7$ transformants. A total of $\sim10^9$ cells from the fully grown library culture were pelleted and induced as described below.

Recombined Sortase A library (R4shuf). In vitro recombination was performed using the NExT procedure[26]. Sortase genes recovered after R4 were amplified with the primers 2F and 6R in PCR reactions containing 50 μM dUTP, 150 μM dTTP, and 200 μM each of dATP, dCTP, and dGTP. After purification by gel extraction, 17 μg of the PCR product was incubated with 7.5 units of uracil deglycosylase (NEB). Piperidine was added (10% vol/vol) and the reaction was heated at 90 °C for 3 min. The resulting gene fragments were purified using the QiaExII kit after neutralization of the piperidine with glacial acetic acid.

Fragments were assembled in PCR reactions containing 1 μg of fragments using the conditions reported by Tawfik[44] In separate fragment assembly reactions, primers 7F, 8F, and 9F were each added to the assembly reaction at 0.5 μM and 1.5 μM to favor the inclusion of P94S, D160N, D165A, and D186G— mutations that appeared to improve catalytic efficiency based on activity assays of individual clones evolved in R3 and R4. Assembly reactions were purified using the Qiaquick kit, re-amplified with the primers 1F and 1R, and purified by gel extraction. Eight μg of each assembled gene product (24 μg total) were mixed with 7 μg of *Nhe*I / *BamH*I-digested pCTCon2CTEV plasmid, concentrated by ethanol precipitation, and electroporated into competent ICY200 cells as described above, resulting in a library of $6.9x10^7$ transformants. A total of $\sim10^9$ cells from the fully grown library culture were pelleted and induced as described below.

Sortase Library R8mut. The R8mut library was cloned into yeast as described above for the R0 library, starting with an equimolar mixture of the genes encoding clones 8.3, 8.4, 8.5, and 8.9 These clones were chosen because they possessed only one extraneous mutation in addition to the tetramutant motif (8.3,8.4,8.9), or because they possessed an altered tetramutant core (8.5). More heavily mutagenized library members (8.11, 8.13) were avoided in order to minimize deviation from the tetramutant core of mutations. The concentrations of dPTP and 8-oxo-dGTP were each 10 μM. Following electroporation into ICY200 as described above, a library of $5x10^7$ transformants was obtained with a bulk mutagenesis rate of 1.5%, corresponding with an amino acid mutagenesis rate of 1.1%.

General Yeast Methods. Yeast cells were transformed with DNA using the lithium acetate method. Plasmid DNA from yeast cultures was harvested using the Zymoprep Yeast

Plasmid Minipreparation Kit (Zymo Research) following the manufacturer's instructions. For sequencing, zymoprepped DNA was amplified by transformation into *E. coli*, or sortase genes were amplified by PCR using the primers 2F and 6R.

S. cerevisiae strain ICY200 was propagated in YPD or growth media consisting of 100 mM phosphate pH 6.6, 2% (w/v) dextrose, 0.67% yeast nitrogen base (Sigma), 100 μg/mL cysteine, 100 μg/mL proline, 30 μg/mL histidine, 30 μg/mL methionine, and complete supplement mixture lacking uracil (MP Biomedical). Growth media for ICY200 transformed with the pCTCon2CTEV yeast display plasmids was the same, except the complete supplement mixture lacked uracil and tryptophan. Induction media was the same as the growth media lacking uracil and tryptophan, except the carbon source consisted of 1.8% galactose and 0.2% dextrose. For induction of display of sortase enzymes on the cell surface, yeast cells from a fully grown culture were pelleted, resuspended in induction media at a density of $7x10^6$ cells/mL, and incubated at 20 °C for 18-36 hours. Cells were pelleted and washed with TBS supplemented with 1 mg/mL BSA (TBS-B) before input into assays.

Protein Expression and Purification

Bacterial Expression of Sortases. *E. coli* BL21(DE3) transformed with pET29 sortase expression plasmids were cultured at 37 °C in LB with 50 μg/mL kanamycin until OD_{600} = 0.5-0.8. IPTG was added to a final concentration of 0.4 mM and protein expression was induced for three hours at 30 °C. The cells were harvested by centrifugation and resuspended in lysis buffer (50 mM Tris pH 8.0, 300 mM NaCl supplemented with 1 mM $MgCl_2$, 2 units/mL DNAseI (NEB), 260 nM aprotinin, 1.2 μM leupeptin, and 1 mM PMSF). Cells were lysed by sonication

and the clarified supernatant was purified on Ni-NTA agarose following the manufacturer's instructions. Fractions that were >95% purity, as judged by SDS-PAGE, were consolidated and dialyzed against Tris-buffered saline (25 mM Tris pH 7.5, 150 mM NaCl). Enzyme concentration was calculated from the measured A_{280} using the published extinction coefficient of 17,420 M^{-1} cm^{-1} [45].

Bacterial Expression of Sfp Phosphopantetheinyl Transferase. *E. coli* BL21(DE3) harboring the pET29 expression plasmid for Sfp phosphopantetheinyl transferase (a gift from the Christopher T. Walsh lab) were cultured at 37 °C in LB with 50 μg/mL kanamycin until OD_{600} ~0.6. IPTG was added to a final concentration of 1 mM, and protein expression was induced at 37 °C for three hours. The cells were harvested by centrifugation and lysed by resuspension in B-PER (Novagen) containing 260 nM aprotinin, 1.2 μM leupeptin, 2 units/mL DNAseI, and 1 mM PMSF. The clarified supernatant was purified on Ni-NTA agarose, and fractions that were >95% pure were consolidated and dialyzed against 10 mM Tris pH 7.5 +1 mM EDTA +5% glycerol. Enzyme concentration was calculated from the measured A_{280} using the published extinction coefficient of 27,220 M^{-1} cm^{-1} [46].

Bacterial Expression of TEV S219V Protease. *E. coli* BL21(DE3) harboring the pRK793 plasmid for TEV S219V expression and the pRIL plasmid (Addgene) were cultured in LB with 50 μg/mL carbenicillin and 30 μg/mL chloramphenicol until OD_{600} ~0.7. IPTG was added to a final concentration of 1 mM, and the cells were induced for three hours at 30 °C. The cells were pelleted by centrifugation and lysed by sonication as described above for the sortases.

The clarified lysate was purified on Ni-NTA agarose, and fractions that were >95% TEV S219V were consolidated and dialyzed against TBS. Enzyme concentration was calculated from the measured A_{280} using the reported extinction coefficient of 32,290 M^{-1} cm^{-1} [47].

Protein Sequences. Amino acid changes relative to wild-type *S. aureus* sortase A are underlined.

Aga2p-srtA C184A (Figure 2-4, Figure 2-10B)

MQLLRCFSIFSVIASVLAQELTTICEQIPSPTLESTPYSLSTTTILANGKAMQGVFEYYKSV
TFVSNCGSHPSTTSKGSPINTQYVFKDNSSTLQASGGGGSGGGGSGGGGSYPYDVPDYA
GSENLYFQGASQAKPQIPKDKSKVAGYIEIPDADIKEPVYPGPATPEQLNRGVSFAEENE
SLDDQNISIAGHTFIDRPNYQFTNLKAAKKGSMVYFKVGNETRKYKMTSIRDVKPTDVE
VLDEQKSKDKQLTLITADDYNEKTGVWEKRKIFVATEVKGSEQKLISEEDL

Aga2p-Clone 8.3 (Figure 2-10B, Figure 2-11A)

MQLLRCFSIFSVIASVLAQELTTICEQIPSPTLESTPYSLSTTTILANGKAMQGVFEYYKSV
TFVSNCGSHPSTTSKGSPINTQYVFKDNSSTLQASGGGGSGGGGSGGGGSYPYDVPDYA
GSENLYFQGASQAKPQIPKDKSKVAGYIEIPDADIKEPVYPGPATSEQLNRGVSFAEENE
SLDDQNISIAGHTFIDRPNYQFTNLKAAKKGSMVYFKVGNETRKYKMTSIRNVKPTAVE
VLDEQKSKDKQLTLITCDDYNEKTGVWETRKIFVATEVKGSEQKLISEEDL

Aga2p-Clone 8.4 (Figure 2-10B, Figure 2-11A)

MQLLRCFSIFSVIASVLAQELTTICEQIPSPTLESTPYSLSTTTILANGKAMQGVFEYYKSV
TFVSNCGSHPSTTSKGSPINTQYVFKDNSSTLQASGGGGSGGGGSGGGGSYPYDVPDYA

GSENLYFQGASQAKPQIPKDKSKVAGYIEIPDADIKEPVYPGPATSEQLNRGVSFAEENE
SLDDQNISIAGHTFIDRPNYQFTNLKAAKKGSMVYFKVGNETRKYKMTSIRNVKPTAVE
VLDEQKSKDKQLTLITCDDYNEETGVWETRKIFVATEVKGSEQKLISEEDL

Aga2p-Clone 8.9 (Figure 2-10B, Figure 2-11A)

MQLLRCFSIFSVIASVLAQELTTICEQIPSPTLESTPYSLSTTTILANGKAMQGVFEYYKSV
TFVSNCGSHPSTTSKGSPINTQYVFKDNSSTLQASGGGGSGGGGSGGGGSYPYDVPDYA
GSENLYFQGASQAKPQIPKDKSKVAGYIEIPDADIKEPVYPGPATSEQLNRGVSFAEENE
SLDDQNISIAGHTFIDRPNYQFTNLKAAKKGSMVYFKVGNETRKYRMTSIRNVKPTAVE
VLDEQKSKDKQLTLITCDDYNEKTGVWETRKIFVATEVKGSEQKLISEEDL

Aga2p-Clone 8.13 (Figure 2-10B, Figure 2-11A)

MQLLRCFSIFSVIASVLAQELTTICEQIPSPTLESTPYSLSTTTILANGKAMQGVFEYYKSV
TFVSNCGSHPSTTSKGSPINTQYVFKDNSSTLQASGGGGSGGGGSGGGGSYPYDVPDYA
GSENLYFQGASQAKPQIPKDKSKVAGYIEIPDADIKEPVYPGPATSEQLNRGVSFAEGNE
SLDDQNISIAGHTYIDRPNYQFTNLKAAKKGSMVYFKVGNETRKYKMTSIRNVKPTAVE
VLDEQKSKDKQLTLITCDDYNEKTGVWETRKIFVATEVKGSEQKLISEEDL

wild-type S. aureus sortase A (Figure 2-10B, Figure 2-11A, Table 2-1)

MQAKPQIPKDKSKVAGYIEIPDADIKEPVYPGPATPEQLNRGVSFAEENESLDDQNISIAG
HTFIDRPNYQFTNLKAAKKGSMVYFKVGNETRKYKMTSIRDVKPTDVEVLDEQKGKD
KQLTLITCDDYNEKTGVWEKRKIFVATEVKLEHHHHHH

srtA P94S (Table 2-1)

MQAKPQIPKDKSKVAGYIEIPDADIKEPVYPGPATSEQLNRGVSFAEENESLDDQNISIAG
HTFIDRPNYQFTNLKAAKKGSMVYFKVGNETRKYKMTSIRDVKPTDVEVLDEQKGKD
KQLTLITCDDYNEKTGVWEKRKIFVATEVKLEHHHHHH

srtA D160N (Table 2-1)

MQAKPQIPKDKSKVAGYIEIPDADIKEPVYPGPATPEQLNRGVSFAEENESLDDQNISIAG
HTFIDRPNYQFTNLKAAKKGSMVYFKVGNETRKYKMTSIRNVKPTDVEVLDEQKGKD
KQLTLITCDDYNEKTGVWEKRKIFVATEVKLEHHHHHH

srtA D165A (Table 2-1)

MQAKPQIPKDKSKVAGYIEIPDADIKEPVYPGPATPEQLNRGVSFAEENESLDDQNISIAG
HTFIDRPNYQFTNLKAAKKGSMVYFKVGNETRKYKMTSIRDVKPTAVEVLDEQKGKD
KQLTLITCDDYNEKTGVWEKRKIFVATEVKLEHHHHHH

srtA K196T (Table 2-1)

MQAKPQIPKDKSKVAGYIEIPDADIKEPVYPGPATPEQLNRGVSFAEENESLDDQNISIAG
HTFIDRPNYQFTNLKAAKKGSMVYFKVGNETRKYKMTSIRDVKPTDVEVLDEQKGKD
KQLTLITCDDYNEKTGVWETRKIFVATEVKLEHHHHHH

Clone 4.2 (Figure 2-10B, Figure 2-11A, Table 2-1)

MQAKPQIPKDKSKVAGYIEIPDADIKEPVYPGPATPEQLNRGVSFAEENESLDDQNISIAG
HTFIDRPNYQFTNLKAAKKGSMVYFKVGNETRKYKMTSIRNVKPTDVEVLDEQKGKD
KQLTLITCDDYNEETGVWETRKIFVATEVKLEHHHHHH

Clone 4.3 (Figure 2-10B, Figure 2-11A, Table 2-1)

MQAKPQIPKDKSKVAGYIEIPDADIKEPVYPGPATSEQLNRGVSFAEENESLDDQNISIAG
HTFIDRPNYQFTNLKAAKKGSMVYFKVGNETRKYKMTSIRDVKPTAVEVLDEQKGKD
KQLTLITCDDYNEKTGVWEKRKIFVATEVKLEHHHHHH

P94S/D160N/D165A/K196T (Table 2-1)

MQAKPQIPKDKSKVAGYIEIPDADIKEPVYPGPATSEQLNRGVSFAEENESLDDQNISIAG
HTFIDRPNYQFTNLKAAKKGSMVYFKVGNETRKYKMTSIRNVKPTAVEVLDEQKGKD
KQLTLITCDDYNEKTGVWETRKIFVATEVKLEHHHHHH

P94S/D160N/K196T (Table 2-1, Figure 2-14)

MQAKPQIPKDKSKVAGYIEIPDADIKEPVYPGPATSEQLNRGVSFAEENESLDDQNISIAG
HTFIDRPNYQFTNLKAAKKGSMVYFKVGNETRKYKMTSIRNVKPTDVEVLDEQKGKD
KQLTLITCDDYNEKTGVWETRKIFVATEVKLEHHHHHH

P94S/D160N/D165A (Table 2-1)

MQAKPQIPKDKSKVAGYIEIPDADIKEPVYPGPATSEQLNRGVSFAEENESLDDQNISIAG
HTFIDRPNYQFTNLKAAKKGSMVYFKVGNETRKYKMTSIRNVKPTAVEVLDEQKGKD
KQLTLITCDDYNEKTGVWEKRKIFVATEVKLEHHHHHH

P94R/D160N/D165A/K190E/K196T (Table 2-1)

MQAKPQIPKDKSKVAGYIEIPDADIKEPVYPGPATREQLNRGVSFAEENESLDDQNISIAG
HTFIDRPNYQFTNLKAAKKGSMVYFKVGNETRKYKMTSIRNVKPTAVEVLDEQKGKD
KQLTLITCDDYNEETGVWETRKIFVATEVKLEHHHHHH

Effective Molarity of Surface-Conjugated Substrate Relative to Yeast-Displayed Sortase. Yeast displaying clones 4.2 and 4.3 were conjugated with GGGK-CoA as described in Materials and Methods. The resulting cells were incubated with 1 μM Biotin-LPETGG in TBS with 5 mM $CaCl_2$, and aliquots were removed at various time points and immediately diluted 1:20 into ice-cold PBS containing 6 μM TEV S219V, 5 mM AAEK2 (an inhibitor of *S. aureus* sortase A[38]), 1 mM berberine chloride (an inhibitor of *S. aureus* sortase A[48]) , and 5 mM of non-biotinylated GGG. After incubation on ice for fifteen minutes, the samples were pelleted and resuspended in ice-cold PBS containing 6 μM TEV S219V, 5 mM AAEK2, 5 mM GGG for one hour. Following staining of the cells with streptavidin-phycoerythrin (for reaction extent) and AlexaFluor488-conjugated anti-hemagglutinin antibody (for display), the mean phycoerythrin (PE) fluorescence intensities (PE MFI) of the AlexaFluor488-positive cells were recorded with a BD Fortessa flow cytometer. When plotted versus time (t), the PE MFI (for reaction extent) for the 488/PE-double positive population of each sample were fit to the Poisson equation representing the proportion of sites converted for a reaction operating at constant velocity v, $f_\infty(1-e^{-v*(t+theta)})+f_0$. The scaling factor f_∞ is taken to represent the fluorescence intensity of a fully labeled cell and is determined by allowing reactions to run for two hours and fixing this as the endpoint. The minimum fluorescence intensity for a library member, f_0, is fixed from the PE MFI of 488-negative cells within the population. The velocity of the reaction, v, and the time

correction factor, theta, were both determined by nonlinear regression of the data to the fit curve using the program Mathematica. The velocity data were then transformed into estimates for the effective molarity of displayed enzymes for [GGG] by the use of the previously determined Michaelis-Menten relations for clones 4.2 and 4.3, [GGG] = $K_{m,GGG}*K_{m,LPETG}*v+K_{m,GGG}*[LPETG]*v/(k_{cat}*[LPETG]-K_{m,LPETG}*v-[LPETG]*v)$

[GGG] estimates were made for two technical replicates each of the 4.2 and 4.3 sortase mutants, and the overall estimate of [GGG] was found to be 0.95 ± 0.11 mM.

References

1 Chapman-Smith, A., Mulhern, T. D., Whelan, F., Cronan, J. E. & Wallace, J. C. The C-terminal domain of biotin protein ligase from E. coli is required for catalytic activity. *Protein Science* **10**, 2608-2617 (2001).

2 Savile, C. K. *et al.* Biocatalytic Asymmetric Synthesis of Chiral Amines from Ketones Applied to Sitagliptin Manufacture. *Science* **329**, 305-309, doi:10.1126/science.1188934 (2010).

3 Uttamapinant, C. *et al.* A fluorophore ligase for site-specific protein labeling inside living cells. *Proceedings of the National Academy of Sciences* **107**, 10914-10919, doi:10.1073/pnas.0914067107 (2010).

4 Yin, J. *et al.* Genetically encoded short peptide tag for versatile protein labeling by Sfp phosphopantetheinyl transferase. *Proceedings of the National Academy of Sciences of the United States of America* **102**, 15815-15820, doi:10.1073/pnas.0507705102 (2005).

5 Popp, M. W., Antos, J. M., Grotenbreg, G. M., Spooner, E. & Ploegh, H. L. Sortagging: a versatile method for protein labeling. *Nat Chem Biol* **3**, 707-708, doi:http://www.nature.com/nchembio/journal/v3/n11/suppinfo/nchembio.2007.31_S1.html (2007).

6 Walsh, G. Biopharmaceutical benchmarks 2006. *Nat Biotech* **24**, 769-776 (2006).

7 Vellard, M. The enzyme as drug: application of enzymes as pharmaceuticals. *Current opinion in biotechnology* **14**, 444-450 (2003).

8 Cherry, J. R. & Fidantsef, A. L. Directed evolution of industrial enzymes: an update. *Current opinion in biotechnology* **14**, 438-443 (2003).

9 Bershtein, S. & Tawfik, D. S. Advances in laboratory evolution of enzymes. *Current opinion in chemical biology* **12**, 151-158 (2008).

10 Bloom, J. D. *et al.* Evolving strategies for enzyme engineering. *Current opinion in structural biology* **15**, 447-452 (2005).

11 Turner, N. J. Directed evolution of enzymes for applied biocatalysis. *Trends in Biotechnology* **21**, 474-478 (2003).

12 Neuenschwander, M., Butz, M., Heintz, C., Kast, P. & Hilvert, D. A simple selection strategy for evolving highly efficient enzymes. *Nature biotechnology* **25**, 1145-1147 (2007).

13 van Sint Fiet, S., van Beilen, J. B. & Witholt, B. Selection of biocatalysts for chemical synthesis. *Proceedings of the National Academy of Sciences of the United States of America* **103**, 1693-1698 (2006).

14 Kelly, B. T., Baret, J.-C., Taly, V. & Griffiths, A. D. Miniaturizing chemistry and biology in microdroplets. *Chemical Communications*, 1773-1788 (2007).

15 Lin, H., Tao, H. & Cornish, V. W. Directed evolution of a glycosynthase via chemical complementation. *Journal of the American Chemical Society* **126**, 15051-15059 (2004).

16 Leconte, A. M., Chen, L. & Romesberg, F. E. Polymerase evolution: efforts toward expansion of the genetic code. *Journal of the American Chemical Society* **127**, 12470-12471 (2005).

17 Seelig, B. & Szostak, J. W. Selection and evolution of enzymes from a partially randomized non-catalytic scaffold. *Nature* **448**, 828-831 (2007).

18 Olsen, M. J. *et al.* Function-based isolation of novel enzymes from a large library. *Nature biotechnology* **18**, 1071-1074 (2000).

19 Gai, S. A. & Wittrup, K. D. Yeast surface display for protein engineering and characterization. *Current opinion in structural biology* **17**, 467-473 (2007).

20 Boder, E. T. & Wittrup, K. D. Yeast surface display for screening combinatorial polypeptide libraries. *Nature biotechnology* **15**, 553-557 (1997).

21 Varadarajan, N., Rodriguez, S., Hwang, B.-Y., Georgiou, G. & Iverson, B. L. Highly active and selective endopeptidases with programmed substrate specificities. *Nat Chem Biol* **4**, 290-294, doi:http://www.nature.com/nchembio/journal/v4/n5/suppinfo/nchembio.80_S1.html (2008).

22 Yin, J., Liu, F., Li, X. & Walsh, C. T. Labeling proteins with small molecules by site-specific posttranslational modification. *Journal of the American Chemical Society* **126**, 7754-7755 (2004).

23 Zhou, Z. *et al.* Genetically encoded short peptide tags for orthogonal protein labeling by Sfp and AcpS phosphopantetheinyl transferases. *ACS Chemical Biology* **2**, 337-346 (2007).

24 Tsukiji, S. & Nagamune, T. Sortase-Mediated Ligation: A Gift from Gram-Positive Bacteria to Protein Engineering. *ChemBioChem* **10**, 787-798 (2009).

25 Zaccolo, M., Williams, D. M., Brown, D. M. & Gherardi, E. An approach to random mutagenesis of DNA using mixtures of triphosphate derivatives of nucleoside analogues. *Journal of molecular biology* **255**, 589-603 (1996).

26 Müller, K. M. *et al.* Nucleotide exchange and excision technology (NExT) DNA shuffling: a robust method for DNA fragmentation and directed evolution. *Nucleic Acids Research* **33**, e117-e117 (2005).

27 Bentley, M. L., Lamb, E. C. & McCafferty, D. G. Mutagenesis studies of substrate recognition and catalysis in the sortase A transpeptidase from Staphylococcus aureus. *Journal of Biological Chemistry* **283**, 14762-14771 (2008).

28 Frankel, B. A., Tong, Y., Bentley, M. L., Fitzgerald, M. C. & McCafferty, D. G. Mutational analysis of active site residues in the Staphylococcus aureus transpeptidase SrtA. *Biochemistry* **46**, 7269-7278 (2007).

29 Kruger, R. G., Dostal, P. & McCafferty, D. G. Development of a high-performance liquid chromatography assay and revision of kinetic parameters for the Staphylococcus aureus sortase transpeptidase SrtA. *Analytical Biochemistry* **326**, 42-48, doi:http://dx.doi.org/10.1016/j.ab.2003.10.023 (2004).

30 Suree, N. *et al.* The structure of the Staphylococcus aureus sortase-substrate complex reveals how the universally conserved LPXTG sorting signal is recognized. *Journal of Biological Chemistry* **284**, 24465-24477 (2009).

31 Agresti, J. J. *et al.* Ultrahigh-throughput screening in drop-based microfluidics for directed evolution. *Proceedings of the National Academy of Sciences* **107**, 4004-4009 (2010).

32 Antipov, E., Cho, A. E., Wittrup, K. D. & Klibanov, A. M. Highly L and D enantioselective variants of horseradish peroxidase discovered by an ultrahigh-throughput selection method. *Proceedings of the National Academy of Sciences* **105**, 17694-17699 (2008).

33 Yang, G. & Withers, S. G. Ultrahigh-throughput FACS-based screening for directed enzyme evolution. *ChemBioChem* **10**, 2704-2715 (2009).

34 Sunbul, M., Marshall, N. J., Zou, Y., Zhang, K. & Yin, J. Catalytic turnover-based phage selection for engineering the substrate specificity of Sfp phosphopantetheinyl transferase. *Journal of molecular biology* **387**, 883-898 (2009).

35 Jiang, L. *et al.* De novo computational design of retro-aldol enzymes. *Science* **319**, 1387-1391 (2008).

36 Röthlisberger, D. *et al.* Kemp elimination catalysts by computational enzyme design. *Nature* **453**, 190-195 (2008).

37 Siegel, J. B. *et al.* Computational design of an enzyme catalyst for a stereoselective bimolecular Diels-Alder reaction. *Science* **329**, 309-313 (2010).

38 Maresso, A. W. *et al.* Activation of inhibitors by sortase triggers irreversible modification of the active site. *Journal of Biological Chemistry* **282**, 23129-23139 (2007).

39 Kapust, R. B. *et al.* Tobacco etch virus protease: mechanism of autolysis and rational design of stable mutants with wild-type catalytic proficiency. *Protein engineering* **14**, 993-1000 (2001).

40 Killenberg, P. G. & Dukes, D. F. Coenzyme A derivatives of bile acids-chemical synthesis, purification, and utilization in enzymic preparation of taurine conjugates. *Journal of lipid research* **17**, 451-455 (1976).

41 Carsten, M. E. & Eisen, H. N. The Interaction of Dinitrobenzene Derivatives with Bovine Serum Albumin1, 2. *Journal of the American Chemical Society* **75**, 4451-4456 (1953).

42 Raymond, C. K., Pownder, T. A. & Sexson, S. L. General method for plasmid construction using homologous recombination. *Biotechniques* **26**, 134-141 (1999).

43 Ilangovan, U., Ton-That, H., Iwahara, J., Schneewind, O. & Clubb, R. T. Structure of sortase, the transpeptidase that anchors proteins to the cell wall of Staphylococcus aureus. *Proceedings of the National Academy of Sciences* **98**, 6056-6061, doi:10.1073/pnas.101064198 (2001).

44 Herman, A. & Tawfik, D. S. Incorporating Synthetic Oligonucleotides via Gene Reassembly (ISOR): a versatile tool for generating targeted libraries. *Protein Engineering Design and Selection* **20**, 219-226 (2007).

45 Kruger, R. G. *et al.* Analysis of the Substrate Specificity of the Staphylococcus aureus Sortase Transpeptidase SrtA†. *Biochemistry* **43**, 1541-1551, doi:10.1021/bi035920j (2004).

46 Mofid, M. R., Finking, R., Essen, L. O. & Marahiel, M. A. Structure-based mutational analysis of the 4'-phosphopantetheinyl transferases Sfp from Bacillus subtilis: carrier protein recognition and reaction mechanism. *Biochemistry* **43**, 4128-4136 (2004).

47 Tropea, J. E., Cherry, S. & Waugh, D. S. in *High Throughput Protein Expression and Purification* 297-307 (Springer, 2009).

48 Kim, S.-H. *et al.* Inhibition of the bacterial surface protein anchoring transpeptidase sortase by isoquinoline alkaloids. *Bioscience, biotechnology, and biochemistry* **68**, 421-424 (2004).

Chapter Three

Immobilization of actively thromboresistant assemblies on sterile blood contacting surfaces

Zheng Qu, Venkat Krishnamurthy, Carolyn A. Haller, Brent M. Dorr, Ulla M. Marzec, Sawan Hurst, Monica T. Hinds, Stephen R. Hanson, David R. Liu, Elliot L. Chaikof

Zheng Qu initiated and performed the major experiments in this chapter. My contributions to this work include providing eSrtA plasmids and protein and developing labeling protocols for the incorporation of amino-PEG-azide into TM-LPETG by eSrtA.

Some of the text in this chapter appears in *Advanced Healthcare Materials*, **2014**, 3 (1), pp 30-35

Abstract

All medical implants that operate in direct contact with blood, such as vascular grafts, stents, and catheters, elicit clot formation with long-term use. Antithrombotic therapies such as Plavix® may prolong device durability, but carry significant cost and an attendant risk of bleeding. Despite advances in bioengineering and medicine, a universally accepted blood compatible material does not exist. This work demonstrates the feasibility of a point-of-care scheme to coat sterilized commercial vascular grafts with thrombomodulin (TM), a clot resistant protein that was more effective than "state of the art" heparin-coated grafts (Gore® Propaten®) in reducing thrombosis in a primate model. Moreover, rapid one-step modification of TM using a mutant Sortase A enzyme may be a key step towards the industrial scaling and clinical translation of our molecularly engineered films that resist thrombosis.

Introduction

All artificial organ systems and medical devices that operate in direct contact with blood elicit activation of coagulation and platelets with long-term use,[1,2] leading to formation of thrombosis or emboli that often necessitates antithrombotic therapies, which carry significant cost and an attendant risk of bleeding.[3,4] None of the existing synthetic arterial substitutes are suitable for small-caliber (< 6 mm) revascularization procedures, which are central to the fields of cardiac, vascular, and plastic surgery, as well as for the implantation of a variety of artificial organs.[5,6] It is now recognized that the adverse events leading to failure of blood contacting devices is largely related to maladaptive biological reactions at the blood-material interface, which contributes to a substantial risk of early and late thrombotic occlusion.[1,7,8] Despite advances in tissue engineering that have yielded biomaterials that mimic the bulk properties of native blood vessels and promote healing,[9-11] a generally accepted blood compatible material

does not exist.[7] This work demonstrates the feasibility of a point-of-care scheme to site-specifically immobilize thrombomodulin (TM) on sterilized commercial vascular grafts, which exhibited superior thromboresistance compared with heparin-coated grafts (Gore® Propaten®) in a non-human primate model of acute graft thrombosis. Rapid one-step modification of TM with synthetic alkylamine derivatives such as azides and PEG using an evolved sortase (eSrtA) mutant may enable the industrial scaling of this approach.

Surface-induced thrombosis hinges on the generation of thrombin, a central mediator that amplifies the intrinsic coagulation cascade, crosslinks fibrin, and activates platelets.[12,13] First demonstrated in 1963,[14] heparin immobilization has been hypothesized to mimic the antithrombin activity of cell surface heparan sulfate proteoglycans (HSPG) expressed by the endothelium.[15] Recent randomized clinical trials show that heparin modified surfaces substantially improved the clinical outcomes of expanded poly(tetrafluoroethylene) (ePTFE) vascular grafts in lower extremity revascularization. Superior 1-year results have been recently reported for heparin-bonded ePTFE (Propaten) when compared to non-coated ePTFE.[16] Preliminary analysis of heparin-bonded ePTFE covered stents in the superficial femoral artery suggests a similar effect.[17,18] Attenuation of thrombin production at the blood-contacting interface, therefore, may be a critical step in the design of blood-compatible materials that improve the clinical performance of blood-contacting implants.

The physiological role of heparin, produced primarily by mast cells, in hemostasis remains unclear[19] as the majority of anticoagulantly active HSPG is not in direct contact with flowing blood[20] and knock-out mice lacking the specific pentasaccharide sequence that inhibits thrombin do not exhibit a procoagulant phenotype.[21] In contrast, TM is the major vasculoprotective molecule localized on the endothelial cell surface and defects therein increase the risk of

thromboembolism, as well as inflammatory disorders.[22] By forming a stoichiometric 1:1 complex with thrombin, TM sequesters thrombin's prothrombotic activity, and simultaneously accelerates thrombin's catalytic activity to generate activated protein C (aPC) by 1000-fold. aPC inhibits the upstream proteases necessary for amplifying thrombin production and represents the primary physiological mechanism which regulates hemostasis.[23,24]

Clinical implementation of strategies reported to date on the immobilization of TM,[24-31] as well as other proteins in therapeutic and diagnostic applications, have been primarily limited by two main factors: the inherent reduction in activity associated with schemes that non-specifically react with free amino, carboxyl, or thiol motifs contained near the catalytically active site, and the necessity for terminal sterilization, which in the medical device industry mainly comprise either ethylene oxide (EtO) or radiation that often perturb the chemical structure and activity of surface-bound biomolecules.[32-34] We were first to demonstrate a bioorthogonal strategy to site-specifically tether recombinant human TM via a single C-terminal azide motif (TM-N_3) by Staudinger Ligation on the luminal surface of 4 mm i.d. ePTFE grafts that preserved the therapeutic activity of TM to catalyze aPC generation.[35] In principle, immobilization of TM on sterilized surfaces with stable anchor sites may provide an alternative to terminal sterilization to manufacture an off-the-shelf product. However, the limited yield and scalability of auxotrophic incorporation of azido-alanine in TM-N_3 as well as the propensity of triphenylphosphines to degrade by air oxidation[36] in our previous report would prohibit the clinical translation of such an approach.

SrtA is a calcium-dependent cysteine transpeptidase found in *Staphylococcus aureus* and other Gram-positive bacteria that anchors proteins containing a C-terminal LPXTG motif (where X denotes any amino acid) by breaking the threonine-glycine bond and forming a new amide

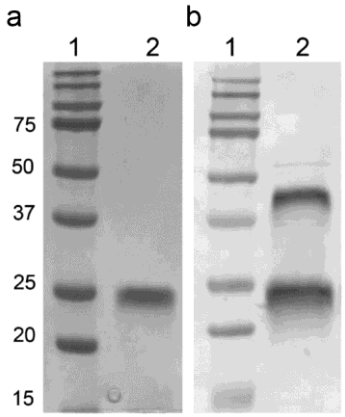

Figure 3-1 SDS-PAGE gel tracking of FLAG-tagged TM_{LPETG}
(a) SDS-PAGE gel tracking of FLAG-tagged TM_{LPETG} purification by anti-FLAG immunoaffinity chromatography. (b) Western blot of purified TM_{LPETG} using an antibody that recognizes TM456. Lanes: 1 – MW markers, 2 – TM_{LPETG}.

bond with oligoglycine-linked molecules.[37-39] Site-specific SrtA transpeptidation of synthetic nucleophiles may be a more efficient alternative to unnatural amino acid approaches[40] to incorporate any of a number of functionalities, such as biotin, fluorophores, and azides, to the termini of recombinant proteins in one step.[41,42] We generated a recombinant human TM fragment (Figure 3-1) containing the minimal functional domains for antithrombotic activity[43,44]

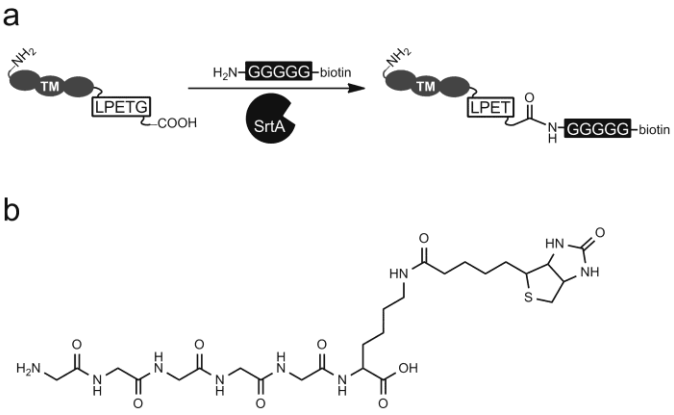

Figure 3-2 Diagrams of SrtA reactions

(**a**) Sortase-catalyzed transpeptidation of biotinylated pentaglycine peptide to the C-terminus of thrombomodulin (TM). (**b**) Chemical structure of the biotinylated pentaglycine peptide (Gly_5-biotin).

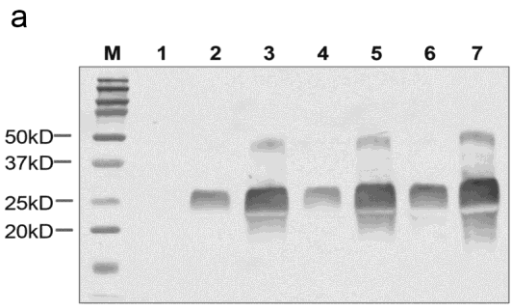

b

Lane	TM	SrtA	Gly_5-biotin	Rxn Time (h)
1	1	0	100	20
2	1	2	10	2
3	1	2	10	20
4	1	2	100	2
5	1	2	100	20
6	1	5	100	2
7	1	5	100	20

Figure 3-3 Sortase catalyzed transpeptidation of TM_{LPETG} with biotinylated pentaglycine peptide (Gly_5-biotin) nucleophiles.

(a) western blot analysis to detect presence of biotin using streptavidin-AP conjugate. (b) Molar ratios of the TM_{LPETG}, WT SrtA, and Gly_5-biotin nucleophile as well as reaction times.

and a C-terminal LPETG se quence (TM_{LPETG}) that facilitated subsequent C-terminal fusion with a biotinylated pentaglycine peptide probe (Gly_5-biotin) and wild-type (WT) SrtA (Figure 3-2). TM_{LPETG} exhibited similar catalytic activity to generate aPC in the presence of thrombin and calcium compared with previous batches of TM generated in our lab.[44] However, high molar excess of WT SrtA (> 2 molar equiv) and Gly_5-biotin (> 10 molar equiv), as well as long reaction times (20 h), were required to drive TM_{LPETG} biotinylation yields (Figure 3-3). Our observations are in agreement with other reported SrtA-catalyzed protein labeling applications,

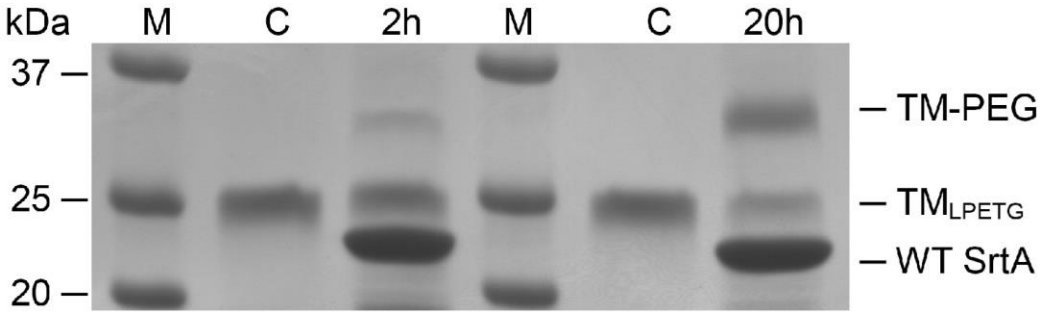

Figure 3-4 Tracking Gel of SrtA Transpeptidation of TM_{LPETG}

SDS-PAGE gel tracking of wild-type (WT) *S. aureus* sortase A (SrtA) catalyzed transpeptidation of an amine-PEG_{113} (MW 5kDa) to thrombomodulin containing a C-terminal LPETG peptide motif (TM_{LPETG}) for 2 h or 20 h reaction time. Notations: C – controls with only TM_{LPETG}, M – molecular weight markers.

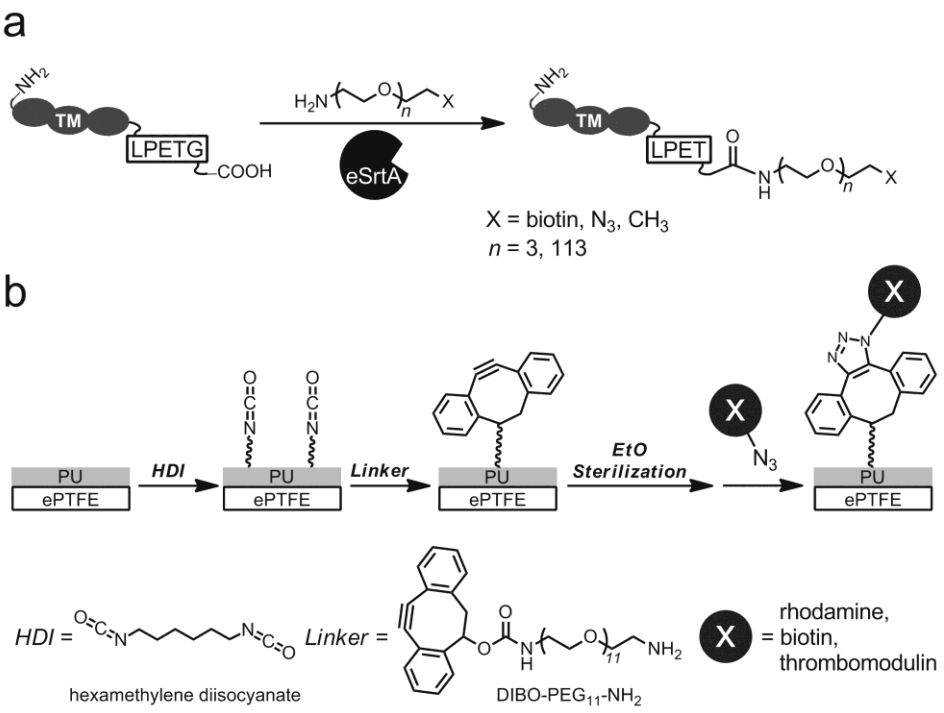

Figure 3-5 Reaction scheme for SrtA-catalyzed azidylation and protein immobilization

(**a**) Covalent site-specific ligation of amine-PEG_n-X to thrombomodulin (TM) containing a C-terminal LPETG peptide motif catalyzed by an evolved *S. aureus* sortase A mutant (eSrtA), where n is the number of PEG repeats and X is a bioorthogonal reactive group such as biotin and azide. (**b**) Surface reaction scheme to modify the lumen of expanded poly(tetrafluoroethylene) (ePTFE) vascular grafts with dibenzocyclooctyne (DIBO) that can be sterilized by ethylene oxide (EtO) prior to strain-promoted [3+2] cycloaddition to immobilize azide derivatives such as rhodamine, biotin, and TM.

which were similarly limited by the low catalytic activity of WT SrtA.[41,42] In addition, we confirmed previous reports showing the suitability of alkylamine nucleophile substrates for SrtA[42,45] by demonstrating WT SrtA-catalyzed PEGylation of TM_{LPETG} in the presence of 100 molar equiv of 5 kDa NH_2-PEG, which achieved ~80% yield after 20 h (Figure 3-4). Despite their lower efficiency as nucleophiles, the relative synthetic simplicity of alkylamine compared with oligoglycine derivatives may further improve the commercial scalability and scope of suitable substrates for SrtA-catalyzed protein labeling.

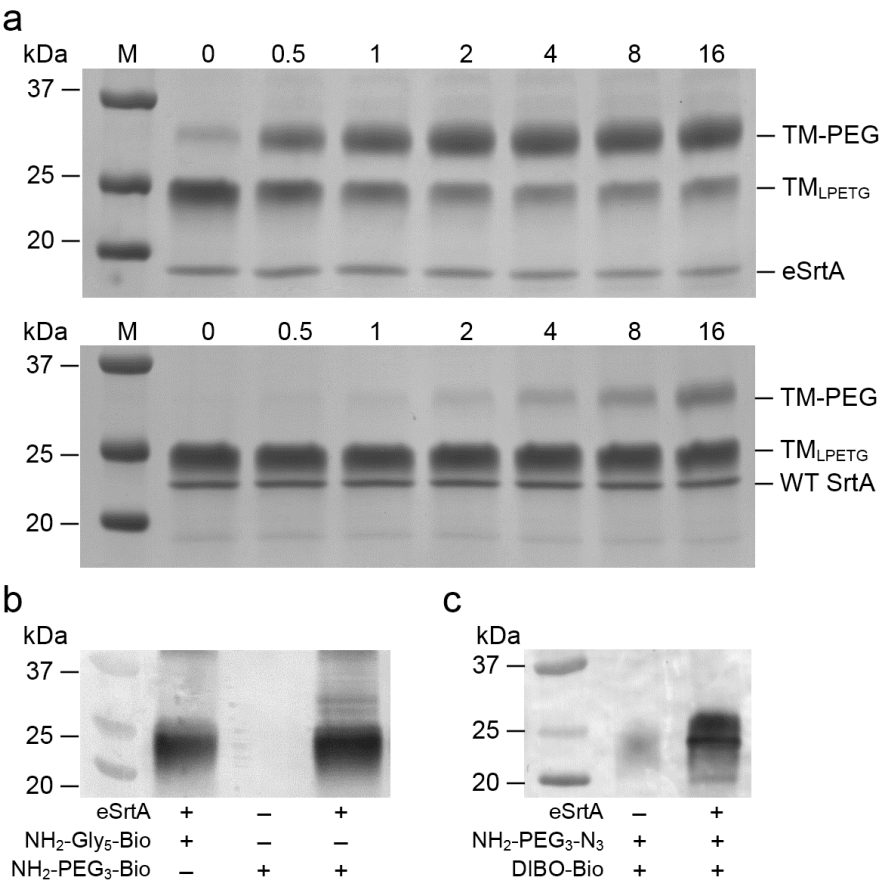

Figure 3-6 Optimization of eSrtA/TM$_{LPETG}$ reaction conditions

(**a**) SDS-PAGE gel tracking of evolved (eSrtA) or wild-type sortase A (WT SrtA) catalyzed transpeptidation of an amine-PEG$_{113}$ (MW 5kDa) to thrombomodulin (TM) containing a C-terminal LPETG peptide motif (TM$_{LPETG}$) over a 16 h time period. (**b**) Western blot comparison of eSrtA-catalyzed transpeptidation of amine-PEG$_3$-biotin (NH$_2$-PEG$_3$-Bio) and biotinylated pentaglycine peptide (NH$_2$-Gly$_5$-Bio) under identical reaction conditions. (**c**) Strain-promoted [3+2] cycloaddition of dibenzocyclooctyne-biotin (DIBO-Bio) with azide-tagged TM, generated by eSrtA-catalyzed ligation of NH$_2$-PEG$_3$-N$_3$ to TM$_{LPETG}$.

The recent development of a general yeast display system has facilitated directed evolution of WT SrtA to generate a SrtA pentamutant (eSrtA), which exhibited 120-fold increase in catalytic activity,[46] and enabled the routine preparation of recombinant proteins that contain a single C-terminal α-thioester.[47] We hypothesized that eSrtA may facilitate rapid labeling of TM$_{LPETG}$ with a single azide motif using the commercially available alkylamine derivative NH$_2$-

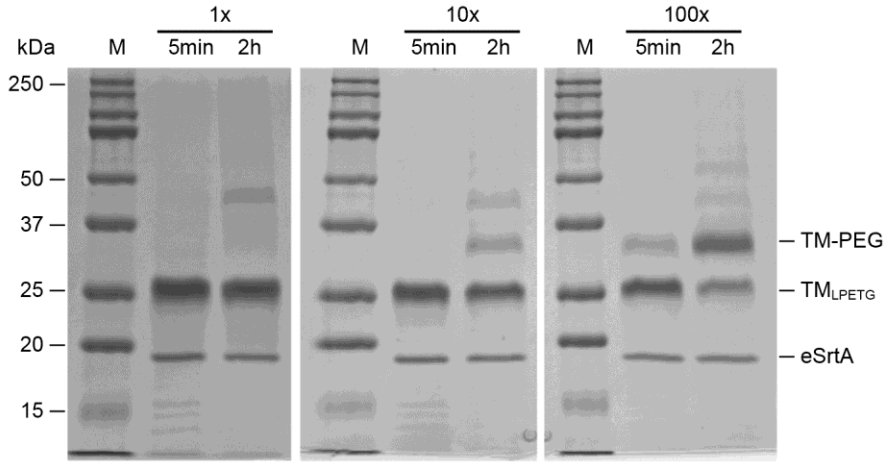

Figure 3-7 Tracking gel of eSrtA transpeptidation

SDS-PAGE gel tracking of pentamutant *S. aureus* sortase A (eSrtA)-catalyzed transpeptidation of 1, 10, or 100 molar equiv amine-PEG_{113} (MW 5kDa) relative to thrombomodulin containing a C-terminal LPETG peptide motif (TM_{LPETG}) for 5 min or 2 h reaction time. Notations: M – molecular weight markers.

PEG_3-N_3 to generate TM-N_3 (Figure 3-5A). As shown in Figure 3-6A, eSrtA dramatically improved the PEGylation efficiency of TM_{LPETG} with 100 molar equiv of 5 kDa NH_2-PEG probe as compared to WT SrtA, achieving nearly 80% yield after 2 h with 0.1 molar equiv eSrtA. This rapid one-step reaction may be broadly applied to site-specifically PEGylate LPETG-tagged recombinant protein therapeutics, which has been routinely performed to optimize half-life and biostability.[48,49] Notably, the reaction of TM_{LPETG} with 1 or 10 molar equiv 5 kDa NH_2-PEG for 2 h yielded minimal TM-PEG product, and no major TM multimer products formed at these conditions (Figure 3-7). These observations indicate minimal non-specific transpeptidation with exposed primary amines on TM_{LPETG} despite the enhanced catalytic activity of eSrtA. eSrtA was equally efficient in catalyzing the biotinylation of TM_{LPETG} (Figure 3-6B) in the presence of 100 molar equiv Gly_5-biotin and NH_2-PEG_3-biotin, demonstrating equivalency of alkylamines as compared to oligoglycines for eSrtA transpeptidation when reacted in high molar excess. Under

optimal reaction conditions, 0.1 equiv eSrtA and 100-fold molar excess NH_2-PEG_3-N_3 relative to TM_{LPETG} yielded a TM-N_3 conjugate in 2 h, which exhibited selective reactivity with alkyne probes (Figure 3-6C). As the high excess of alkylamine derivatives could be removed or recovered by established dialysis methods due to their small molecular weight, and His-tagged

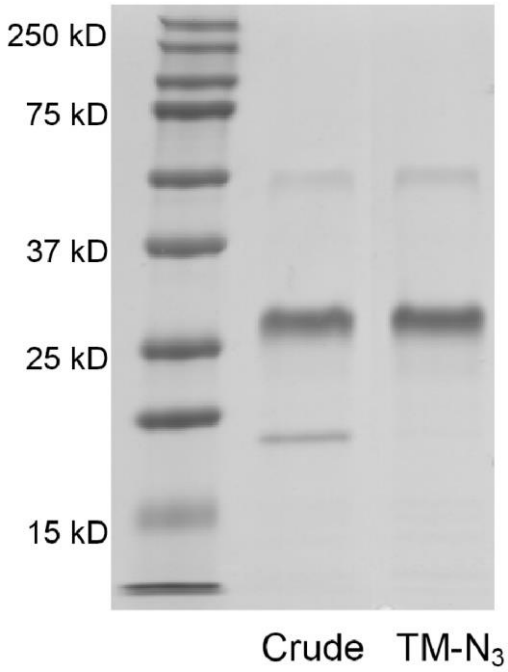

Figure 3-8 Removal of eSrtA by metal affinity pulldown

SDS-PAGE gel tracking of the removal of His-tagged evolved Sortase A (eSrtA, ~17kD) by metal affinity chromatography of the crude reaction mixture following reaction of TM_{LPETG} with NH_2-PEG-N_3.

eSrtA could be efficiently removed by applying the crude reaction mixture onto a metal-affinity column (Figure 3-8), commercial scale-up of TM-N_3 production by eSrtA transpeptidation should be feasible.

Optimization of strained alkynes has yielded variants that exhibit substantially higher reaction kinetics than Staudinger Ligation, while maintaining bioorthogonality to undergo cycloaddition with azide without copper catalysis.[50,51] Dibenzocyclooctyne (DIBO) has been

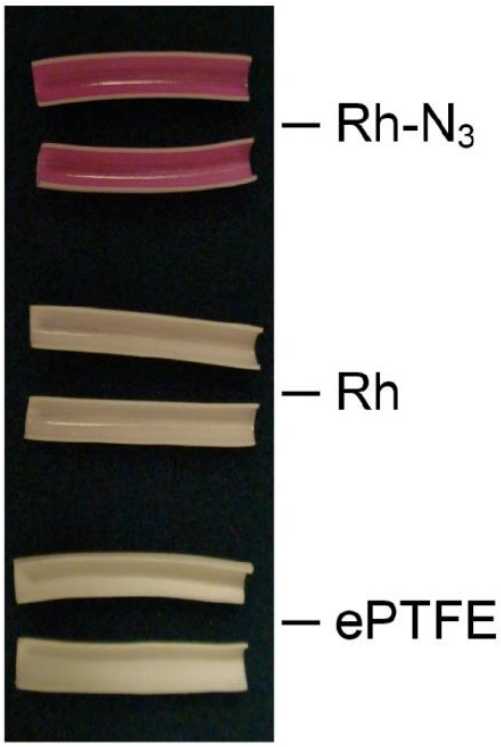

Figure 3-9 Immobilization of rhodamine azide on DIBO functionalize ePTFE grafts

Visual assessment of rhodamine azide (Rh-N_3) or rhodamine B (Rh) immobilization on DIBO functionalized ePTFE grafts, compared with plain ePTFE control.

among the most well char acterized strained alkynes and has been commercialized for cell imaging applications.[52] We synthesized a DIBO-PEG_{11}-NH_2 linker that enabled the activation of the luminal surface of 4 mm i.d. ePTFE vascular grafts, as well as solvent-cast polyurethane (PU) films, with DIBO anchor groups using an approach reported previously[35] and outlined in Figure 3-5B. Commercial ePTFE gr afts activated with DIBO reacted specifically with Rh-N_3, as verified visually (Figure 3-9). Significantly, we demonstrated that EtO sterilization of DIBO modified surfaces did not impair their capacity to bind azide derivatives. Figure 3-10A shows the capacity of DIBO to specifically react with rhodamine azide (Rh-N_3) was not diminished

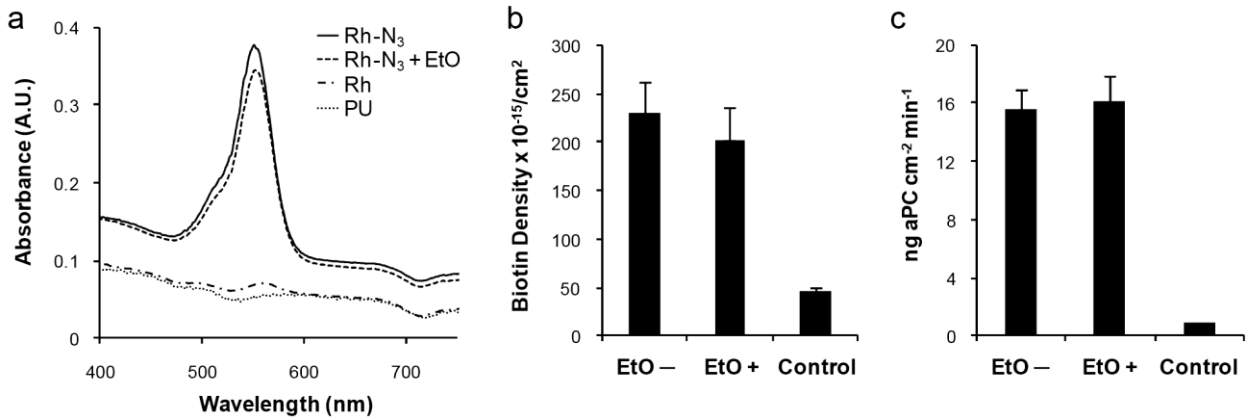

Figure 3-10 Test immobilization on EtO sterilized films

(**a**) UV-vis spectroscopy of rhodamine-azide (Rh-N_3) or rhodamine B (Rh) immobilized on ethylene oxide (EtO) sterilized and non-sterilized thin polyurethane (PU) films functionalized with dibenzocyclooctyne (DIBO). (**b**) Surface density of biotin-PEG_3-N_3 immobilized on EtO sterilized and non-sterilized expanded poly(tetrafluoroethylene) (ePTFE) grafts modified with DIBO. (**c**) Activated protein C (aPC) production by EtO treated and non-treated ePTFE grafts.

following EtO sterilization of DIBO modified PU films. Quantitative measurement of surface biotin density in Figure 3-10B confirmed no significant change in DIBO

reactivity with azide-PEG_3-biotin following EtO sterilization of DIBO modified ePTFE grafts. Covalent immobilization of TM-N_3 on EtO sterilized ePTFE grafts modified with DIBO maintained similar levels of catalytic activity to generate ~15 ng aPC cm^{-2} min^{-1} as TM-N_3 immobilized on non-sterile DIBO modified grafts. Collectively, these results support the feasibility of immobilizing TM-N_3 on sterilized DIBO-modified surfaces that would be carried out in the operating room prior to implantation. Similar point-of-care approaches have been described, for example, electrospinning of polymer wraps for autologous vein grafts,[53] as well as endothelial cell seeding of ePTFE grafts[54] prior to implantation, though these methods may carry a higher risk of microbial contamination.

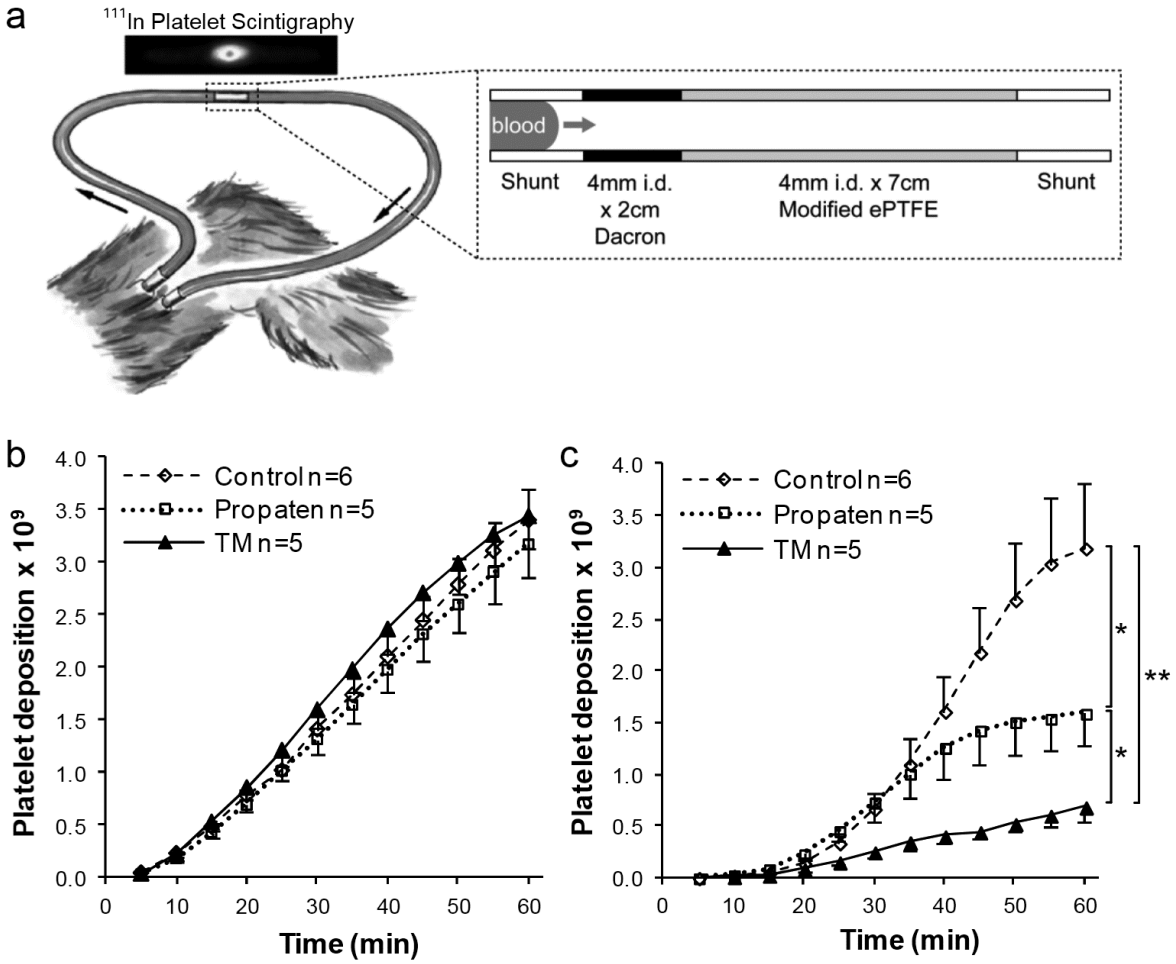

Figure 3-11 Baboon shunt model for antithrombotic efficacy testing

(**a**) Baboon arteriovenous shunt model to measure deposition of platelets on modified expanded poly(tetrafluoroethylene) (ePTFE) grafts in the presence of an upstream prothrombotic Dacron segment. (**b**) Quantity of platelets deposited over a 1 h period on the Dacron segment. (**c**) Quantity of platelets deposited over a 1 h period on unmodified ePTFE control grafts, heparin modified Propaten grafts, and TM modified grafts (* $p < 0.05$, ** $p < 0.01$).

Due to the lack of clinical data that establish the minimal aPC flux required to reduce risk of graft thrombosis, the therapeutic characteristics of TM modified ePTFE grafts was evaluated in an animal model. Chronic arteriovenous shunt models in baboons, whose hemostatic systems most closely mirror that of man, are routinely used to assess the thrombogenicity of blood contacting materials under dynamic flow *in vivo*.[55-57] Due to tissue injury at the graft

anastomosis, which results in exposure of highly thrombogenic tissue factor and collagen motifs to flowing blood,[13] we devised a multi-compartment shunt configuration that inserted an upstream Dacron graft segment that serves as a thrombogenic stress to test the therapeutic activity of aPC generated in a downstream TM modified graft segment (Figure 3-11A). We postulated that the Dacron segment may provide a more clinically relevant test bed by reconstituting the *in vivo* thrombogenic stress exerted on implanted graft materials. Thrombogenicity of materials was evaluated by measuring the real-time deposition of radio-labeled autologous platelets on the luminal surface of unmodified ePTFE, TM modified ePTFE, as well as commercial heparin modified ePTFE (Propaten) vascular grafts.

Dacron was prone to platelet deposition as evident by steady accumulation over a 1 h perfusion period (Figure 3-11B), which was similar to previous reports.[58,59] TM modified ePTFE graft segments reduced platelet deposition by ~80% (Figure 3-11C) when compared to unmodified grafts ($n=5$, $p < 0.01$). The therapeutic efficacy of TM was significantly greater than the commercial heparin coating, which resulted in a ~50% reduction in platelet deposition relative to unmodified grafts ($n=5$, $p < 0.05$). Minimal deposition of platelets on heparin modified ePTFE in non-human primates had previously been reported in shunt configurations that lacked the upstream Dacron segment,[60] but our current studies suggest that the antithrombin III activity catalyzed by heparin may be overwhelmed in the presence of a high upstream thrombogenic source. Given the many factors that dictate the durability of an arterial substitute, the benefit afforded by TM immobilization will need to be evaluated in long-term surgically implanted bypass configurations *in vivo*.[13]

In summary, we have demonstrated the feasibility of covalently immobilizing TM-N_3 on EtO sterilized ePTFE grafts as a point-of-care delivery scheme, which may be a key step in the clinical translation of biologically active films for permanent implants as a sterile off-the-shelf product. Significantly, we demonstrated the superior blood-contacting properties of TM-modified vascular grafts as compared to current commercial heparin modified grafts in a primate model of acute graft thrombosis. Moreover, we have optimized the scalability of producing TM-N_3 by rapid one-step eSrtA transpeptidation of alkylamine azide, and demonstrated the suitability of this approach to site-specifically PEGylate or biotinylate TM. Based on growing reports to date on the application of WT SrtA, the enhanced reactivty of eSrtA may be a key enabling step in the industrial scaling of these strategies.

Materials and Methods

All reagents were purchased from Aldrich, St Louis and used without further purification unless otherwise noted. Expression and purification of recombinant TM_{LPETG} and sortases, as well as solution phase sortase transpeptidation reactions are detailed in the supplementary information section. Gly_5-biotin was obtained from Genscript, Piscataway and used without further purification.

Synthesis of DIBO-PEG_{11}-NH_2. The activated DIBO was synthesized according to a previously published protocol.[52] DIBO-PEG_{11}-NH_2 was synthesized by reaction between the activated DIBO and t-Boc-N-amido-dPEG11-amine (Quanta BioDesign, Powell) followed by TFA deprotection, as detailed previously.[61]

Modification of ePTFE Grafts. 5% w/v Elasthane 80A (Polymer Tech, Berkeley) in *N*,*N*-dimethylformamide (DMF) was extruded through 4 mm i.d. ePTFE thin wall vascular grafts

(Bard, Tempe) and dried under vacuum at 60°C for 20 min. Additional PU was deposited in multiple flow-through/drying cycles over the base layer, and dried overnight under vacuum at 60 °C. PU coated grafts were inserted into tubular rotary reactors, as described previously for surface reactions.[35] Grafts were first reacted with HDI (16% v/v) and TEA (4% v/v) in toluene at 50 °C for 1 h and rinsed in toluene for 6 h. Isocyanate activated grafts were reacted with DIBO-PEG_{11}-NH_2 linker (5 mg/mL) and DMSO (1% v/v) in toluene at 40 °C overnight, rinsed with toluene for 6 h, and dried under vacuum at 25 °C overnight. Standard EtO sterilization was carried out at the Beth Israel Deaconess Medical Center Central Processing (Boston MA). DIBO activated grafts were reacted with 1 mg/mL tetramethylrhodamine-5-carbonyl azide (Invitrogen, Carlsbad) in 1:4 tert-butanol/TBS at 37 °C for 24 h followed by rinsing in methanol for 2 days, 1 mM biotin-PEG_3-N_3 (Pierce, Rockford) in TBS at 37 °C for 24 h followed by rinsing in TBS for 24 h, or 20 μM TM-N_3 in Tris buffered saline (TBS, 20mM Tris, 100mM NaCl, pH 7.5) at 37 °C for 24 h and rinsed with TBS for 24 h. Grafts coated with PU and activated with DIBO were reacted with rhodamine B or TM_{LPETG} as controls.

Modification of polyurethane films. Thin clear PU films were solvent cast by drying 12.5% w/v PU in DMF for 24 h at 60 °C under vacuum. Films were subjected to isocyanate, DIBO, and rhodamine reactions in a glass vial using identical conditions as graft substrates, and characterized by UV-Vis spectroscopy (Cary 50 Bio UV-visible spectrophotometer, Varian).

TM graft cofactor activity assay. A 4 mm graft segment was incubated in 200 μL of 0.2 μM human protein C (Calbiochem, Gibbstown), 5 mM calcium chloride, and 2 nM human α-thrombin (Haematologic Technologies, Essex Junction) in Tris buffer (20 mM Tris, 100 mM NaCl, pH 7.5) with 0.1% bovine serum albumin (BSA) at 37 °C for 1 h, and quenched with 2

IU/mL human anti-thrombin III (American Diagnostica, Stamford) for 5 min. The generation of aPC was quantified using 0.2 mM of an enzymatically digestible chromogenic substrate, Spectrozyme PCa (American Diagnostica).

Determination of biotin surface density with streptavidin-HRP probe: All assay reactions were run in a 96-well plate, per manufacturer's instructions (Pierce). Moles of biotin motifs bound to graft samples were determined using a standard curve generated by known concentrations of streptavidin-HRP incubated with TMB substrate. At the end of each assay, graft segments were flattened between glass slides and scanned at 600 dpi using a HP ScanJet 5370C scanner and the reactive area of each test sample was measured using ImageJ software.

In vivo baboon arteriovenous shunt model. Chronic exteriorized Silastic tubings were implanted in male baboons, as described previously.[62,63] All studies were approved by the Institutional Animal Care and Use Committee at Oregon Health and Science University. Mean blood flow rate through the shunt was measured continuously using a Doppler ultrasonic flow meter and held constant by an external screw clamp at 100 mL/min. Autologous platelets were radiolabeled one day prior to shunt study with Indium-111 oxine and re-injected into the baboon. Platelet deposition in the individual compartments of the shunt assembly was measured over a 60-minute perfusion period using a high sensitivity 99Tc collimator and scintillation camera (GE 400T, General Electric) imaging of the 172 keV ^{111}In photon peak at 5-min intervals. Thrombogenic devices were assembled and inserted into shunts, as detailed previously.[35]

Statistical Analysis. Two-tailed student's t-test assuming unequal variances was used to test for statistical significance between the means of two groups.

Generation of TM_{LPETG} The minimal fragment of human thrombomodulin, epidermal growth factor-like domains 4 – 6 (TM456) was cloned into the Sigma pFLAG ATS expression vector. Amino acid changes relative to the native TM456 sequence are underlined:

TM_{LPETG} (15.2 kDa):

MKKTAIAIAVALAGFATVAQADYKDDDDKVKLVEPVDPCFRANCEYQCQPLNQTS

YLCVCAEGFAPIPHEPHRCQLFCNQTACPADCDPNTQASCECPEGYILDDGFICTDID

ECENGGFCSGVCHNLPGTFECICGPDSALAGQIGTDCGGGGSGGGGSLPETGG

Note that highlighted in blue and underlined is the OmpA tag that facilitates transport of TM_{LPETG} to the periplasmic space of E coli to optimize folding, this sequence is cleaved in final mature TM_{LPETG}. The FLAG peptide sequence is DYKDDDDK at the N-terminus. It has been previously demonstrated that the conversion of the internal methionine residue to leucine maximizes the stability of TM. A second mutation was made to convert the internal RH sequence, which is an active trypsin cleavage site, to GQ. The additional sequence at the C-terminus includes a GGGGSGGGGS spacer and the LPETG sortase recognition motif. An extra glycine was added at the C-terminus as this was previously demonstrated to maximize sortase activity.

Following transformation of chemically competent cells, a fresh LB agar plate was streaked with methionine auxotrophic cells containing the appropriate TM vector and incubated at 37 ºC overnight. A single cell colony was then inoculated into 50 mL of Novagen media supplemented with 0.4 % glucose and 50 µg/mL ampicillin and cultured at 37 ºC, 225 RPM, for 16 h. A total of 25 mL of fully grown starter culture (OD600 = 1.20) was added per 500 mL of Novagen media supplemented with 0.4 % glucose and 50 µg/mL ampicillin, and cultured at 37 ºC, 225 RPM. Upon cell growth to OD600 = ~0.9, IPTG was added at a final concentration of 1 mM to

induce TM_{LPETG} expression, and the culture was incubated for an additional 4 h at 37 ºC, 225 RPM. Cell cultures were centrifuged at 4,000x RCF at 4 ºC for 10 minutes and stored at 4 ºC.

Standard osmotic shock protocol was performed on stored cell pellets to extract the crude periplasmic proteins. Cell pellets were first warmed to room temperature and re-suspended in 40 ml/g cells of 0.5 M sucrose, 0.03 M Tris-HCl (pH 8.0) at a final pH of 8.0 per gram of cells. Suspended cells were evenly distributed into round bottom centrifuge tubes (60 mL per tube). A total of 120 µL of 500 mM sucrose was added to each tube to achieve final 1 mM EDTA concentration and incubate with gentle shaking for 10 minutes at RT. The cell suspension was centrifuged at 3,500x g for 10 min at 10 °C and the supernatant decanted. The cell pellet was rapidly resuspended in 25 mL/g cell pellet ice-cold, distilled water (40 mL per tube is sufficient) for 10 minutes and the cell suspension centrifuged at 3,500x RCF for 10 min at 4 °C. A total of 35 mL of supernatant was removed from each tube and transferred to clean round bottom centrifuge tubes. These were clarified by further centrifugation at 25,000x RCF for 25 min at 4 °C and sterilized using a 0.22 µm filtration system. Anti-FLAG immunoaffinity chromatography (Sigma) was performed on the clarified supernatant per manufacturer's instructions. SDS-PAGE analysis and total protein quantification were performed using standard Bradford assay (Bio-Rad) protocols from the manufacturer.

Bacterial Expression of Evolved Sortase and Wild-type Sortase. The amino acid sequence of the wild-type sortase and evolved sortase is provided below:

Wild-type sortase with N-terminal His-tag (19.5 kDa):

MASSHHHHHHDYDIPTTENLYFQGSQAKPQIPKDKSKVAGYIEIPDADIKEPVYPGPA

TPEQLNRGVSFAEENESLDDQNISIAGHTFIDRPNYQFTNLKAAKKGSMVYFKVGNE

TRKYKMTSIRDVKPTDVGVLDEQKGKDKQLTLITCDDYNEKTGVWEKRKIFVATEV
K

Evolved sortase with C-terminal His-tag (17.9 kDa) and mutations underlined:

MQAKPQIPKDKSKVAGYIEIPDADIKEPVYPGPATREQLNRGVSFAEENESLDDQNIS
IAGHTFIDRPNYQFTNLKAAKKGSMVYFKVGNETRKYKMTSIR**N**VKPTAVEVLDEQ
KGKDKQLTLITCDDYNEETGVWE**T**RKIFVATEVKLEHHHHHH

E. coli BL21 transformed with pET29 wild-type sortase or evolved sortase expression plasmids were cultured at 37 °C and 225 RPM in LB media supplemented with 50 μg/mL kanamycin. Upon OD600 = 0.8, IPTG was added to a final concentration of 0.4 mM and protein expression was induced for 3 h at 30 °C. The cells were harvested by centrifugation and resuspended in lysis buffer (50 mM Tris pH 8.0, 300 mM NaCl supplemented with 1 mM MgCl2, 2 units/mL DNAseI (NEB), 260 nM aprotinin, 1.2 μM leupeptin, and 1 mM PMSF). Cells were lysed by sonication on ice and the clarified supernatant was purified by column chromatography using Cobalt Talon Resin (Clontech Laboratories) following the manufacturer's instructions. Fractions that were >95 % purity, as judged by SDS-PAGE, were consolidated and dialyzed against Tris-buffered saline (25 mM Tris pH 7.5, 150 mM NaCl) using PD-10 columns (GE Healthcare) and stored as 5 mg/mL stocks at 4 °C.

Solution phase sortase transpeptidation reactions. TM_{LPETG} was reacted with 0.1 or 2 molar equiv WT or 0.1 molar equiv eSrtA and 1, 10, or 100 molar equiv NH_2-PEG_{5kDa} (Nektar) at room temperature. At various reaction time points, a 2 μg aliquot was removed and frozen at -80 °C. Upon completion of the study, all aliquots were thawed at room temperature and

incubated at 100 °C in 1x reducing buffer (Fisher Scientific), and run on a 12 % Tris PAGE gel (Biorad) and visualized by Coommassie staining. The stained gels were dried and scanned at 1200 dpi on an Epson Perfection 1660 photo scanner, and quantification of the extent of TM-PEG formation relative to unreacted TM_{LPETG} was performed using the Gel Analyzer function in ImageJ software.

To generate TM-PEG_3-N_3 using sortase catalyzed transpeptidation, TM_{LPETG} was reacted with 0.1 molar equiv eSrtA and 100 molar excess NH_2-PEG_3-N_3 (Sigma) for 2 h at room temperature. The crude reaction mixture was run through a chromatography column containing Cobalt Talon Resin to remove His-tagged eSrtA, and the flow through was collected and dialyzed against TBS buffer (20 mM Tris pH 7.5, 100 mM NaCl) to remove excess unreacted NH_2-PEG_3-N_3. Following 2 days of dialysis with regular buffer exchanges approximately every 8 h, the final reaction mixture was concentrated and the final yield determined by total protein quantification per manufacturer's protocol (Bio-Rad).

The extent of azide tagging of TM_{LPETG} was determined by incubating the final reaction mixture with excess DBCO-biotin (Invitrogen) overnight at 37 °C. Unreacted DBCO-biotin was removed by 2x sequential dialysis using Zeba Spin Desalting Columns with a 7 kDa MWCO (Fisher Scientific). Final concentration of the dialyzed reaction mixture was determined by total protein quantification per manufacturer's protocol (Bio-Rad). The extent of biotinylation of TM-N_3 by DBCO-biotin was confirmed using a fluorescent biotin quantification kit per manufacturer's instructions (Fisher Scientific).

References

1 Jordan, S. W. & Chaikof, E. L. Novel thromboresistant materials. *Journal of vascular surgery* **45**, A104-A115 (2007).

2 Li, S. & Henry, J. J. Nonthrombogenic approaches to cardiovascular bioengineering. *Annual review of biomedical engineering* **13**, 451-475 (2011).

3 Douketis, J. D. *et al.* The Perioperative Management of Antithrombotic TherapyAmerican College of Chest Physicians Evidence-Based Clinical Practice Guidelines. *CHEST Journal* **133**, 299S-339S (2008).

4 Tatterton, M., Wilshaw, S.-P., Ingham, E. & Homer-Vanniasinkam, S. The use of antithrombotic therapies in reducing synthetic small-diameter vascular graft thrombosis. *Vascular and endovascular surgery* **46**, 212-222 (2012).

5 Conte, M. S. The ideal small arterial substitute: a search for the Holy Grail? *The FASEB journal* **12**, 43-45 (1998).

6 Kapadia, M. R., Popowich, D. A. & Kibbe, M. R. Modified prosthetic vascular conduits. *Circulation* **117**, 1873-1882 (2008).

7 Ratner, B. D. The catastrophe revisited: blood compatibility in the 21st century. *Biomaterials* **28**, 5144-5147 (2007).

8 Zilla, P., Bezuidenhout, D. & Human, P. Prosthetic vascular grafts: wrong models, wrong questions and no healing. *Biomaterials* **28**, 5009-5027 (2007).

9 Ma, P. X. Biomimetic materials for tissue engineering. *Advanced Drug Delivery Reviews* **60**, 184-198 (2008).

10 Place, E. S., Evans, N. D. & Stevens, M. M. Complexity in biomaterials for tissue engineering. *Nature materials* **8**, 457-470 (2009).

11 Crapo, P. M., Gilbert, T. W. & Badylak, S. F. An overview of tissue and whole organ decellularization processes. *Biomaterials* **32**, 3233-3243 (2011).

12 Qu, Z. & Chaikof, E. L. Interface between hemostasis and adaptive immunity. *Current opinion in immunology* **22**, 634-642 (2010).

13 Furie, B. & Furie, B. C. Mechanisms of thrombus formation. *New England Journal of Medicine* **359**, 938-949 (2008).

14 Gott, V. L., Whiffen, J. D. & Dutton, R. C. Heparin bonding on colloidal graphite surfaces. *Science* **142**, 1297-1298 (1963).

15 Linhardt, R. J., Murugesan, S. & Xie, J. Immobilization of heparin: approaches and applications. *Current topics in medicinal chemistry* **8**, 80-100 (2008).

16 Lindholt, J. S. *et al.* The Scandinavian Propaten< sup>®</sup> Trial–1-Year Patency of PTFE Vascular Prostheses with Heparin-Bonded Luminal Surfaces Compared to Ordinary Pure PTFE Vascular Prostheses–A Randomised Clinical Controlled Multi-centre Trial. *European Journal of Vascular and Endovascular Surgery* **41**, 668-673 (2011).

17 Bosiers, M. *et al.* Heparin-bonded expanded polytetrafluoroethylene vascular graft for femoropopliteal and femorocrural bypass grafting: 1-year results. *Journal of vascular surgery* **43**, 313-318 (2006).

18 Lensvelt, M. *et al.* Results of heparin-bonded ePTFE-covered stents for chronic occlusive superficial femoral artery disease. *Journal of vascular surgery* **56**, 118-125 (2012).

19 Bishop, J. R., Schuksz, M. & Esko, J. D. Heparan sulphate proteoglycans fine-tune mammalian physiology. *Nature* **446**, 1030-1037 (2007).

20 de Agostini, A. I., Watkins, S. C., Slayter, H. S., Youssoufian, H. & Rosenberg, R. D. Localization of anticoagulantly active heparan sulfate proteoglycans in vascular endothelium: antithrombin binding on cultured endothelial cells and perfused rat aorta. *The Journal of cell biology* **111**, 1293-1304 (1990).

21 HajMohammadi, S. *et al.* Normal levels of anticoagulant heparan sulfate are not essential for normal hemostasis. *Journal of Clinical Investigation* **111**, 989-999 (2003).

22 Conway, E. M. in *Seminars in immunopathology.* 107-125 (Springer).

23 Esmon, C. T. The roles of protein C and thrombomodulin in the regulation of blood coagulation. *J Biol Chem* **264**, 4743-4746 (1989).

24 Dahlbäck, B. & Villoutreix, B. O. Regulation of Blood Coagulation by the Protein C Anticoagulant Pathway Novel Insights Into Structure-Function Relationships and Molecular Recognition. *Arteriosclerosis, thrombosis, and vascular biology* **25**, 1311-1320 (2005).

25 Kishida, A., Ueno, Y., Maruyama, I. & Akashi, M. Immobilization of human thrombomodulin onto biomaterials: Comparison of immobilization methods and evaluation of antithrombogenicity. *ASAIO journal* **40**, M840-M845 (1994).

26 Sperling, C. *et al.* Immobilization of human thrombomodulin onto PTFE. *Journal of Materials Science: Materials in Medicine* **8**, 789-791 (1997).

27 Vasilets, V. *et al.* Microwave CO< sub> 2</sub> plasma-initiated vapour phase graft polymerization of acrylic acid onto polytetrafluoroethylene for immobilization of human thrombomodulin. *Biomaterials* **18**, 1139-1145 (1997).

28 Li, J.-m. *et al.* Immobilization of human thrombomodulin to expanded polytetrafluoroethylene. *Journal of surgical research* **105**, 200-208 (2002).

29 Sperling, C., Salchert, K., Streller, U. & Werner, C. Covalently immobilized thrombomodulin inhibits coagulation and complement activation of artificial surfaces in vitro. *Biomaterials* **25**, 5101-5113 (2004).

30 Wu, B., Gerlitz, B., Grinnell, B. W. & Meyerhoff, M. E. Polymeric coatings that mimic the endothelium: combining nitric oxide release with surface-bound active thrombomodulin and heparin. *Biomaterials* **28**, 4047-4055 (2007).

31 Yeh, H.-Y. & Lin, J.-C. Bioactivity and platelet adhesion study of a human thrombomodulin-immobilized nitinol surface. *Journal of Biomaterials Science, Polymer Edition* **20**, 807-819 (2009).

32 Allison, D. A review: taking the sterile out of sterility. *Journal of applied microbiology* **87**, 789-793 (1999).

33 Lambert, B. J., Mendelson, T. A. & Craven, M. D. Radiation and ethylene oxide terminal sterilization experiences with drug eluting stent products. *AAPS PharmSciTech* **12**, 1116-1126 (2011).

34 Mendes, G. C., Brandao, T. R. & Silva, C. L. Ethylene oxide sterilization of medical devices: a review. *American journal of infection control* **35**, 574-581 (2007).

35 Qu, Z. *et al.* A biologically active surface enzyme assembly that attenuates thrombus formation. *Advanced functional materials* **21**, 4736-4743 (2011).

36 Lin, F. L., Hoyt, H. M., Van Halbeek, H., Bergman, R. G. & Bertozzi, C. R. Mechanistic investigation of the Staudinger ligation. *Journal of the American Chemical Society* **127**, 2686-2695 (2005).

37 Ton-That, H., Liu, G., Mazmanian, S. K., Faull, K. F. & Schneewind, O. Purification and characterization of sortase, the transpeptidase that cleaves surface proteins of Staphylococcus aureus at the LPXTG motif. *Proceedings of the National Academy of Sciences* **96**, 12424-12429 (1999).

38 Huang, X. *et al.* Kinetic mechanism of Staphylococcus aureus sortase SrtA. *Biochemistry* **42**, 11307-11315 (2003).

39 Frankel, B. A., Kruger, R. G., Robinson, D. E., Kelleher, N. L. & McCafferty, D. G. Staphylococcus aureus sortase transpeptidase SrtA: insight into the kinetic mechanism

and evidence for a reverse protonation catalytic mechanism. *Biochemistry* **44**, 11188-11200 (2005).

40 Xie, J. & Schultz, P. G. An expanding genetic code. *Methods* **36**, 227-238 (2005).

41 Popp, M. W. L. & Ploegh, H. L. Making and breaking peptide bonds: protein engineering using sortase. *Angewandte Chemie International Edition* **50**, 5024-5032 (2011).

42 Proft, T. Sortase-mediated protein ligation: an emerging biotechnology tool for protein modification and immobilisation. *Biotechnology letters* **32**, 1-10 (2010).

43 Fuentes-Prior, P. *et al.* Structural basis for the anticoagulant activity of the thrombin–thrombomodulin complex. *Nature* **404**, 518-525 (2000).

44 Cazalis, C. S., Haller, C. A., Sease-Cargo, L. & Chaikof, E. L. C-terminal site-specific PEGylation of a truncated thrombomodulin mutant with retention of full bioactivity. *Bioconjugate chemistry* **15**, 1005-1009 (2004).

45 Tsukiji, S. & Nagamune, T. Sortase-Mediated Ligation: A Gift from Gram-Positive Bacteria to Protein Engineering. *ChemBioChem* **10**, 787-798 (2009).

46 Chen, I., Dorr, B. M. & Liu, D. R. A general strategy for the evolution of bond-forming enzymes using yeast display. *Proceedings of the National Academy of Sciences*, doi:10.1073/pnas.1101046108 (2011).

47 Ling, J. J., Policarpo, R. L., Rabideau, A. E., Liao, X. & Pentelute, B. L. Protein Thioester Synthesis Enabled by Sortase. *Journal of the American Chemical Society* **134**, 10749-10752, doi:10.1021/ja302354v (2012).

48 Pisal, D. S., Kosloski, M. P. & Balu-Iyer, S. V. Delivery of therapeutic proteins. *Journal of pharmaceutical sciences* **99**, 2557-2575 (2010).

49 Larson, N. & Ghandehari, H. Polymeric conjugates for drug delivery. *Chemistry of Materials* **24**, 840-853 (2012).

50 Sletten, E. M. & Bertozzi, C. R. Bioorthogonal chemistry: fishing for selectivity in a sea of functionality. *Angewandte Chemie International Edition* **48**, 6974-6998 (2009).

51 Jewett, J. C. & Bertozzi, C. R. Cu-free click cycloaddition reactions in chemical biology. *Chemical Society Reviews* **39**, 1272-1279 (2010).

52 Ning, X., Guo, J., Wolfert, M. A. & Boons, G. J. Visualizing metabolically labeled glycoconjugates of living cells by copper-free and fast Huisgen cycloadditions. *Angewandte Chemie International Edition* **47**, 2253-2255 (2008).

53 El-Kurdi, M. S. *et al.* Transient elastic support for vein grafts using a constricting microfibrillar polymer wrap. *Biomaterials* **29**, 3213-3220 (2008).

54 Deutsch, M. *et al.* Long-term experience in autologous in vitro endothelialization of infrainguinal ePTFE grafts. *Journal of vascular surgery* **49**, 352-362 (2009).

55 Myers Jr, D. D. Nonhuman primate models of thrombosis. *Thrombosis research* **129**, S65-S69 (2012).

56 Cadroy, Y., Maraganore, J. M., Hanson, S. R. & Harker, L. A. Selective inhibition by a synthetic hirudin peptide of fibrin-dependent thrombosis in baboons. *Proceedings of the National Academy of Sciences* **88**, 1177-1181 (1991).

57 Hanson, S. R. & Sakariassen, K. S. Blood flow and antithrombotic drug effects. *American heart journal* **135**, S132-S145 (1998).

58 Gruber, A. & Hanson, S. R. Factor XI–dependence of surface-and tissue factor–initiated thrombus propagation in primates. *Blood* **102**, 953-955 (2003).

59 Harker, L. A. *et al.* Clopidogrel inhibition of stent, graft, and vascular thrombogenesis with antithrombotic enhancement by aspirin in nonhuman primates. *Circulation* **98**, 2461-2469 (1998).

60 Lin, P. H. *et al.* Small-caliber heparin-coated ePTFE grafts reduce platelet deposition and neointimal hyperplasia in a baboon model. *Journal of vascular surgery* **39**, 1322-1328 (2004).

61 Krishnamurthy, V. R. *et al.* Chemoselective immobilization of peptides on abiotic and cell surfaces at controlled densities. *Langmuir* **26**, 7675-7678 (2010).

62 Hanson, S. R. *et al.* Antithrombotic effects of thrombin-induced activation of endogenous protein C in primates. *Journal of Clinical Investigation* **92**, 2003 (1993).

63 Jordan, S. W. *et al.* The effect of a recombinant elastin-mimetic coating of an ePTFE prosthesis on acute thrombogenicity in a baboon arteriovenous shunt. *Biomaterials* **28**, 1191-1197 (2007).

Chapter Four

In situ Regeneration of Bioactive Coatings

Zheng Qu, Brent M. Dorr, Erbin Dai, Carolyn A. Haller, Wookhyun Kim, Hyun O. Ham, David R. Liu & Elliot L. Chaikof

Zheng Qu initiated and performed the catheter synthesis, TM synthesis and stripping/recharging experiments in this chapter. I provided eSrtA protein and plasmids and developed the whole blood labeling protocols. Zheng and I jointly developed the idea for the reversible immobilization scheme.

Some of the text in this chapter is currently under review for publication.

Abstract

The immobilization of biologically active catalysts on solid supports is a central paradigm in bioprocessing industries and in the design of medical device and diagnostics. Degradation of surface activity in the operating environment by stresses such as oxidation, hydrolysis, and proteolysis often limits their long term performance. Here we show the site-specific covalent immobilization of biologically active molecules and their regeneration through a two-step stripping and recharging cycle. Reversible transpeptidation by a laboratory-evolved *Staphylococcus aureus* Sortase A (eSrtA) enabled the rapid immobilization of an antithrombogenic film in the presence of whole blood, as well as multiple cycles of film regeneration *in vitro* that preserved its biological activity. Moreover, medical devices can be modified *in situ* by eSrtA transpeptidation after *in vivo* implantation to immobilize or remove film constituents. These studies establish a rapid, orthogonal, and reversible surface chemistry scheme to regenerate selective molecular constitutents that can dramatically extend the lifetime of bioactive films in a manner akin to living systems.

Introduction

Medical devices in blood contacting applications such as stents, extracorporeal support systems, and vascular access catheters are prone to life threatening complications initiated by maladaptive host biological responses at the blood-material interface[1,2]. Immobilization of bioactive molecules and drug eluting assemblies on implantable devices has yielded promising combination products that abrogate thrombotic cascades and detrimental inflammation[3], enhance device integration and regeneration of healthy tissue[4,5], and inhibit microbial colonization[6]. Clinical translation of these strategies for permanent implants has been constrained, in part, by the limited therapeutic duration afforded by a finite surface reservoir of bioactive agents, as well

as degradation of surface components following exposure to the physiological environment[6,7]. Efforts to improve biostability and bioactivity have included the manipulation of surface properties such as hydrophilicity, charge, and topography[8], immobilization chemistry[9,10], as well as rational and evolutionary protein engineering[11]. Despite recent progress in these areas, a surface coating for implantable devices that reliably retains biological activity for a commercially and clinically viable time scale has not been developed.

Local or systemic delivery of bioactive therapeutic payloads that target the blood contacting surface of medical implants may facilitate *in situ* regeneration of bioactivity. This concept has been explored previously in clinical applications such as targeted drug delivery[12,13], molecular imaging[14], and minimally invasive cell therapy[15]. In principle enzyme ligation offers an opportunity for catalyzing reversible bond forming reactions that could enable the molecular regeneration of bioactive thin films *in situ*. *Staphylococcus aureus* sortase A (SrtA) catalyzes the

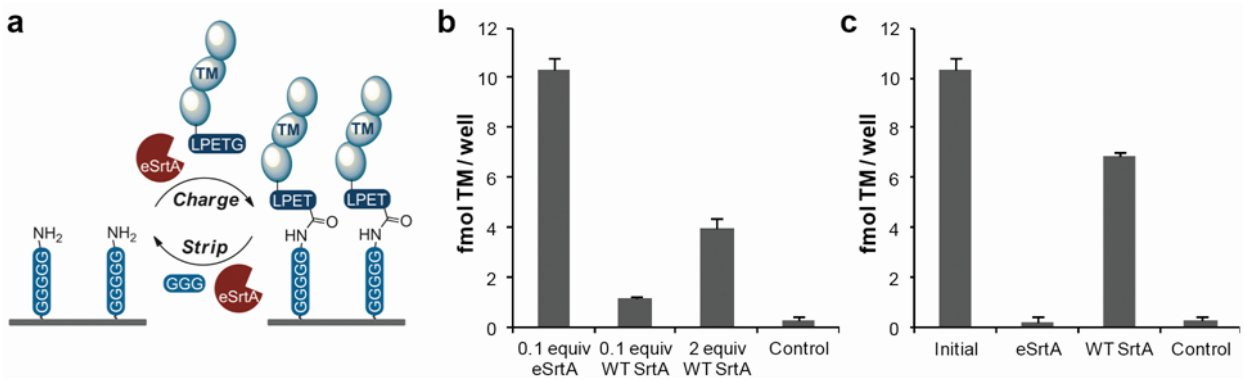

Figure 4-1 Sortase-catalyzed rechargeable assembly of LPETG-labeled thrombomodulin (TM_{LPETG}) on pentaglycine modified model surfaces.

(A) Two-step "rechargeable" surface assembly cycle initiated by sortase-catalyzed charging of LPETG-tagged biomolecules on pentaglycine modified surfaces, followed by sortase-catalyzed stripping to regenerate pentaglycine anchor sites for additional surface reaction cycles. (B) Immobilization of 1 µM TM_{LPETG} on pentaglycine coated microwells using 0.1 molar equivalents evolved sortase (eSrtA), 0.1 and 2 molar equivalents wild-type sortase (WT SrtA), or no sortase as a negative control. (C) Following immobilization of 1 µM TM_{LPETG} on pentaglycine coated microwells using 0.1 molar equivalents eSrtA, removal of bound TM was carried out using 20 µM of either evolved eSrtA or WT SrtA with 1 mM triglycine. Error bars denote standard deviation ($n \geq 3$).

covalent tra nspeptidation of a C-terminal "sorting motif" LPXTG to N-terminal oligoglycine (e.g. GGG) nucleophiles through an acyl-enzyme complex forming a LPXT-GGG bond[16]. Due to its synthetic simplicity and the very limited occurrence of the LPXTG motif in native proteins, SrtA-catalyzed transpeptidation has been broadly applied in protein purification, labeling, and immobilization onto solid supports[17-19]. However, the low catalytic activity and substrate affinity of wild type (WT) SrtA necessitates high molar excess of the enzyme and long incubation times to approach reaction completion, limiting its effectiveness and applicability. An evolved SrtA mutant (eSrt A) has recently been generated that exhibits 120-fold higher LPETG-ligation activity than the wild-type enzyme.[20] This enzyme raises the possibility of multiple rapidly catalyzed c ycles of removal and reversible assembly of bioactive molecular films onto oligoglycine mo dified surfaces both *in vitro* and *in vivo*.

Results

Reversible assembly of thrombo modulin.

We were the first to characterize the effectiveness of thrombomodulin (TM) in abrogating

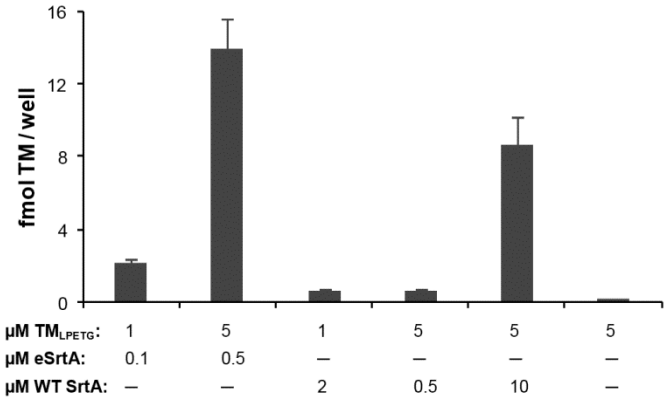

Figure 4-2 Sortase-catalyzed immobilization of LPETG-tagged thrombomodulin (TM_{LPETG}) on pentaglycine surfaces in the presence of whole blood.

Direct sortase-catalyzed assembly of TM_{LPETG} in 50% v/v heparinized whole blood (20 U heparin/mL blood) at 37 °C for 1 h without additional calcium. Evolved and wild-type (WT) sortases were tested at 2 different TM_{LPETG} concentrations as well as TM_{LPETG}/sortase ratios. Error bars denote standard deviation ($n \geq 4$).

tissue factor induced thrombin production under controlled venous and arterial flow conditions[21-23]. Materials functionalized with TM, a major physiological inhibitor of thrombin generation[24,25], exhibit reduced thrombogenicity *in vitro* and *in vivo*[26-35], thereby, supporting the clinical feasibility of a new paradigm in an tithrombotic surface design. To demonstrate the site-specific reversible assembly of TM on oligoglycine surfaces (Figure 4-1A), we first generated a recombinant human TM fragment containing a C-terminal LPETG motif (TM_{LPETG}). WT SrtA and an eSrtA produced by directed evolution using a yeast display system were generated, as previously reported[20] Model pentaglycine surfaces, which match the natural SrtA substrate on the *S. aureus* cell wall,[36] were generated by immobilizing a biotinylated pentaglycine peptide (NH_2-GGGGGK-biotin) on surfaces pre-coated with streptavidin. Surface immobilization of TM_{LPETG} by eSrtA yielded ~9-fold higher surface TM density than WT SrtA. Notably, this surface density of TM would require at least 20-fold higher quantities of WT SrtA catalyst than

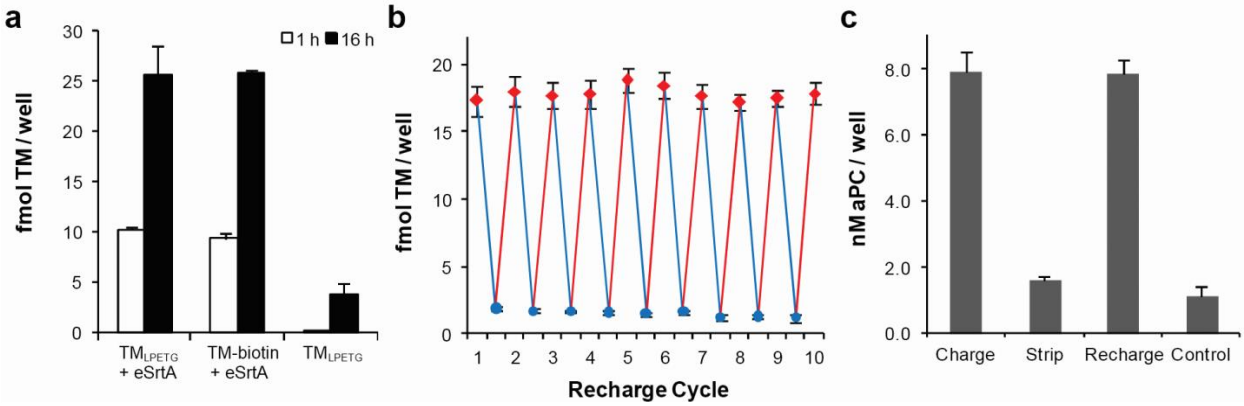

Figure 4-3 Rapid repetitive recharging of LPETG-tagged thrombomodulin (TM_{LPETG}) on pentaglycine surfaces by evolved sortase A (eSrtA).

(A) Sortase-catalyzed binding of TM_{LPETG} on pentaglycine modified model surfaces following 1 and 16 h reaction were compared with the binding of biotinylated TM (TM-biotin) directly on streptavidin coated microwells. In parallel, TM_{LPETG} was incubated in microwells without sortase as a negative control. (B) Sequential eSrtA-catalyzed charging (red) and stripping (blue) cycles of TM_{LETPG} performed on model pentaglycine surfaces. (C) Cofactor activity of immobilized TM to catalyze production of activated protein C (aPC) following the initial assembly of TM_{LPETG}, stripping by eSrtA, and regeneration of TM_{LPETG} by eSrtA. Error bars denote standard deviation ($n \geq 3$).

eSrtA (Figure 4-1B). Near complete removal of immobilized TM films could be achieved with eSrtA in 30 minutes, whereas WT SrtA was substantially less efficient w hen reacted under identical conditions (Figure 4-1C). In this surface coupling scheme, the surface-binding kinetics of TM_{LPETG} by eSrtA nearly matched that of biotin-avidin binding (Figure 4-2A), a well-established bioconjugation met hod. Up to ten repetitive recharge cycles were accomplished using eSrtA to reproducibly regenerate the TM film assembly (Figure 4-2B) with no significant loss of the ability of the TM films to catalyze generation of activated protein C (Figure 4-2C). These results confirm the enhanced catalytic activity of eSrtA as a critical enabling step in the application of a two-step strip/recharge scheme for rapid and repetitive regeneration of biologically active molecular films.

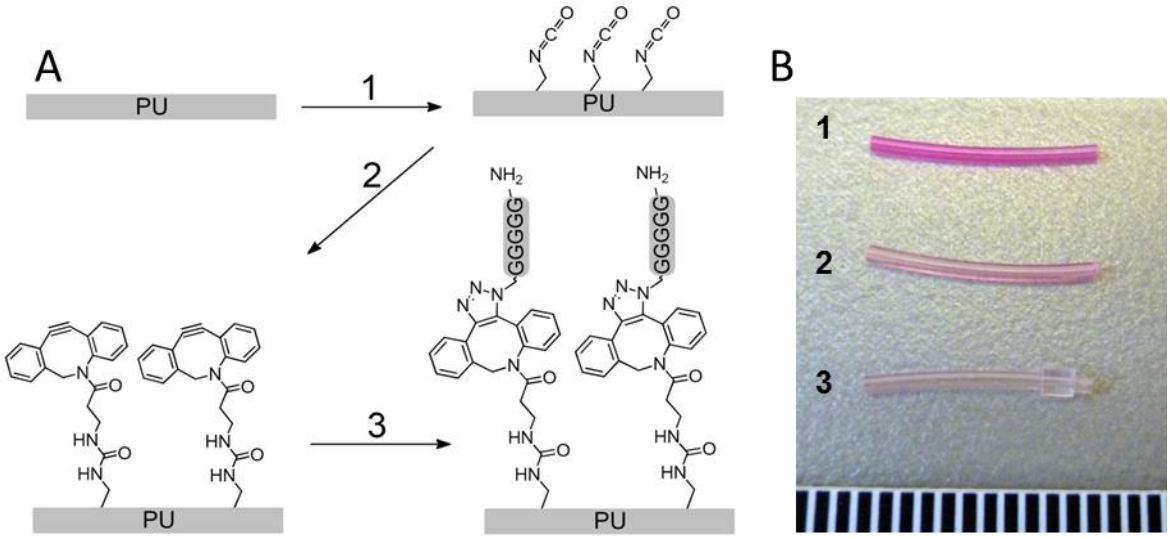

Figure 4-4 Sequential surface reaction scheme to modify polyurethane catheters with pentaglycine motifs.

(A) Reaction conditions: (1) hexamethylene diisocyanate / triethylamine; (2) DBCO-amine / triethylamine; (3) NH_2-GGGGG-N_3

(B) Dibenzocyclooctyne (DBCO) modified polyurethane catheters reacted specifically with rhodamine azide probes. Representative image of samples: (1) DBCO catheters reacted with rhodamine azide; (2) plain catheter reacted with rhodamine azide; (3) DBCO modified catheter reacted with rhodamine B**.**

Assembly of thrombomoduli n in whole blood.

Due to the rarity of LPETG and GGG motifs in the physiological environment, the two-step strip/recharge reaction by eSrtA should provide a feasible strategy to regenerate films on medical implants *in situ*. As a proof-of-concept, we demonstrated the ability to immobilize TM_{LPETG} on pentaglycine surfaces in 50% v/v whole blood at 37 ºC We observed that eSrtA was capable of efficiently functionalizing these model surfaces >20-fold more effectively than WT SrtA (Figure 4-3), consistent with predictions based upon their *in vitro* kinetics, and at levels comparable to what we achieved in completely defined reaction buffer. These results highlight the enhanced activity of eSrtA as an enabling step towards *in situ* assembly of molecular films at the blood contacting interface of medical implants.

Reversible assembly of molecular films on venous access catheters in vivo.

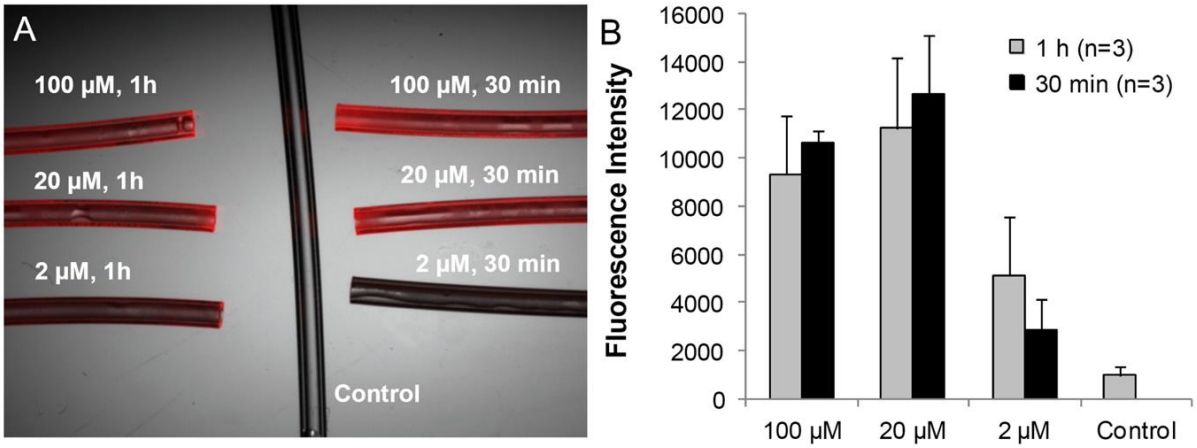

Figure 4-5 Immobilization of LPETG-tagged biotin on pentaglycine modified polyurethane (PU) catheters by eSrtA.

(A) Representative merged fluorescent and bright field microscopy image of PU catheters modified with pentaglycine motifs, and reacted with various concentrations of biotin-LPETG peptide for 30 min or 1 h. A total of 0.1 molar equivalent eSrtA relative to biotin-LPETG was used for all reaction conditions. At the end of reaction, Cy3-labeled streptavidin was incubated at 0.1mg/mL with catheters for 30 min to assess the surface density of biotin. (B) Fluorescence intensity was measured using Image J and expressed as mean ± std. dev. for 3 individual catheter segments per concentration of biotin-LPETG used.

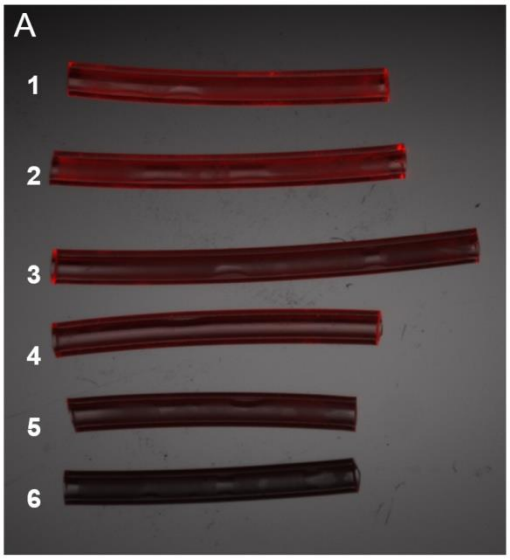

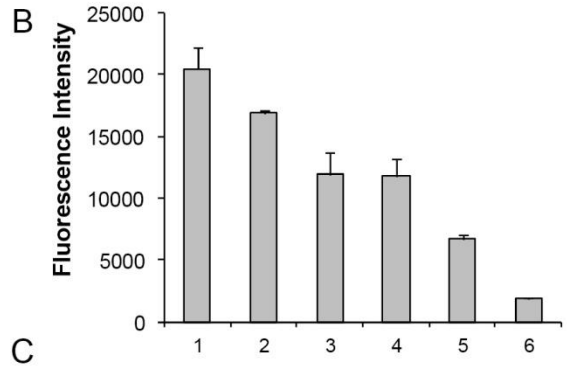

C

	Reaction Condition	% Stripped
1	Biotin-LPETGGGG-catheter (positive control)	–
2	100 μM GGG + 2 μM SrtA, 10 min	20
3	100 μM GGG + 10 μM SrtA, 10 min	50
4	100 μM GGG + 2 μM SrtA, 30 min	50
5	100 μM GGG + 10 μM SrtA, 30 min	70
6	GGG-catheter (negative control)	–

Figure 4-6 Removal of LPETG-tagged biotin immobilized on pentaglycine modified polyurethane (PU) catheters.

(A) Representative merged fluorescent and bright field microscopy image of PU catheters modified with pentaglycine motifs and reacted with biotin-LPETG/eSrtA, and stripped using various concentrations of GGG peptide and eSrtA as summarized in (C). Cy3-labeled streptavidin was incubated at 0.1mg/ml with catheters for 30 min to assess the surface density of biotin. (B) Fluorescence intensity was measured using Image J and expressed as mean ± standard deviation for three individual catheter segments per reaction condition.

Polyurethane (PU) venous access catheters are routinely used in the clinic, but have substantial complications related to thrombosis and infection that may be reduced by surface immobilization of bioactive molecular films[37-39]. *In situ* eSrtA transpeptidation was used to imm obilize and remove LPETG-tagged probes on pentaglycine modified PU catheters deployed in the mouse vena cava. PU catheters were modified with cyclooctyne motifs using a sequential scheme (Figure 4-4A), as previously reported[35], and azide reactivity was confirmed using rhodamine azide probes (Figure 4-4B). Azide-tagged pentaglycine peptide (NH_2-GGGGG-N_3) was used to generate pen taglycine motifs on PU catheters. Optimal reaction parameters that maximized eSrtA-catalyzed assembly of a biotin-LPETG probe were first determined *ex vivo* (Figures 4-5 and 4-6). Pentaglycine- modified catheters were deployed in the vena cava of live mice, followed by systemic administration of eSrtA and either LPETG tagged probes or

triglycine (GGG) to charge or strip the catheter surface, respectively. Real time fluorescent imaging confirmed near complete removal of LPETG tagged near-IR probes from pentaglycine catheters in the presence of eSrtA and GGG within 1 h (Figures 4-7a and Figure 4-8). Analysis of explanted catheters confirmed the selective immobilization or removal of biotin-LPETG probes from pentaglycine catheters *in vivo* by intravenously delivered eSrtA in 1 h (Fig. 4-7B–C and Figure 4-8).

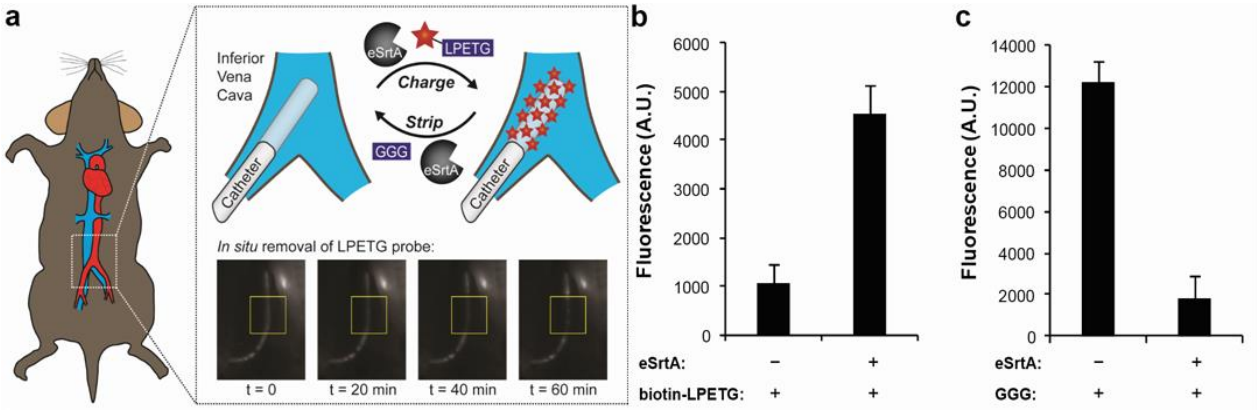

Figure 4-7 Sortase-catalyzed *in situ* assembly of LPETG-labeled probes on pentaglycine modified catheters deployed in mice vena cava.

(A) Reversible assembly of LPETG-labeled probes on pentaglycine modified catheters deployed *in vivo* may be achieved by intravenous delivery of eSrtA and triglycine peptide. Representative real time fluorescent imaging of a pentaglycine modified polyurethane catheter functionalized with LPETG-labeled Alexa Fluor 750 deployed in mouse vena cava and stripped by intravenous delivery of eSrtA and triglycine. (**B**) *In situ* eSrtA-catalyzed immobilization of LPETG-tagged biotin (biotin-LPETG) probes on pentaglycine modified catheters deployed in mice vena cava following 1 h reaction after intravenous delivery of biotin-LPETG and eSrtA. (C) *In situ* eSrtA-catalyzed removal of LPETG-tagged biotin probes from pentaglycine modified catheters deployed in mice vena cava following 1 h reaction after intravenous delivery of triglycine (GGG) and eSrtA. Error bars denote standard deviation ($n \geq 3$).

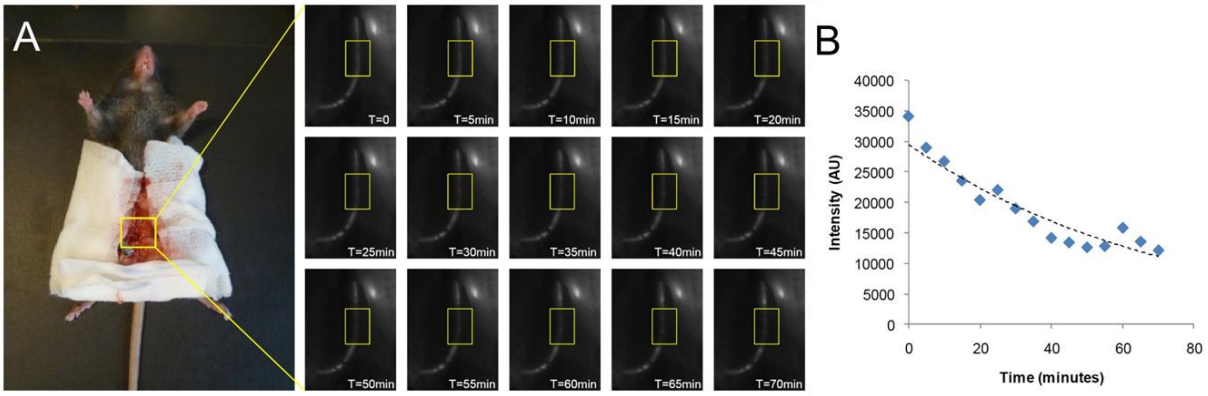

Figure 4-8 *In situ* removal of LPETG-tagged near-IR probes from pentaglycine modified polyurethane catheters deployed in mouse vena cava.

(A) Catheters modified with pentaglycine peptide and conjugated with LPETG labeled Alexa Fluor 750 was stripped by IV delivery of triglycine (400 µg) and 5'SrtA (700 µg). The near-IR fluorescent signal from the modified catheter was monitored using the Maestro multi-spectral fluorescence imaging system in real time over 70 min and (B) quantitative image analysis was performed to evaluate the fluorescent signal intensity of the modified catheters.

Discussion

The principle that anti-thrombogenic films on blood contacting devices may yield improved clinical outcomes has been supported by promising results reported from randomized clinical trials of heparin-bonded prostheses in the femoropopliteal position. Enhanced 1-yr patency was demonstrated for heparin-bonded Dacron® grafts when compared to non-coated PTFE (75% vs. 58%, $p = 0.037$)[40]. Likewise, superior 1-year results have been recently reported for heparin-bonded PTFE (Propaten®) when compared to non-coated PTFE (81% vs. 69%, $p = 0.03$), particularly for those patients with critical limb ischemia (80% vs. 58%, $p = 0.03$)[41]. Initial analysis of heparin-bonded PTFE covered stents in the superficial femoral artery suggests a similar effect[42,43]. Nonetheless, the surface heparin effect is not sustained; with loss of heparin activity on Dacron grafts within 3 months and within 6 months after implantation of Propaten grafts in a sheep model[44,45].

Current techniques to covalently modify surfaces with bioactive compounds have largely involved bioconjugate techniques that link nucleophilic motifs such as amines, thiols, and hydroxyls to their partner electrophiles[46]. Abundant presentation of these motifs in the complex chemical landscape of biological systems reduces the efficiency of targeting payloads for regenerating these device surfaces[47]. Recent efforts to modify blood contacting surfaces with bioactive molecules has lead to the application of a variety of bioorthogonal coupling chemistries, notably Staudinger Ligation and native chemical ligation, as well as Click cycloaddition and intein-mediated splicing[35,48-53]. However, these irreversible bond-forming approaches prohibit the *in situ* removal and regeneration of surface assemblies. Non-covalent strategies for "recharging" bioactive surfaces have been proposed through the use of metal-affinity[54], N-halamine structures[55], disulfide bonds[56], as well as biotin-avidin interaction[57], nonetheless, even under controlled *in vitro* conditions, repetitive regeneration using these schemes is challenging and would not be easily adaptable to surface regeneration *in vivo*.

We have determined that SrtA-catalyzed transpeptidation to site-specifically immobilize LPETG-tagged agents on pentaglycine modified surfaces enables the capacity to engineer highly specific, covalent, and rapidly "rechargeable" surfaces to sustain long term biological activity. In comparison with other chemoenzymatic approaches[58-60], the enhanced kinetics and bond forming efficiency afforded by directed evolution of SrtA was a critical enabling technology for this concept. We confirmed the capacity of eSrtA to catalyze multiple cycles of rapid assembly and removal of LPETG tagged biomolecules and established that such a strategy could be performed in the presence of whole blood. Taken together, our findings establish the capacity to rapidly and reproducibly regenerate selective molecular constituents after device implantation with the potential to dramatically extend the lifetime of bioactive films in a manner akin to living

systems. It is anticipated that such a strategy could be applied to stripping and regenerating any of a number of potential film constituents that display finite stability or activity.

Materials and Methods

Unless otherwise specified, all reagents were purchased from Sigma-Aldrich and used without further purification. The peptides NH_2-GGGGG-N_3, NH_2-GGGGGK-biotin, biotin-LPETG, and NH_2-LPETG were obtained from Genscript. LPETG-tagged Alexa Fluor 750 was synthesized using NH_2-LPETG peptide and Alexa Fluor 750 succinimidyl ester per manufacturer's instructions (Invitrogen).

Modification of catheters *in vitro*. Polyurethane catheters (SAI Infusion) with a 2 cm length and 1 F tip were first modified with pentaglycine anchor motifs. Catheters were reacted with 16% v/v hexamethylene diisocyanate (HDI) and 4% v/v triethylamine (TEA) in toluene at 50 °C for 1 h and rinsed in toluene for 6 h. Isocyanate activated catheters were reacted with 1 mg/mL dibenzocyclooctyne (DBCO)-amine linker (Click Chemistry Tools) and TEA (1% v/v) in toluene at 40 °C overnight, rinsed with toluene for 6 h, and dried under vacuum at 25 °C overnight. DBCO activated catheters were reacted with 1 mg/mL tetramethylrhodamine -5-carbonyl azide (Invitrogen) in 1:4 tert-butanol/PBS at 37 °C for 24 h followed by rinsing in methanol for 24 h to confirm surface cyclooctyne reactivity. DBCO activated catheters were reacted with NH_2-GGGGG-N_3 at 37 °C overnight and rinsed in TBS buffer (20 mM Tris pH 7.5, 100 mM NaCl). Pentaglycine modified catheters were incubated with biotin-LPETG or LPETG-labeled Alexa Fluor 750 peptide (2 µM to 100 µM) and 0.1 molar equivalents of eSrtA with relative to the LPETG probe concentration for 30 min or 1 h and rinsed for 4 h in TBS. Biotinylated catheters were incubated in 0.1 mg/mL Cy3-labeled streptavidin in TBS with 0.05%

Tween 20 for 30 min and rinsed overnight in TBS. Imaging of catheters was carried out using the Zeiss Discovery V20 Stereo Microscope and quantitative image analysis by ImageJ was performed to determine fluorescence intensity.

***In situ* modification of catheters deployed in mice.** Pentaglycine modified catheters were deployed approximately 1 cm within the vena cava via the femoral vein of C57BL/6 mice. All animals were maintained under anesthesia with isoflurane or ketamine on a heating pad. In order to functionalize pentaglycine modified catheters *in situ*, a 200 µL dose of 4 nmol eSrtA, 40 nmol LPETG-tagged biotin, and 20 U of heparin were injected intravenously through the catheter inlet. To demonstrate *in situ* removal of LPETG probes from pentaglycine modified catheters, a 200 µL dose of 40 nmol eSrtA, 2 µmol triglycine peptide, and 20 U of heparin were injected intravenously through the catheter inlet. After 1 h reaction, the mice were sacrificed and catheters were explanted and incubated in streptavidin-Cy3 (30 min) and washed with TBS buffer (2 h). Fluorescent and bright field microscopy images were obtained to detect biotin groups on the catheter surface. Real time tracking of the *in situ* removal of LPETG-tagged Alexa Fluor 750 was carried using a Maestro Multi-Spectral *in vivo* fluorescence imaging system with near-IR filter sets. Images were taken using a monochromatic 12-bit camera, and analyzed using ImageJ to determine fluorescence intensity.

Statistical Analysis. Two-tailed student's *t*-test assuming unequal variances was used to test for statistical significance between the means of two groups.

All other methods are as described in Chapter 3

References

1 Anderson, J. M., Rodriguez, A. & Chang, D. T. in *Seminars in immunology*. 86-100 (Elsevier).

2 Helmus, M. N., Gibbons, D. F. & Cebon, D. Biocompatibility: meeting a key functional requirement of next-generation medical devices. *Toxicologic pathology* **36**, 70-80 (2008).

3 Jordan, S. W. & Chaikof, E. L. Novel thromboresistant materials. *Journal of vascular surgery* **45**, A104-A115 (2007).

4 Ma, P. X. Biomimetic materials for tissue engineering. *Advanced Drug Delivery Reviews* **60**, 184-198 (2008).

5 de Mel, A., Jell, G., Stevens, M. M. & Seifalian, A. M. Biofunctionalization of biomaterials for accelerated in situ endothelialization: a review. *Biomacromolecules* **9**, 2969-2979 (2008).

6 Banerjee, I., Pangule, R. C. & Kane, R. S. Antifouling coatings: recent developments in the design of surfaces that prevent fouling by proteins, bacteria, and marine organisms. *Advanced Materials* **23**, 690-718 (2011).

7 Olsen, S. M., Pedersen, L. T., Laursen, M., Kiil, S. & Dam-Johansen, K. Enzyme-based antifouling coatings: a review. *Biofouling* **23**, 369-383 (2007).

8 Talbert, J. N. & Goddard, J. M. Enzymes on material surfaces. *Colloids and Surfaces B: Biointerfaces* **93**, 8-19 (2012).

9 Mateo, C., Palomo, J. M., Fernandez-Lorente, G., Guisan, J. M. & Fernandez-Lafuente, R. Improvement of enzyme activity, stability and selectivity via immobilization techniques. *Enzyme and Microbial Technology* **40**, 1451-1463 (2007).

10 Sheldon, R. A. Enzyme immobilization: the quest for optimum performance. *Advanced Synthesis & Catalysis* **349**, 1289-1307 (2007).

11 WoÈrn, A. & PluÈckthun, A. Stability engineering of antibody single-chain Fv fragments. *Journal of molecular biology* **305**, 989-1010 (2001).

12 Wu, A. M. & Senter, P. D. Arming antibodies: prospects and challenges for immunoconjugates. *Nature biotechnology* **23**, 1137-1146 (2005).

13 Ruoslahti, E., Bhatia, S. N. & Sailor, M. J. Targeting of drugs and nanoparticles to tumors. *The Journal of cell biology* **188**, 759-768 (2010).

14 Massoud, T. F. & Gambhir, S. S. Molecular imaging in living subjects: seeing fundamental biological processes in a new light. *Genes & development* **17**, 545-580 (2003).

15 Karp, J. M. & Leng Teo, G. S. Mesenchymal stem cell homing: the devil is in the details. *Cell stem cell* **4**, 206-216 (2009).

16 Marraffini, L. A., DeDent, A. C. & Schneewind, O. Sortases and the art of anchoring proteins to the envelopes of gram-positive bacteria. *Microbiology and Molecular Biology Reviews* **70**, 192-221 (2006).

17 Parthasarathy, R., Subramanian, S. & Boder, E. T. Sortase A as a novel molecular "stapler" for sequence-specific protein conjugation. *Bioconjugate chemistry* **18**, 469-476 (2007).

18 Chan, L. *et al.* Covalent attachment of proteins to solid supports and surfaces via sortase-mediated ligation. *PLoS one* **2**, e1164 (2007).

19 Ito, T. *et al.* Highly Oriented Recombinant Glycosyltransferases: Site-Specific Immobilization of Unstable Membrane Proteins by Using Staphylococcus aureus Sortase A. *Biochemistry* **49**, 2604-2614, doi:10.1021/bi100094g (2010).

20 Chen, I., Dorr, B. M. & Liu, D. R. A general strategy for the evolution of bond-forming enzymes using yeast display. *Proceedings of the National Academy of Sciences,* doi:10.1073/pnas.1101046108 (2011).

21 Tseng, P.-Y., Rele, S. S., Sun, X.-L. & Chaikof, E. L. Membrane–mimetic films containing thrombomodulin and heparin inhibit tissue factor-induced thrombin generation in a flow model. *Biomaterials* **27**, 2637-2650 (2006).

22 Tseng, P.-Y., Rele, S. M., Sun, X.-L. & Chaikof, E. L. Fabrication and characterization of heparin functionalized membrane-mimetic assemblies. *Biomaterials* **27**, 2627-2636 (2006).

23 Tseng, P.-Y., Jordan, S. W., Sun, X.-L. & Chaikof, E. L. Catalytic efficiency of a thrombomodulin-functionalized membrane-mimetic film in a flow model. *Biomaterials* **27**, 2768-2775 (2006).

24 Qu, Z. & Chaikof, E. L. Interface between hemostasis and adaptive immunity. *Current opinion in immunology* **22**, 634-642 (2010).

25 Esmon, C. T. Regulation of blood coagulation. *Biochimica et Biophysica Acta (BBA)-Protein Structure and Molecular Enzymology* **1477**, 349-360 (2000).

26 Kishida, A., Ueno, Y., Maruyama, I. & Akashi, M. Immobilization of human thrombomodulin on biomaterials: evaluation of the activity of immobilized human thrombomodulin. *Biomaterials* **15**, 1170-1174 (1994).

27 Kishida, A., Ueno, Y., Maruyama, I. & Akashi, M. Immobilization of human thrombomodulin onto biomaterials: Comparison of immobilization methods and evaluation of antithrombogenicity. *ASAIO journal* **40**, M840-M845 (1994).

28 Sperling, C. *et al.* Immobilization of human thrombomodulin onto PTFE. *Journal of Materials Science: Materials in Medicine* **8**, 789-791 (1997).

29 Sperling, C., Salchert, K., Streller, U. & Werner, C. Covalently immobilized thrombomodulin inhibits coagulation and complement activation of artificial surfaces in vitro. *Biomaterials* **25**, 5101-5113 (2004).

30 Vasilets, V. *et al.* Microwave CO< sub> 2</sub> plasma-initiated vapour phase graft polymerization of acrylic acid onto polytetrafluoroethylene for immobilization of human thrombomodulin. *Biomaterials* **18**, 1139-1145 (1997).

31 Wu, B., Gerlitz, B., Grinnell, B. W. & Meyerhoff, M. E. Polymeric coatings that mimic the endothelium: combining nitric oxide release with surface-bound active thrombomodulin and heparin. *Biomaterials* **28**, 4047-4055 (2007).

32 Yeh, H.-Y. & Lin, J.-C. Bioactivity and platelet adhesion study of a human thrombomodulin-immobilized nitinol surface. *Journal of Biomaterials Science, Polymer Edition* **20**, 807-819 (2009).

33 Li, J.-m. *et al.* Immobilization of human thrombomodulin to expanded polytetrafluoroethylene. *Journal of surgical research* **105**, 200-208 (2002).

34 Jiang, R., Weingart, J., Zhang, H., Ma, Y. & Sun, X.-L. End-point immobilization of recombinant thrombomodulin via sortase-mediated ligation. *Bioconjugate chemistry* **23**, 643-649 (2012).

35 Qu, Z. *et al.* A biologically active surface enzyme assembly that attenuates thrombus formation. *Advanced functional materials* **21**, 4736-4743 (2011).

36 Popp, M. W. L. & Ploegh, H. L. Making and breaking peptide bonds: protein engineering using sortase. *Angewandte Chemie International Edition* **50**, 5024-5032 (2011).

37 Nichols, A. B. *et al.* Effect of heparin bonding on catheter-induced fibrin formation and platelet activation. *Circulation* **70**, 843-850 (1984).

38 Heyman, P. W., Cho, C., McRea, J., Olsen, D. & Kim, S. Heparinized polyurethanes: in vitro and in vivo studies. *Journal of biomedical materials research* **19**, 419-436 (1985).

39 Klement, P., Du, Y. J., Berry, L. R., Tressel, P. & Chan, A. K. Chronic performance of polyurethane catheters covalently coated with ATH complex: a rabbit jugular vein model. *Biomaterials* **27**, 5107-5117 (2006).

40 Devine, C. & McCollum, C. Heparin-bonded Dacron or polytetrafluorethylene for femoropopliteal bypass: five-year results of a prospective randomized multicenter clinical trial. *Journal of vascular surgery* **40**, 924-931 (2004).

41 Lindholt, J. S. *et al.* The Scandinavian Propaten< sup>®</sup> Trial–1-Year Patency of PTFE Vascular Prostheses with Heparin-Bonded Luminal Surfaces Compared to

Ordinary Pure PTFE Vascular Prostheses–A Randomised Clinical Controlled Multi-centre Trial. *European Journal of Vascular and Endovascular Surgery* **41**, 668-673 (2011).

42 Bosiers, M. *et al.* Heparin-bonded expanded polytetrafluoroethylene vascular graft for femoropopliteal and femorocrural bypass grafting: 1-year results. *Journal of vascular surgery* **43**, 313-318 (2006).

43 Lensvelt, M. *et al.* Results of heparin-bonded ePTFE-covered stents for chronic occlusive superficial femoral artery disease. *Journal of vascular surgery* **56**, 118-125 (2012).

44 Devine, C., Hons, B. & McCollum, C. Heparin-bonded Dacron or polytetrafluoroethylene for femoropopliteal bypass grafting: a multicenter trial. *Journal of vascular surgery* **33**, 533-539 (2001).

45 Pedersen, G., Laxdal, E., Ellensen, V., Jonung, T. & Mattsson, E. Improved patency and reduced intimal hyperplasia in PTFE grafts with luminal immobilized heparin compared with standard PTFE grafts at six months in a sheep model. *The Journal of cardiovascular surgery* **51**, 443-448 (2010).

46 Hermanson, G. T. *Bioconjugate techniques*. (Academic press, 2013).

47 Stephan, M. T. & Irvine, D. J. Enhancing cell therapies from the outside in: Cell surface engineering using synthetic nanomaterials. *Nano today* **6**, 309-325 (2011).

48 Stabler, C. L. *et al.* Surface re-engineering of pancreatic islets with recombinant azido-thrombomodulin. *Bioconjugate chemistry* **18**, 1713-1715 (2007).

49 Sun, X.-L., Stabler, C. L., Cazalis, C. S. & Chaikof, E. L. Carbohydrate and protein immobilization onto solid surfaces by sequential Diels-Alder and azide-alkyne cycloadditions. *Bioconjugate chemistry* **17**, 52-57 (2006).

50 Wilson, J. T. *et al.* Biomolecular surface engineering of pancreatic islets with thrombomodulin. *Acta biomaterialia* **6**, 1895-1903 (2010).

51 Jewett, J. C. & Bertozzi, C. R. Cu-free click cycloaddition reactions in chemical biology. *Chemical Society Reviews* **39**, 1272-1279 (2010).

52 Chen, Y.-X., Triola, G. & Waldmann, H. Bioorthogonal chemistry for site-specific labeling and surface immobilization of proteins. *Accounts of chemical research* **44**, 762-773 (2011).

53 Debets, M. F. *et al.* Bioconjugation with strained alkenes and alkynes. *Accounts of chemical research* **44**, 805-815 (2011).

54 Akgöl, S. & Denizli, A. Novel metal-chelate affinity sorbents for reversible use in catalase adsorption. *Journal of Molecular Catalysis B: Enzymatic* **28**, 7-14 (2004).

55 Hui, F. & Debiemme-Chouvy, C. Antimicrobial N-Halamine Polymers and Coatings: A Review of Their Synthesis, Characterization, and Applications. *Biomacromolecules* **14**, 585-601 (2013).

56 Boitieux, J., Groshemy, R., Thomas, D. & Ergan, F. Reversible immobilization of an antibody with a thiol-substituted sorbent: application to enzyme immunoassays. *Analytica chimica acta* **197**, 229-237 (1987).

57 Scouten, W. H. & Konecny, P. Reversible immobilization of antibodies on magnetic beads. *Analytical Biochemistry* **205**, 313-318 (1992).

58 Rashidian, M., Song, J. M., Pricer, R. E. & Distefano, M. D. Chemoenzymatic reversible immobilization and labeling of proteins without prior purification. *Journal of the American Chemical Society* **134**, 8455-8467 (2012).

59 Kosa, N. M., Haushalter, R. W., Smith, A. R. & Burkart, M. D. Reversible labeling of native and fusion-protein motifs. *Nature methods* **9**, 981-984 (2012).

60 Rabuka, D. Chemoenzymatic methods for site-specific protein modification. *Current opinion in chemical biology* **14**, 790-796 (2010).

Chapter Five

Directed Evolution of Orthogonal Sortase Enzymes with Reprogrammed Specificity

Brent M. Dorr, Hyun Ok Ham, Elliot L. Chaikof, David R. Liu

Hyun Ok Ham performed the material labeling experiments and GGG-Diblock labeling experiments, while I developed and performed all other experiments and analysis in this chapter.

Some of the text in this chapter is currently being prepared for publication.

Abstract

S. aureus sortase A catalyzes the transpeptidation of an LPXTG peptide acceptor and a glycine-linked peptide donor and has proven to be a powerful tool for site-specific protein modification. The substrate specificity of sortase A is fairly stringent, limiting its broader utility. Here we report the directed evolution of sortase A to recognize two altered substrates, LAXTG and LPXSG, with high activity and specificity. Following nine rounds of yeast display screening integrated with negative selection based on competitive inhibition with off-target substrates, the evolved sortases exhibit specificity changes of up to 51,000-fold relative to the starting sortase without substantial loss of catalytic activity. The specificities of these reprogrammed sortases are sufficiently orthogonal to enable the simultaneous conjugation of multiple peptide substrates to their respective targets in a single solution. We demonstrated the utility of these evolved sortases by using them to effect the site-specific labeling of unmodified, endogenous fetuin A in human plasma, the conjugation of orthogonal fluorescent peptides onto surfaces, and the synthesis of tandem fluorophore-protein-PEG conjugates in two therapeutically relevant fibroblast growth factor proteins, FGF1 and FGF2.

Introduction

The modification of proteins enables applications including the manipulation of protein pharmacokinetics,[1,2] the study of protein biochemistry[3], the immobilization of proteins on solid support[4], and the synthesis of protein-protein fusions that cannot be expressed in cells[5,6]. An attractive approach for the synthesis of such conjugates attaches molecules site-specifically to proteins using epitope-specific enzymes. Such a strategy can bypass the challenges of bioorthogonality and chemoselectivity through the careful choice of enzyme and tag.

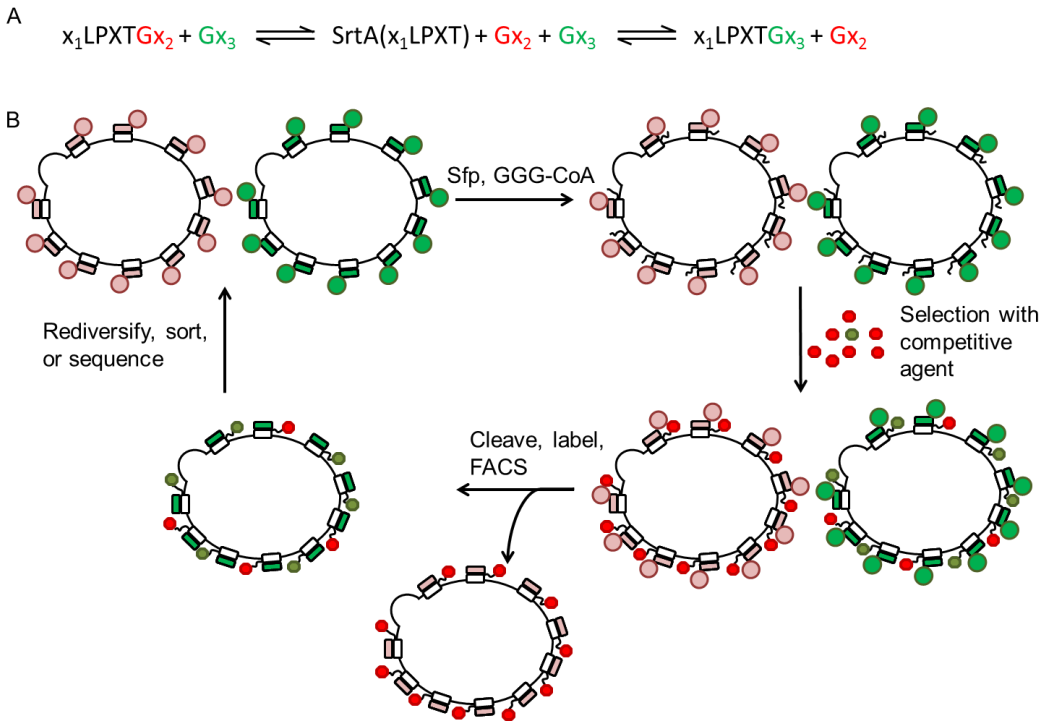

Figure 5-1 Schematic of yeast display-based negative selection
A. Schematic representation of the Sortase A reaction. SrtA recognizes the LPXTG peptide sequence, then cleaves between the T-G bond to form a covalent intermediate, SrtA(LPXT) while ejecting the C-terminal region. This stable thioester then catalyzes the equilibration with externally provided C-terminal regions. B. Bond-forming yeast display selection scheme incorporating negative selection. Clockwise from top left: Specific (red) and promiscuous (blue) enzymes are displayed as C-terminal Aga2p fusions in our bond forming yeast display system. Next, S6 peptide-containing Aga1p molecules are loaded with a selection acceptor substrate, such as GGG-CoA, displaying it at high effective molarity to the displayed enzyme. Modified cells are incubated with a small amount of a biotinylated target moiety (red) and a large amount of an unbiotinylated off-target moiety (blue). Enzyme is then cleaved away by TEV protease and cells are labeled for biotinylation as well as protein display, sorted for activity and display levels, and optionally rediversified for further selection.

Techniques to implement this approach, however, are commonly limited by the requirement of cumbersome and poorly-tolerated fusion tags, or by rigidly defined donor substrate specificity.

The bacterial transpeptidase *S. Aureus* sortase A (SrtA) mediates the anchoring of proteins to the bacterial cell wall and has been widely exploited in bioconjugate synthesis[7]. SrtA recognizes a small, 5-amino acid "sorting motif" (-LPXTG, where X = any amino acid) that can be incorporated into many proteins of interest. Upon binding a sorting motif, SrtA cleaves the scissile Thr-Gly peptide bond via a cyste ine protease-like mechanism, resulting in loss of the C-

terminal glycine to yield a thioacyl intermediate. This intermediate then reacts with an N-terminal Gly-Gly-Gly motif to result in a -LPXTGGG- conjugate (Figure 5-1a). The small size of the SrtA sorting motif and the synthetic accessibility of Gly-Gly-Gly-linked substrates have led to the use of SrtA in a wide variety of applications, including the synthesis of protein-protein[6], protein-nucleic acid[8], protein-lipid[9], and protein-surface[10] conjugates.

The utility of wild-type SrtA has been limited by two key factors. First, its poor catalytic activity limits its use primarily to applications in which it can be used in superstoichiometric amounts, and over long timescales, such as small-scale bioconjugate synthesis. The modest catalytic activity of wild-type SrtA also reduces reaction yield and can lead to the formation of substantial quantities of stable thioacyl intermediates. To overcome this limitation, we previously reported the development of a selection for the evolution of bond-forming enzymes (Figure 5-1b), and the application of this selection to evolve a highly active SrtA variant, eSrtA, with five mutations relative to wild-type SrtA and approximately 140-fold higher catalytic activity than the wild-type enzyme.[11]

A second limitation of both SrtA[12] and eSrtA is their fairly stringent requirement for substrates containing LPXTG. This constraint precludes the use of these enzymes to modify proteins lacking this particular sequence (naturally or through genetic modification), and also prevents their use in more complex syntheses in which multiple sortase enzymes conjugate orthogonal substrates onto a single protein scaffold or onto multiple protein targets. Previous approaches to addressing this limitation have included the directed evolution of a catalytically weakened but promiscuous SrtA variant recognizing XPXTG motifs[13], as well as the use of homologous sortase enzymes possessing different specificity[14]. These approaches, however,

have thus far produced enzymes with substantially lower activity relative to wild-type SrtA or eSrtA and cannot be used to modify arbitrary targets of interest [13,15].

In this work we developed and applied a modified version of a bond-forming enzyme screening system to evolve SrtA variants with dramatically altered, rather than broadened, substrate specificity. Over the course of nine rounds of mutagenesis and fluorescence-activated cell sorting (FACS), we isolated eSrtA variants that recognize either LPX**S**G or L**A**XTG with a minimal loss of activity and up to a 51,000-fold change in specificity relative to eSrtA. We applied these reprogrammed sortases to the synthesis of doubly modified fluorophore-protein-PEG conjugates to demonstrate the rapid construction of complex protein conjugates through multi-step transpeptidation. In addition, we used these evolved sortases to achieve the post-translational modification of endogenous fetuin A, a protein that cannot be efficiently modified by eSrtA because it lacks an LPXTG motif, in unmodified human plasma. Finally, we used the evolved sortases to immobilize fluorophore-linked peptides onto GGG-modified well plates to demonstrate orthogonal surface functionalization. Collectively, these findings represent a facile approach for generating sortase enzymes with tailor-made substrate specificities and expand substantially the number of highly active, orthogonal sortase enzymes available for protein conjugation applications.

Results

A competitive inhibition strategy for sortase evolution

To evolve eSrtA variants with altered substrate specificity, we combined our previously described modified yeast display screen[11] with competitive inhibition to enable negative selection pressure against promiscuous enzymes (Figure 5-1b). We hypothesized that presenting an enzyme with a limiting quantity of biotinylated target substrate in the presence of a large

excess of non-biotiny lated off-target substrate, followed by screening for biotinylated cells, would create evolutionary pressure favoring enzymes with both high activity and high specificity. Enzymes that survive sc reening will preferentially process the target substrate, resulting in cell biotinylation, rather than expend their single turnovers on processing off-target substrates that do not result in cell biotinylation (Figure 5-1b). We envisioned that positive and negative selection pressures could be modulated by varying the concentrations of biotinylated target substrate and non-biotinylated off-target substrates.

To test the ability of cognate LPETG substrate (K_m = 0.2 mM) to compete with a

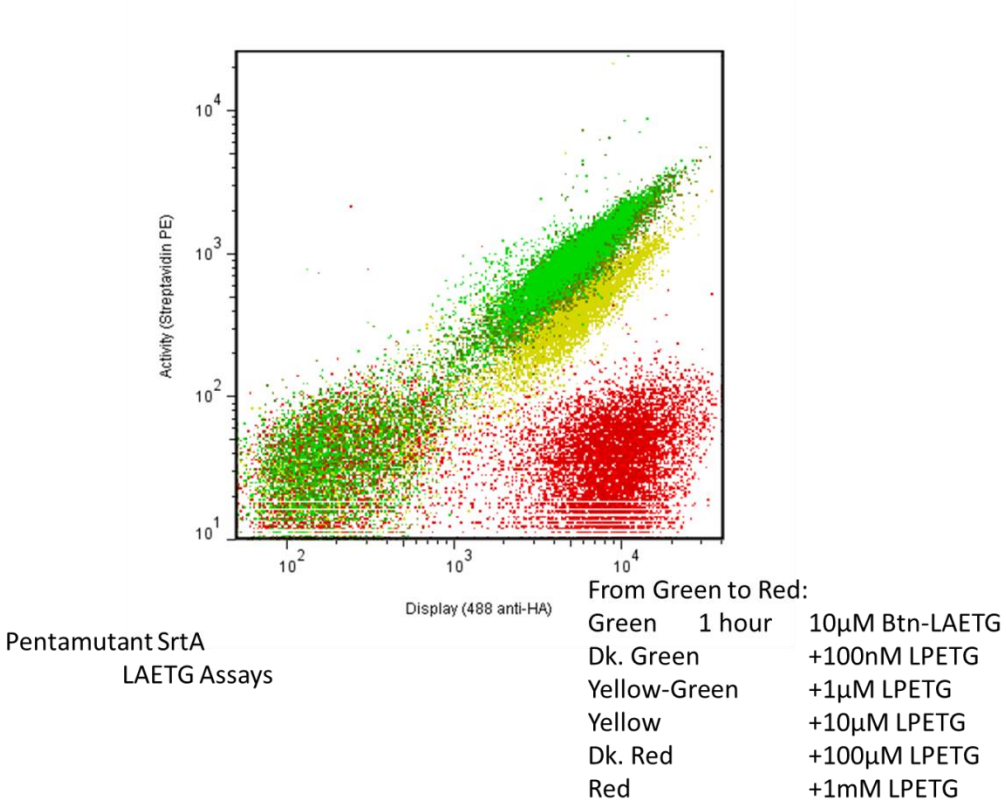

Figure 5-2 Validation of SrtA competitive negative selection.
ICY200 Yeast displaying eSrtA were induced overnight with SGR media, then incubated for one hour with 10µM Btn-LAETGG peptide and between 100nM and 1mM non-biotinylated LPETGG peptide in TBS supplemented with 5mM $CaCl_2$. Cells were then cleaved using TEV, labeled for expression and activity as described and assayed flow cytometrically. Signal reduced to that of unlabeled control at levels above 10µM LPETG.

Table 5-1 Complete evolution program for eSrtA(2A) and eSrtA(4S) substrates.
In each case, libraries were iteratively selected against increasing concentrations of the undesired substrate LPETGG in the presence of decreasing concentrations of biotinyl-LAETGG or LPESGG.

Substrate	Round	Library Size	# Sorts	Final Substrate Concentration (μM)	Final Inhibitor Concentration (μM)	Final Incubation Time (mins)	Final Library Size
LAETG	1	1.0×10^8	4	10	0.1	60	1×10^5
LAETG	2	4.6×10^7	4	10	10	60	1×10^5
LAETG	3	6.8×10^7	4	1	10	60	1×10^5
LAETG	4	4.8×10^7	6	0.1	100	60	8.2×10^4
LAETG	5	3.8×10^7	5	0.01	100	60	7×10^4
LAETG	6	5.4×10^7	7	0.01	1000	60	7.2×10^4
LAETG	7	4.1×10^7	3	0.01	1000	60	3.2×10^4
LAETG	8	2.6×10^7	4	0.01	1000	5	5×10^4
LAETG	9	8.9×10^7	5	0.008	1000	5	4×10^4
LPESG	1	1.0×10^8	4	1	0.1	60	1×10^5
LPESG	2	6.0×10^7	4	0.1	10	60	1×10^5
LPESG	3	4.7×10^7	4	0.01	100	60	1×10^5
LPESG	4	6.1×10^7	6	0.01	100	60	9×10^4
LPESG	5	3.2×10^7	6	0.01	1000	60	3×10^4
LPESG	6	5.1×10^7	7	0.01	1000	60	7×10^4
LPESG	7	4.8×10^7	3	0.01	1000	60	1.6×10^4
LPESG	8	2.8×10^7	4	0.01	1000	5	1.5×10^5
LPESG	9	1.0×10^8	5	0.006	3000	5	1.2×10^5

candidate LAETG target (K_m = 6.1 mM), we used a strain of *S. cerevisiae* displaying eSrtA in the context of our bond-forming scre en. Loading the Aga1 domain with GGG-CoA, we incubated cells with 10 μM bioti n-LAETG and a range of 100 nM to 1 mM non-biotinylated LPETG for 1 hour (Figure 5-2). We observed 50% inhibition of cell biotinylation with 10 μM LPETG, and virtually complete inhibition b y 100 μM LPETG. These results suggest that in the context of our screen, th e K_I of a free competitive substrate i s substantially more potent than its K_m when treated as a substrate, possibly because the single-turnover nature of the yeast display system strongly penalizes candidate enzymes that accept non-biotinylated substrates. Taking this observation into account, we perform ed all subsequent screens for altered SrtA specificity in the presence of 1 μM to 1 mM LPETG.

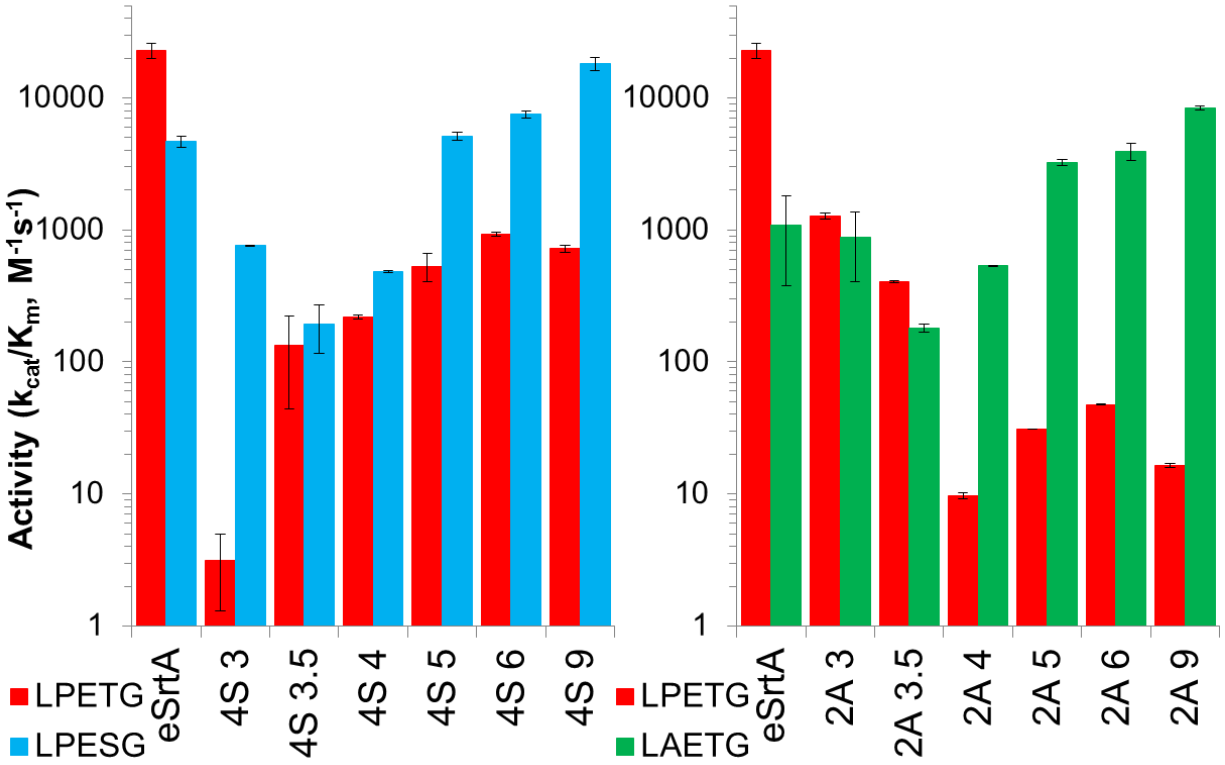

Figure 5-3 Activity levels (k_{cat}/K_m, in $M^{-1}s^{-1}$) of the most abundant clones from each of the measured rounds of selection.
In each case, the most abundant single clone from each round was expressed and purified from *E. coli*, then characterized using an *in vitro* HPLC assay against either Abz-LPETGK(Dnp)$_{CONH2}$, Abz-L**A**ETGK(Dnp)$_{CONH2}$ or Abz-LPE**S**GK(Dnp)$_{CONH2}$ in order to determine k_{cat}, K_m and k_{cat}/K_m for each enzyme against either the wild type substrate LPETG or the new target substrates (Table 5-3). $(k_{cat}/K_m)_{target}$:$(k_{cat}/K_m)_{LPETG}$ was observed to change significantly across nine rounds of screening and mutagenesis, changing by a factor of 51,000 for LAETG, from 1:103 (eSrtA) to 510:1 (eSrtA(2A-9)) and by a factor of 125 for LPESG, from 1:5 (eSrtA) to 25:1 (eSrtA(4S-9)).

Initial evolution of eSrtA variants with altered substrate preference

Because binding-pocket geometries of SrtA in the previously reported apo-LPETG crystal structure[16], apo-LPETG NMR structure[17], and holo-LPETG NMR structure[18] are diverse, we used broad, unbiased mutagenesis to gen erate initial eSrtA diversity. We randomized at a 2% level the entire SrtA gene (441 bp) via chemical mutagenesis (8 mutations per gene on average), transformed the resulting gene pool into y east to generate libraries of 10^7 to 10^8 eSrtA variants, and then screened the resulting libraries with either biotin-L**A**ETG or biotin-LPE**S**G in

the presence of inhibitory concentrations of LPETG (Table 5-1). Starting eSrtA exhibits a 103-fold preference for LPETG over LAETG, and a 5-fold preference for LPETG over LPESG (Figure 5-3).

Three rounds of whole-gene mutagenesis and screening yielded two converged clones, eSrtA(2A-3) and eSrtA(4S-3), each of which containe d between eight and ten coding mutations

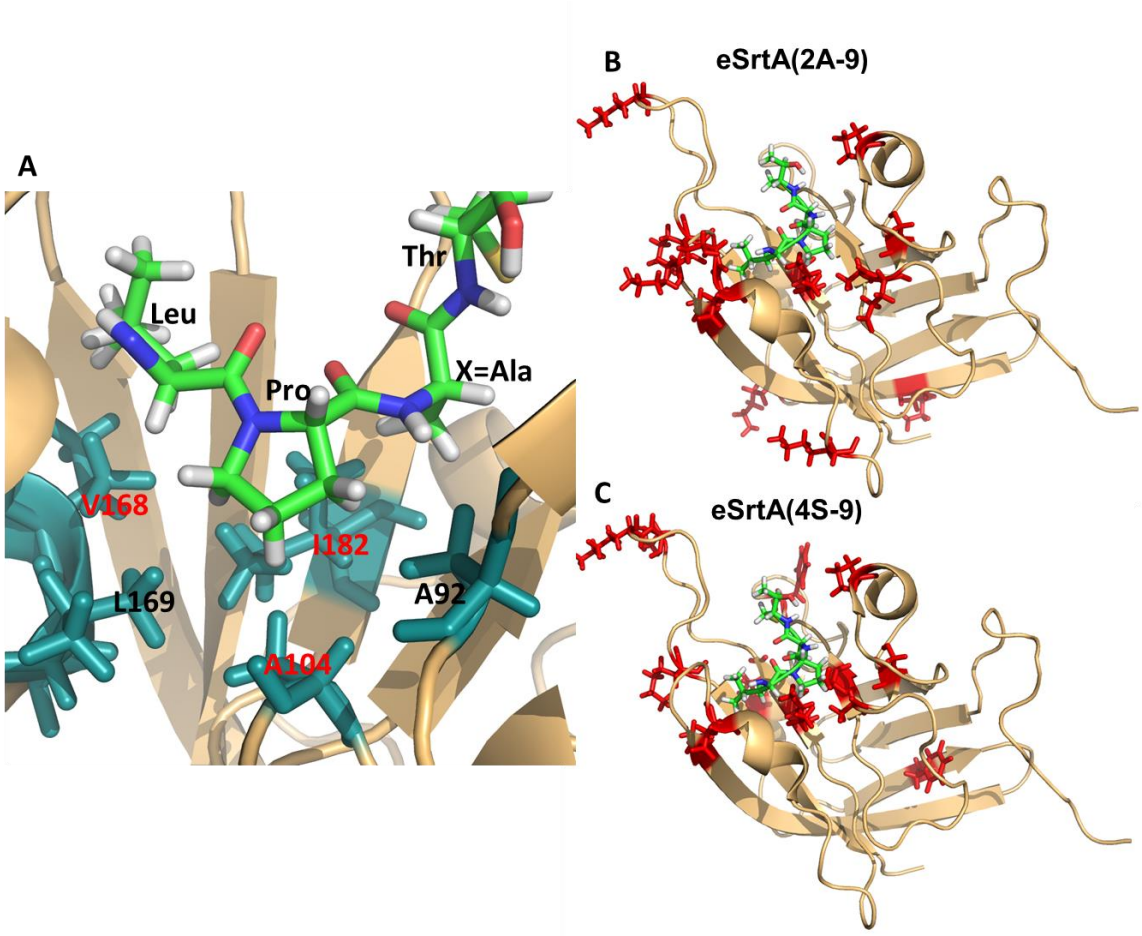

Figure 5-4 Mutational context of eSrtA variants of altered specificity.
A. The holo-enzyme structure is shown with a model LPET-thioester bound, with the mutated residues I182 and V168 highlighted in addition to their surrounding amino acid context. Notably, further mutation of A92 or L169 failed to improve the specificity or activity of the evolved mutants. B,C. Mutations present in C, eSrtA(2A-9) and D, eSrtA(4S-9) highlighted in red on the wild type holo-SrtA NMR structure.

relative to eSrtA. Using an established HPLC assay[19], we determined that mutants 2A-3 and 4S-3 exhibited substantially altered substrate preferences of 1.4-fold preference for LPETG over LAETG (reduced from 103-fold) and a 245-f old preference for LPESG over LPETG (reversed from a 5-fold preference for LPETG), but at the expense of > 10-fold reduced catalytic efficiency (Figure 5-3). By analyzing the mutations that emerged after round 3 in the context of the SrtA holo-LPETG NMR structure, we identified a cluster of three mutations in each mutant that are predicted to make contacts with the LPETG substrate in eSrtA. In the case of eSrtA(2A-3), these mutations are K162R, V168I and I182F, while in the case of eSrtA(4S-3), these changes are A104T, A118T and I182V (Figure 5-4). We hypothesized that these mutations were principally responsible for altering the substrate binding site geometry to accommodate the new targets, with V168I and I182F collectively providing additional steric bulk to complement the smaller alanine side chain at substrate position 2, and A104T and A1 18T altering the active site geometry to discriminate the extra methyl group in threonine from serine at substrate position 4.

To test this hypothesis, we generated candidate "minimal mutant" eSrtA(2A-3.5) and eSrtA(4S-3.5) enzymes containing only those three mutations corresponding to predicted first-shell contacts in each evolved sortase. Both minimal mutants exhi bited substrate promiscuity, processing both the wild-type LPETG and their new respective LAETG or LPESG targets with comparable efficiency (Figure 5-3), albeit with ~100-fold lower activity than that of eSrtA processing its own native LPETG substrate. While these variants showed dramatically reduced performance in nearly all respects, their broad substrate scope led us to suspect that they would serve as strong starting points for the further evolution of altered sortase specificity. Moreover, these results validated the importance of the A104/A118/I182 cluster for recognition of the T4 residue and of the V162/V168/I182 cluster for recognition of the P2 residue. Taken together,

these results suggest that mutations in the binding groove of eSrtA contribute to changes in specificity, but are not sufficient to impart high substrate specificity and activity.

Secondary evolution of eSrtA variants with altered substrate specificity

Next we generated site-saturation libraries based on the eSrtA(2A-3.5) and eSrtA(4S-3.5) minimal mutants. Using degenerate NNK codons, we randomized residues 104, 168, and 182 in eSrtA(2A-3.5), and residues 104, 118, and 182 in eSrtA(4S-3.5). Additionally, we used PCR mutagenesis to further diversify the se libraries in an untargeted manner at a frequency of ~1% per residue. Screening of these librar ies against their target substrate s in the presence of ten-fold higher concentrations of non-biotinylated LPETG yielded the round 4 variants eSrtA(2A-4) and eSrtA(4S-4), each of which acquired novel mutations. In eSrtA(2A-4), A104H, V168I, and I182V resulted in a dramatic specificity change relative to eSrtA(2A-3.5), for the first time generating an enzyme that reacted preferentially with LAETG over LPETG (73-fold preference) (Figure 5-3). In the case of eSrtA(4S-4), A104V, A118T, F122S, and I182V imparted slightly improved preference t owards LPESG relative to the promiscuous mutant eSrtA(4S-3.5), resulting in a 2-fold preference for LPESG over LPETG.

To more fully explore the sequence space of residues mutated in round 4 clones, we subjected these loci to site saturation mutagenesis. In round 5, we applied NNK mutagenesis to the most frequently mutated residues among clones emerging from round 4 (positions 162, 168, and 182 in eSrtA(2A-4), and positions 118, 122, and 182 in eSrtA(4S-4)), and also mutated the rest of the eSrtA gene at a ~1% frequency. Screening of the resulting libraries yielded variants eSrtA(2A-5) and eSrtA(4S-5), each of which included a mixture of mutations at targeted and untargeted residues. In the case of eSrtA(2A-5), we observed library-wide convergence towards R99H and K138I mutations in addition to I168V reversion mutations. In the case of eSrtA(4S-

5), we identified N98D, F122A and A118S mutations, with A118T mutations forming a minor subpopulation, not present in the consensus eSrtA(4S-5) sequence. Expression, purification, and assaying of these round 5 clones revealed that eSrtA(2A-5) possessed 2-fold improved substrate specificity and 6-fold improved catalytic efficiency when compared with eSrtA(2A-4), while eSrtA(4S-5) possessed 4-fold improved substrate specificity and 10-fold improved catalytic efficiency when compared with eSrtA(4S-4) (Figure 5-3).

Following these gains, we repeated this approach of saturation mutagenesis on both newly discovered mutations, as well as revisiting the original pentamutant mutations from the eSrtA starting material. Starting from eSrtA(2A-5), we combines five libraries in which positions 99 and 138 were randomized, in addition to either residue 160, 165, 189, 190, or 196. Similarly, starting from eSrtA(4S-5), we randomized position 132, in addition to one of residues in positions 160, 165, 189, 190, or 196, before combining the resulting five libraries. Untargeted mutagenesis and screening as before provided variants eSrtA(2A-6) and eSrtA(4S-6). We observed the reversion H99R as well as D160K, K152I, and K138P in eSrtA(2A-6). In the case of eSrtA(4S-6), A118T was a predominant mutation, in addition to K134R and E189F. These variants exhibited only marginal improvements in catalytic activity and specificity relative to round 5 clones (Figure 5-3), suggesting that further targeted mutagenesis would not yield further gains in performance.

Given that substrate specificity and catalytic activity were comparable among clones emerging from rounds 5 and 6, we hypothesized that the selective advantage of eSrtA(2A-6) and eSrtA(4S-6) over their ancestors must have arisen from reduced substrate hydrolysis. To decouple hydrolysis from overall enzymatic efficiency, we measured the concentration of GGG at which the rates of acyl-enzyme hydrolysis and transpeptidation are equal, which we define as

the parameter K_H. We found that eSrtA(2A-6) (K_H = 149 ± 63 μM) possessed significantly improved hydrolytic performance when compared with eSrtA(2A-5) (K_H = 731 ± 235) and that eSrtA(4S-6) (K_H = 116 ± 10 μM) was significantly improved relative to eSrtA(4S-5) (K_H = 190 ± 16 μM).

Taken together, these results suggest that the use of whole-gene mutagenesis to identify target loci for site saturation mutagenesis provides access to eSrtA variants with substantially altered substrate specificities. Despite the strong gains observed in rounds 4 and 5, however, we observed no significant activity gains in round 6, suggesting that these evolved enzymes were in a local fitness maximum.

Evolving improved activity in eSrtA mutants with altered specificities

Next we partially randomized all of the sites that were mutated among clones in rounds 4-6. For each target site, we created degenerate codon libraries designed to achieve a 27% mutagenesis rate at each nucleotide of each codon observed to change from our eSrtA starting scaffold. We applied this scheme to residues 94, 98, 99, 104, 160, 162, 165, 182, 189, 190, and 196 in both eSrtA(2A-6) and eSrtA(4S-6) and further applied broad spectrum mutagenesis to each library at a level of approximately 1%.

We screened each library at slowly increasing stringency. Round 7 was sorted three times at stringency levels comparable to that of round 6 (Table 5-1) in order to enable neutral drift, and when tested for activity *en masse* revealed significant cell biotinylation after only five minutes of incubation with substrate. The round 7 survivors were then randomly mutagenized to yield the round 8 library. Round 8 was sorted four times at a reduced five-minute incubation time, maintaining the library at the maximum activity level attained during round 7. At this point, significantly improved activity was observable in the final round 8 population. Harvesting

and randomly mutating the round 8 library led to the round 9 library, which was then subjected to five rounds of sorting with 5-minute incubation times as well as gradually decreasing concentrations of biotinylated substrate (down to a minimum of 6 nM in the case of LPESG selections and 8 nM in the case of LAETG selections) and increasing concentrations of up to 4 mM of non-biotinylated LPETG. These libraries converged on variants eSrtA(2A-9) and eSrtA(4S-9), each of which possessed four to five mutations relative to their round 6 counterparts. Expression, purification and testing of these mutants revealed them to be highly active on their target substrates, with minimal off-target activity against their starting LPETG substrates. The overall changes in substrate specificity of eSrtA(2A-9) and eSrtA(4S-9) relative to eSrtA are 51,000- and 120-fold, respectively (Figure 5-3).

Clone eSrtA(4S-9) showed greatly improved specificity for LPESG over LPETG (25-fold) when compared with eSrtA's opposite starting preference for LPETG over LPESG (5-fold) with negligible activity on LAETG substrates. We hypothesized that this much higher specificity for LPESG was in part caused by the LPXS-eSrtA(4S-9) intermediate coupling more efficeintly to GGG compared to the LPXT-eSrtA(4S-9) intermediate. In order to test this hypothesis, we measured K_H of eSrtA(4S-9) for LPETG and for LPESG, and observed that $K_{H,LPETG}$ (295 ± 18 μM) was nearly twice that of $K_{H,LPESG}$ (174 ± 32 μM). These results show that eSrtA(4S-9) achieves its specificity via a combination of selectively binding LPESG over LPETG, as well as reduced stability of the mis-charged LPET-SrtA intermediate.

Similarly, eSrtA(2A-9) showed much higher specificity than eSrtA for its target substrate, with a nearly 500-fold preference for LAETG over LPETG as compared to eSrtA's 103-fold opposite starting specificity for LPETG over LAETG, and negligible activity on LPESG. Unfortunately, the poor affinity of eSrtA(2A-9) for LPETG precluded the measurement

Table 5-2 Table of eSrtA(2A) and eSrtA(4S) small amino acid specificity.
As described above, 6.4, 64 or 640 nM eSrtA(2A), or 5.5, 55 or 550 nM eSrtA(4S) were incubated with 10μM of the listed peptide substrates in SrtA reaction buffer for 15 minutes, then quenched and analyzed by HPLC. eSrtA(2A-9) showed significant (greater than on LPETG) reactivity only with LAETG, LSETG and LGETG, while eSrtA(4S-9) showed significant reactivity only with LPESG and LPEAG.

Enz	Sub	%Labeling, 1xEnz	%Labeling, 10xEnz	%Labeling, 100xEnz
eSrtA(2A-9)	L**A**ETG	5.73	51.10	98.5
eSrtA(2A-9)	L**G**ETG	0.78	2.45	8.21
eSrtA(2A-9)	L**P**ETG	0.00	1.51	5.70
eSrtA(2A-9)	L**S**ETG	0.65	3.68	25.70
eSrtA(2A-9)	L**V**ETG	0.59	1.53	5.54
eSrtA(4S-9)	LPE**A**G	5.33	50.80	98.00
eSrtA(4S-9)	LPE**G**G	1.30	3.41	14.40
eSrtA(4S-9)	LPE**S**G	7.91	73.40	97.90
eSrtA(4S-9)	LPE**T**G	0.77	5.01	42.40
eSrtA(4S-9)	LPE**V**G	0.72	2.19	10.60

of $K_{H,LPETG}$ for this variant. However, measuring $K_{H,LAETG}$ (18.7 ± 3.3 μM) revealed it to have substantially improved hydrolytic performance compared to that of eSrtA, and comparable to that of wild-type SrtA.

In order to test if eSrtA(2A-9) and eSrtA(4S-9) retain similar global specificity profiles to that of wild-type SrtA, we assayed the activity of both enzymes on peptides related to their reprogrammed targets, as well as on the LPETG starting peptide (Table 5-2). Among substrates containing A, G, P, S or V at position 2, eSrtA(2A-9) exhibited greatest activity on LAETG, with LSETG showing more than 10-fold lower activity, and LGETG and LPETG both showing more than 100-fold diminished conversion, and LVETG showing no detectable activity (Table 5-2).

Table 5-3 Selected kinetic parameters for Wild Type, eSrtA, eSrtA(2A.9) and eSrtA(4S.9) for each of their selected substrates.

In each case, rate constants were determined by measuring enzyme velocity at 8 different substrate concentrations by HPLC assay, then fit using nonlinear regression to the Michaelis-Menten equation, yielding k_{cat} and K_m. K_H was measured by determining the enzyme hydrolysis rate in the absence of GGG k_H, in addition to the k_{cat} and $K_{m,GGG}$ for GGG with acceptor substrate concentration fixed. K_H was then calculated by the direct assay using the modified Michaelis-Menten equation $v = [Enz]k_{cat}\frac{[GGG]+K_H}{[GGG]+K_{m,GGG}}$.

Enz	Sub	k_{cat} (Hz)	K_m (μM)	k_{cat}/K_m ($M^{-1}s^{-1}$)	Rel. Activity	K_H (μM)
SrtA	LPETG	1.5 ± 0.2	7600 ± 500	200 ± 30	--	14.3 ± 0.8
eSrtA	LPETG	5.4 ± 0.4	230 ± 20	23000 ± 3000	1	32.9 ± 2.3
eSrtA	L**A**ETG	1.31 ± 0.26	6160 ± 870	221 ± 75	99.6	--
eSrtA	LPE**S**G	1.74 ± 0.17	672 ± 167	2650 ± 440	8.7	--
2A.9	LPETG	0.02126 ± 0.00004	1290 ± 30	16.5 ± 0.4	794	--
2A.9	L**A**ETG	2.03 ± 0.02	154 ± 1	13100 ± 200	1	19.3 ± 3.2
2A.9	LPE**S**G	0.03 ± 0.03	37000 ± 35000	0.8 ± 0.2	16400	--
2A.9	L**S**ETG	0.115 ± 0.007	331 ± 67	354 ± 54	24	--
4S.9	LPETG	--	--	517	34	--
4S.9	L**A**ETG	0.0079 ± 0.0003	391 ± 17	20.3 ± 0.3	867	--
4S.9	LPE**S**G	2.15 ± 0.12	123 ± 13	17600 ± 1900	1	305 ± 112
4S.9	LPE**A**G	2.24 ± 0.02	197 ± 4	11370 ± 191	1.6	--

For eSrtA(4S-9), similar substrate profiling on A, G, S, T and V substitutions at position 4 revealed that eSrtA(4S-9) has ve ry low activity on LPEGG, LPETG, and LPEVG substrates, but considerable activity against LPEAG substrates (Table 5-2). Indeed, eSrt(4S- 9) possesses 62% of LPESG-type activity on LPEAG substrates (Table 5-3).

Collectively, these results establish that eSrtA(2A-9) and eSrtA(4S-9) evolved altered but fairly stringent specificity compared with eSrtA, at least in part modulated through the

hydrolytic stability of their acyl-enzyme intermediates. Both evolved round 9 clones strongly prefer their new LAXTG or LPXSG targets over the canonical LPXTG substrate, yet maintain overall catalytic efficiency within 2-fold of that of eSrtA (Table 5-3).

eSrtA(4S-9) modifies endogenous fetuin A in human plasma

In light of the known activity of eSrtA in human serum[20] and the highly altered specificity of eSrtA(4S-9), we hypothesized that eSrtA(4S-9) could catalyze the site-selective modification of endogenous LPXSG or LPXAG motifs in the human proteome. Based on an initial survey of the Uniprot protein database[21], we identified 199 candidate proteins with LPXSG or LPXAG motifs known to exist in the human proteome. Cross-validation against the Plasma Proteome Database[22] identified only 36 proteins known to be present at detectable concentrations in human plasma. Due to th e frequent occlusion of such tags in their folded

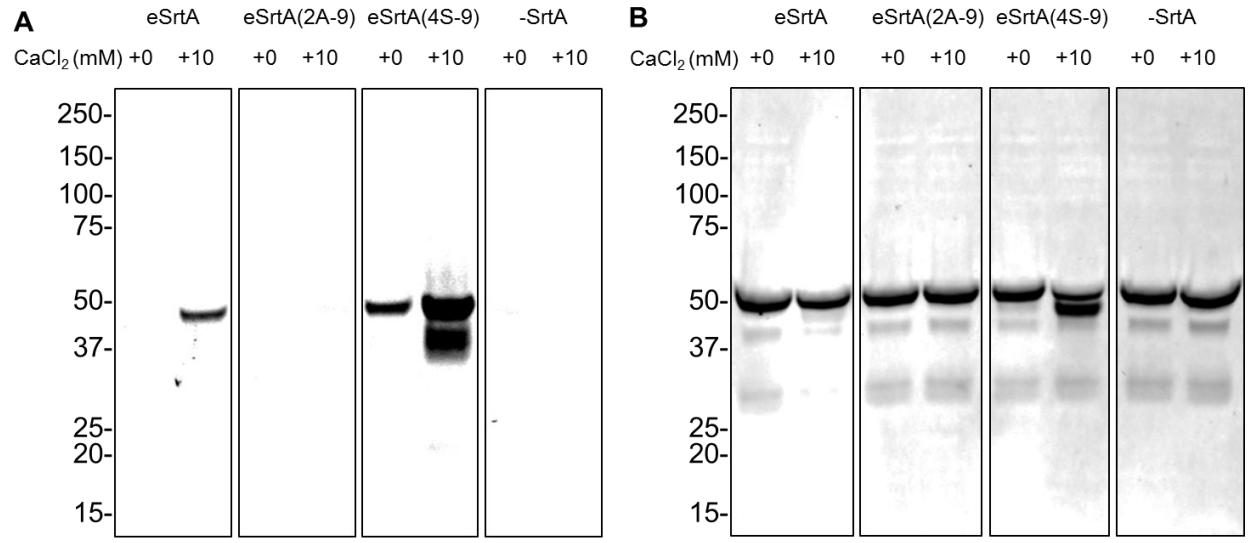

Figure 5-5 Use of evolved eSrtA variants to label endogenous substrates.
(A) Treatment of human plasma with 1μM selected SrtA variants for 2 hours at room temperature in the presence of 1mM GGGK(Biotin) and with or without 10mM $CaCl_2$ supplement. A clear labeling product is produced with a molecular weight of approximately 50 kDa. Scale-up and biotin pulldown followed by proteomic analysis identified this protein as fetuin A, which subsequent antibody labeling (B) confirmed. The ~1kDa mass shift corresponding with GGG-Btn installation is clearly visible in the eSrtA(4S-9), 10mM supplemental $CaCl_2$ sample. Densitometry of these bands suggest overall labeling efficiency of 0.6% by eSrtA in the presence supplemental calcium, 1.8% by eSrtA(4S-9) in the absence of supplemental calcium, and 57.6% by eSrtA(4S-9) in the presence of supplemental calcium.

state, we hypothesized that only a small fraction of the se 36 candidate proteins would be accessible to transpeptidation by a functional enzyme.

We tested the ability of eSrtA(4S-9) to label proteins in human plasma by co-incubating whole plasma with 1 μM eSrtA(4S-9) in the presence of 1 mM Gly-Gly-Gly-Lys(Biotin) for 2 hours at room temperature in the presence or absence of 10 mM $CaCl_2$. Immunoblot and biotin capture each identified a single transp eptidation product (Figure 5-5), identified by mass spectrometry and confirmed by Western blot as fetuin A. As a systematic regulator of tissue mineralization,[23] the selective *in vivo* and *in vitro* modification of fetuin A may be useful in the study of pathogenic biomineralization, as well as the diagnosis or potential therapeutic intervention of fetuin-associated hemodialysis outcomes[24], malnutrition-inflammation-atherosclerosis syndrome[25] and *P. berghei* pathogenesis[26]. Fetuin A contains an LPPAG sequence that our studies above suggest should be a substrate for eSrtA(4S-9), but that should not be a substrate for eSrtA. Ind eed, eSrtA showed no processing of fetuin A in the absence of supplemental calcium, and only modest fetuin A conjugation efficiencies (90-fold lower than that of eSrtA(4S-9)) in the presence of 10 mM supplemental $CaCl_2$.

These findings demonstrate the ability of evolved reprogrammed sortase enzymes to conjugate substrates to endogenous human proteins without chemical or genetic intervention. The high activity level of eSrtA(4S-9) in the absence of supplemental calcium demonstrates that evolved eSrtA variants can modify endogenous proteins with no additional cofactors.

Reprogrammed sortases enable the facile synthesis of complex bioconjugates

The multiple modification of a protein's N- and C- terminus using only a single SrtA variant is severely hindered by competing reactions of protein oligomerization and circularization whenever a reactive C-terminal sorting signal and N-terminal GGG are both

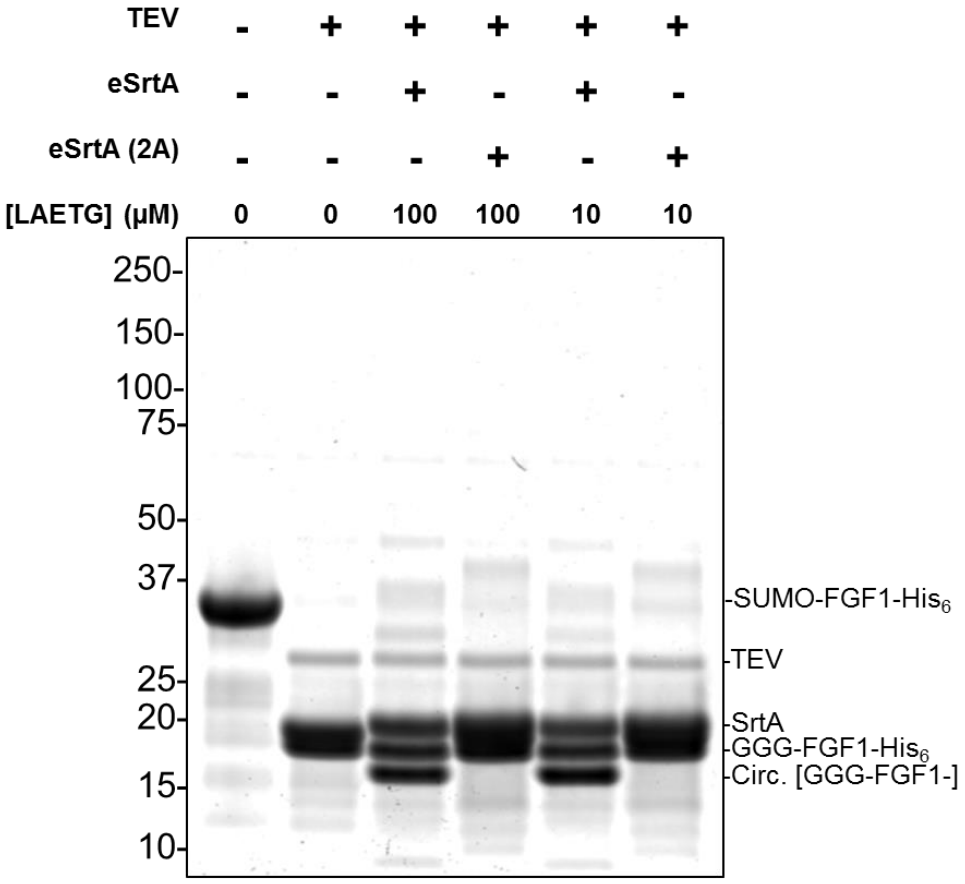

Figure 5-6 Circularization of GGG-FGF-LPESG by eSrtA in Dual Labeling.
Reactions between SUMO-TEV site-FGF1-LPESG-His_6, 0.5eq TEV Protease, and either 0.2eq eSrtA or eSrtA(2A) in the presence of 10 or 100μM Btn-LAETG for 4 hours. *In situ* digestion of the TEV cleavage site exposes an N-terminal GGG, which is ideally then reacted with LAETG. However, in the presence of the off target site LPESG, a promiscuous sortase irreversibly reacts with it to cleave away the C-terminal his tag, and circularize the resulting protein. This competing side-reaction introduces a side product that copurifies with nearly all FGF conjugates, significantly reducing both purity and yield in the absence of orthogonal enzymes.

present (Figure 5-6). Orthogonal SrtA variants have previously been used in the N- and C-terminal functionalization of target proteins[14,27]. However, in these applications the low activity and poor orthogonality of the enzymes greatly limited the scope of available reactions[27]. In order to test whether the high activity and altered specificity of eSrtA(2A-9) and eSrtA(4S-9) can overcome these limitations, we attempted to synthesize dual N- and C-terminally functionalized

Table 5-4 Yields of FGF/GGG-PEG Semisynthesis.
750-FGF-GGG-PEG conjugates were synthesized as described in main text, using intermediate purification by Ni-NTA filtration to remove SrtA catalyst and unreacted starting material, then concentrated against 10kDa membranes to eliminate residual GGG-PEG and leaving groups. These conjugates were assayed for purity via denaturing gel, and for overall yield by BCA assay, shown above. Notably, FGF2 conjugates showed uniformly poorer yield than FGF1 conjugates, owing both to their lower starting purity than FGF1 (<50%, as opposed to >90%) and to their smaller reaction scale (0.5mg vs 8mg).

Protein	C-terminal Modifier	Starting Protein, mg	Conjugate Protin, mg	Molar Yield
FGF1	GGG	8.08	1.48	31.0 %
FGF1	GGG-PEG_{10kDa}	8.08	1.25	16.7 %
FGF1	GGG-*bis*-PEG_{10kDa}	8.08	0.84	11.2 %
FGF1	GGG-4arm-PEG_{10kDa}	8.08	1.48	19.6 %
FGF1	GGG-PEG_{10kDa}-Biotin	8.08	0.84	11.1 %
FGF2	GGG	0.54	0.01	0.4 %
FGF2	GGG-PEG_{10kDa}	0.54	0.10	2.0 %
FGF2	GGG-*bis*-PEG_{10kDa}	0.54	0.10	1.8 %
FGF2	GGG-4arm-PEG_{10kDa}	0.54	0.10	1.9 %
FGF2	GGG-PEG_{10kDa}-Biotin	0.54	0.08	1.6 %

proteins of biomedical importance. Fibroblast Growth Factor 1 (FGF1) is currently being evaluated for the treatment of ischemic disease and is limited in its efficacy by low *in vivo* stability[28]. Fibroblast Growth Factor 2 (FGF2) is an angiogenic factor that has been investigated previously as a wound healing factor[29], but its translation into the clinic has been also limited by poor biostability[30].

We expressed recombinant FGF1 and FGF2 as SUMO-TEV-GGG-FGF-LPESG-His_6 constructs. Due to the close proximity of the FGF N- and C-termini, transpeptidation attempts using an unprotected N-terminus, or using non-orthogonal enzymes, generated only circularized

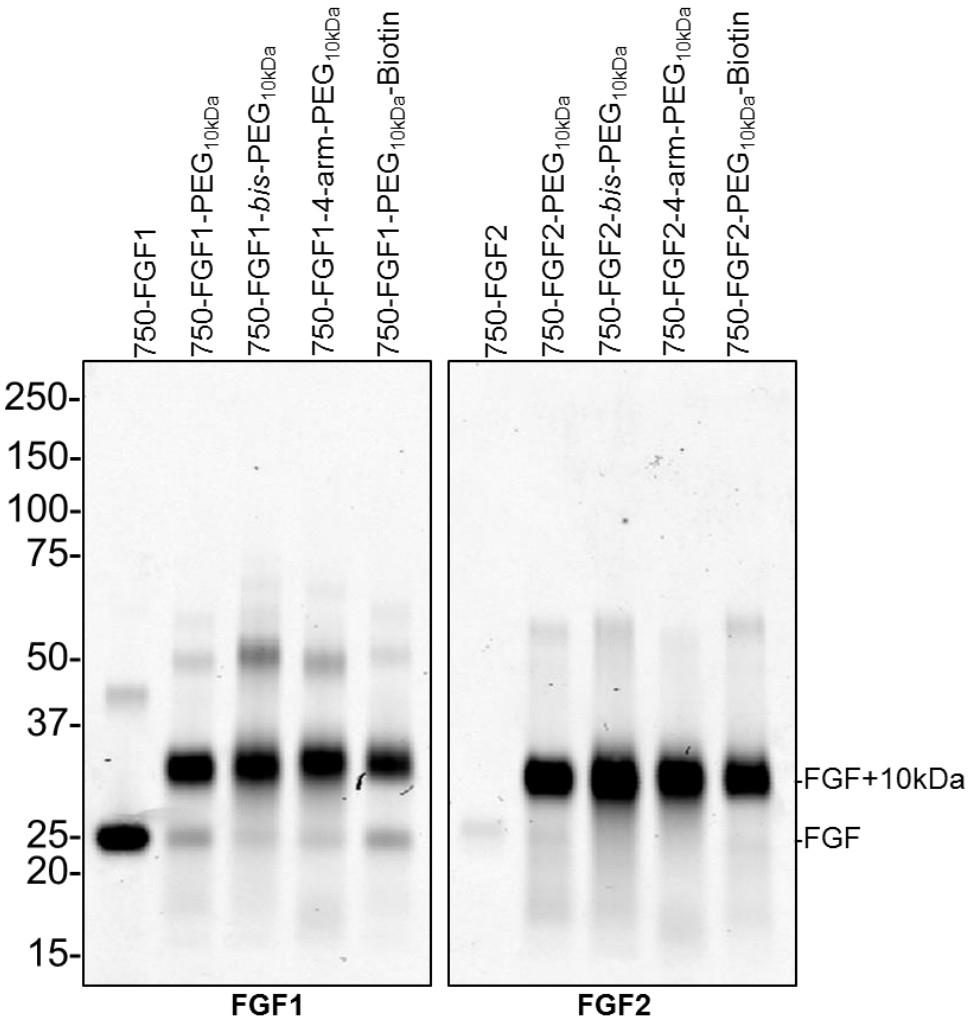

Figure 5-7 N- and C-terminal labeling of the Fibroblast Growth Factors FGF1 and FGF2.

Tandem SUMO-TEV Cleavage Site-FGF1/2-LPESG-His_6 constructs were expressed in BL21 (DE3) cells and purified by Ni(NTA) chromatography. These constructs were then treated with 0.2 eq eSrtA(4S-9) in the presence of 1mM GGG-PEG and purified by filtration through a plug of Ni-NTA resin followed by concentration against a 10kDa MWCO membrane. These were then treated with 0.2 eq eSrtA(2A-9) in the presence of 10eq AlexaFluor750-LAETGG and purified once more by ion exchange chromatography to give the expected conjugates in listed yield. To assess labeling specificity, conjugates were run on an SDS-PAGE gel and scanned for fluorescence at 700 nm

FGF as product (Figure 5-6). We used evolved eSrtA(4S-9) to conjugate 10 kDa PEG-GGG, 10 kDa *bis*-PEG-GGG, 10 kDa 4-arm PEG-GGG, or 10 kDa Biotin-PEG-GGG to this protein. The loss of the C-terminal His_6 tag, along with the use of His_6-tagged reagents, allowed the facile

purification of these conjugates from the initial reaction mixture. *In situ* cleavage of the linker by TEV protease generated an N-terminal GGG, which was then reacted with an Alexa Fluor® 750-linked LAETG peptide using evolved eSrtA(2A-9) to afford the final 750-LAETG-FGF-LPESG-PEG bioconjugates in moderate yield (15-30% yield at 8mg scale, see Table 5-4) and high purity (Figure 5-7).

These results establish that eSrtA(2A-9) and eSrtA(4S-9) collectively form an orthogonal protein conjugation enzyme pair, enabling the facile synthesis of complex bioconjugates at substantially improved scale and yield relative to previous methods[14]. The facile and parallel synthesis of milligram quantities of dual PEG- and fluorophore-conjugated proteins of clinical interest may facilitate the high-throughput synthesis and screening of bioconjugates at scales relevant to preclinical studies.

eSrtA(2A-9) and eSrtA(4S-9) modify material surfaces orthogonally and with high activity

Finally, encouraged by the effectiveness of eSrtA(2A-9) and eSrtA(4S-9) for protein semisynthesis, we tested their potential utility for functionalizing surface materials. Previous methods of biofunctionalization have been successful in generating materials with improved biocompatibility[31-33], however these methods are only compatible with end-point immobilization of a single protein. Techniques for the orthogonal or multi-component immobilization of several proteins to a single material target could enable the synthesis of more sophisticated protein-linked materials.

To test the ability of our evolved eSrtA variants to selectively modify their cognate substrates in complex mixtures, we measured their ability to modify GGG-functionalized amphiphilic diblock polypeptide surfaces, rather than soluble substrates, using fluorophore-conjugated LAETG or LPESG (Figure 5-8). We generated GGG-PEG-functionalized 96-well

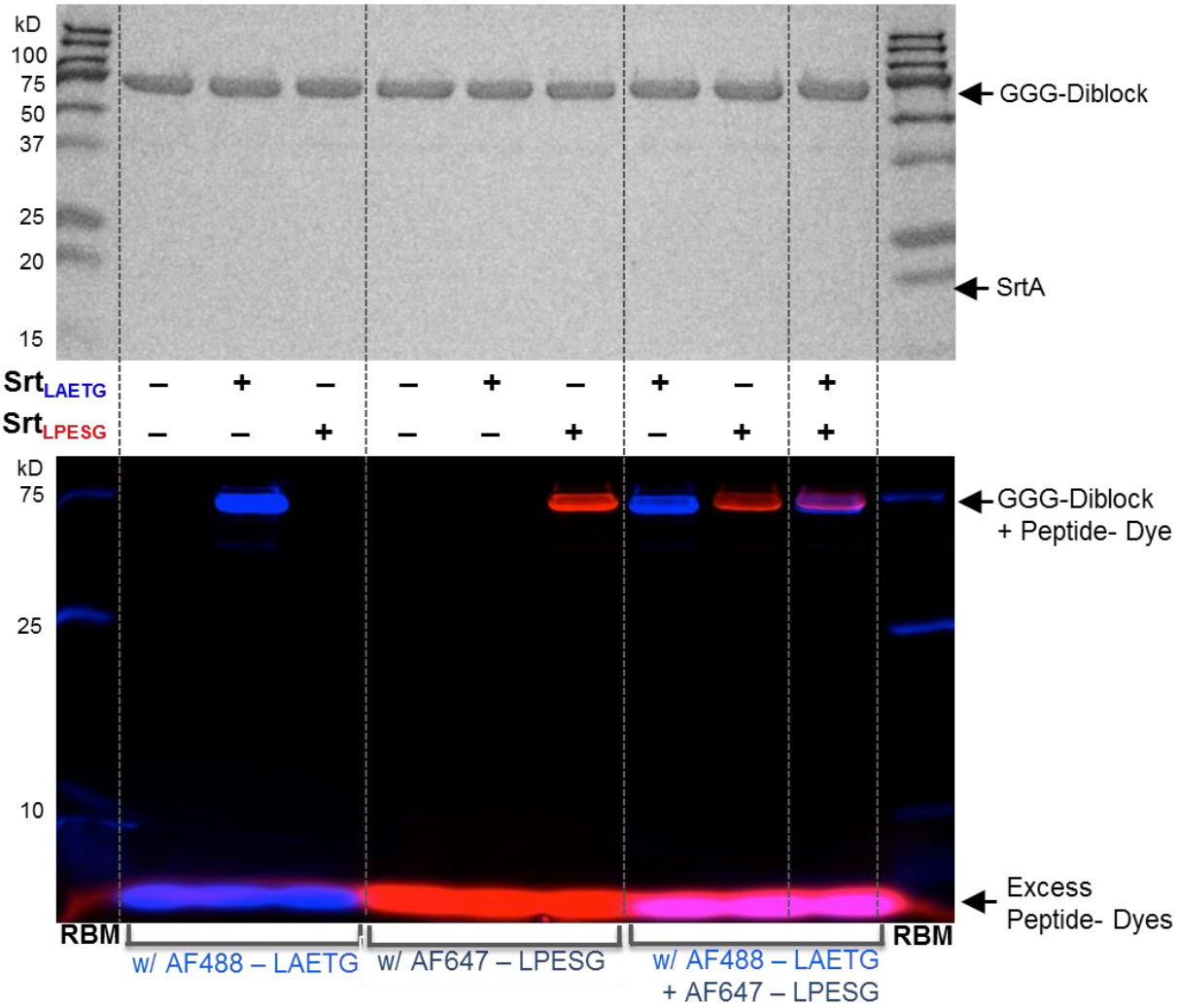

Figure 5-8 Functionalization of GGG-Diblock by eSrtA(2A) and eSrtA(4S).
Reactions between eSrtA(2A), eSrtA(4S) and amphiphilic diblock polypeptide (ADP). ADP was co-incubated with Alexa Fluor® 488-LAETG, Alexa Fluor® 647-LPESG, eSrtA(2A) and/or eSrtA(4S). These reactions were then run out on denaturing gel and visualized using either coomassie stain, 488 fluorescence or 647 fluorescence. As shown, significant peptide-diblock reaction was observed only for cognate pairs of enzyme and sorting signal, with no detectable off-target interactions.

plates, to which we added either Alexa Fluor® 488-LAETG or Alexa Fluor® 647-LPESG in the

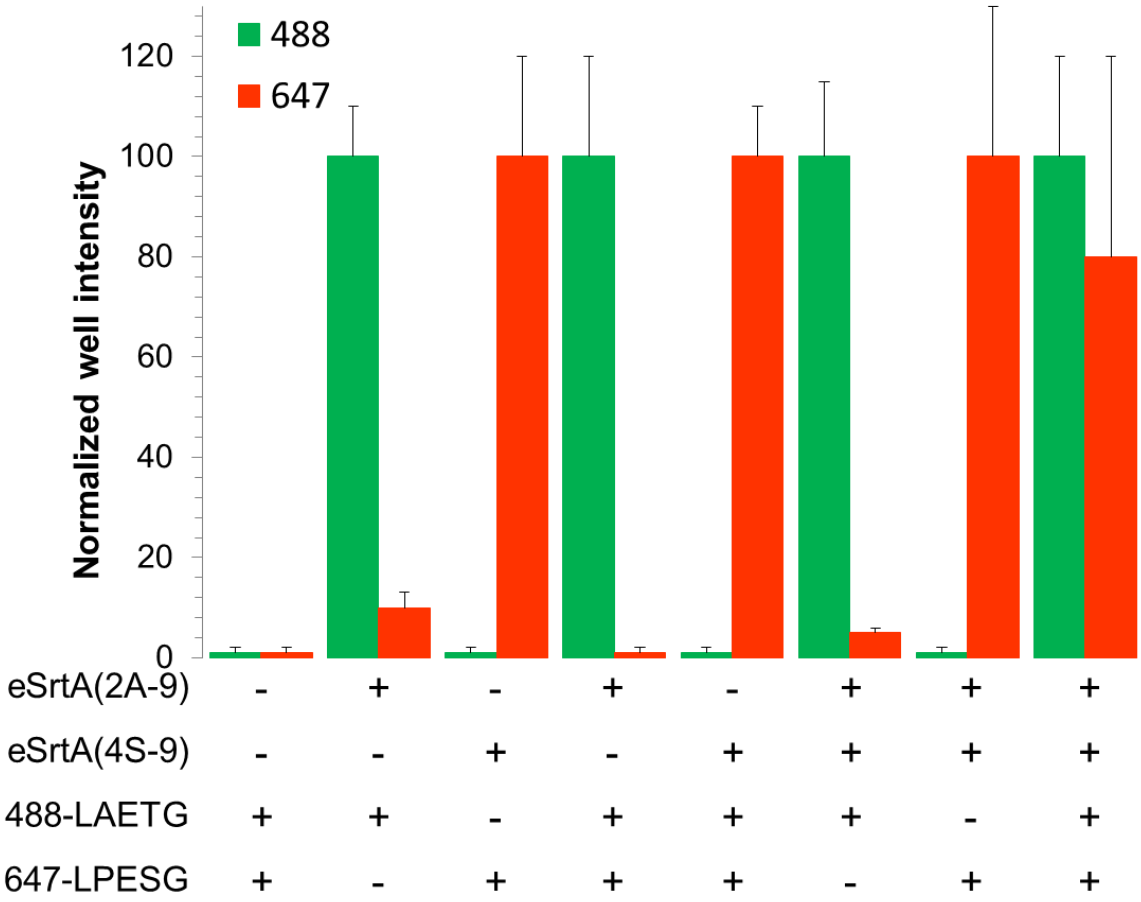

Figure 5-9 Functionalization of solid substrate using eSrtA(2A-9) and eSrtA(4S-9).
GGG-PEG(5kDa) coated 96 well plates were reacted with pools containing enzyme and fluorophore-peptide conjugates, then their total fluorescence was measured at 488 nm or 647 nm, and collectively normalized to the fluorescent intensities obtained from the groups 'eSrtA(2A-9) + 488-LAETG' or 'eSrt(4S-9) + 647-LPESG'. In each case, overall labeling was maintained at a high level using only small amount of enzyme, with minimal cross-reactivity owing to the high overall specificity of eSrtA(2A-9) and eSrtA(4S-9).

presence of eSrtA(2A-9), eSrtA(4S-9), or both. Each enzyme exhibited significant activity only on its cognate substrate, and each was capable of modifying surfaces to a high degree of functionalization when combined with its cognate substrate (Figure 5-9). These results collectively suggest that eSrtA(2A-9) and eSrtA(4S-9) are capable of mediating the simultaneous conjugation of multiple distinct compounds onto GGG-functionalized surfaces with very little cross-reactivity.

Discussion

We applied a modified yeast display selection strategy to evolve highly active eSrtA into reprogrammed, orthogonal variants eSrtA(2A-9) and eSrtA(4S-9) with a 51,000- or 120-fold change in substrate specificity, respectively. eSrtA(2A-9) and eSrtA(4S-9) both have catalytic activity comparable to that of eSrtA, but strongly prefer LAXTG and LPXSG substrates, respectively, over the wild-type LPXTG substrate. We demonstrated the utility of SrtA reprogramming by showing that eSrtA(4S-9), unlike eSrtA or wild-type SrtA, is capable of modifying the human protein fetuin A in unmodified human plasma with high efficiency and specificity. We further demonstrated the utility of these reprogrammed sortases by using them to synthesize the bioconjugates Alexa Fluor® 750-LAETG-FGF1-PEG and Alexa Fluor® 750-LAETG-FGF2-PEG using a set of four different PEG building blocks, and by using these evolved enzymes to simultaneously and orthogonally functionalize GGG-linked surfaces with target peptides.

The evolution of eSrtA(2A-9) and eSrtA(4S-9) revealed a number of biochemical features of the enzyme, including the role of the channel formed by A118, A104, I182, and V168 in directing and coordinating transpeptidation. While this channel had been implicated as part of the sorting signal binding groove in previous structural studies[18,34], this study represents the first modification of these residues to retarget the specificity of the enzyme. Our use of broad spectrum mutagenesis to identify biochemically valuable loci in the enzyme active site for further interrogation by site-saturation mutagenesis also proved a valuable strategy for the study and engineering of this structurally dynamic protein.

The features of eSrtA(4S-9) suggest a complex mechanism underlying substrate specificity. The high hydrolytic instability of the enzyme suggests that the thioester intermediate

is destabilized in this mutant, a feature that may play a role in its high substrate specificity by selectively hydrolyzing mis-charged enzyme. In comparison, the very low hydrolytic instability of eSrtA(2A-9) suggests increased stability of the thioester intermediate, comparable to that of the wild type SrtA and increasing its potential utility for downstream applications in cases where GGG-linked substrates are difficult to access.

In agreement with Piotukh et al[13]'s report of a promiscuous SrtA recognizing XPETG peptides, we observed that eSrtA is capable of evolving significant changes in substrate specificity. This capability is somewhat surprising given the mechanistic similarity between sortases and cysteine proteases[18] and the well-appreciated difficulty of successful engineering or evolving proteases with altered substrate specificities[35,36]. Our successful reprogramming of two out of eSrtA's four specificity-determining amino acids suggests that it is unusually reprogrammable, making it an appealing target for the further evolution of user-defined protease-like enzymes.

The high activity and specificity of eSrtA(4S-9) enabled the successful chemical modification of the human serum glycoprotein fetuin A, the major carrier protein of calcium phosphate *in vivo* and a potent anti-inflammatory protein and inhibitor of soft tissue calcification[23]. While fetuin A is traditionally difficult to purify away from its natively interacting partners[37], our strategy of site-specific reaction and pull-down afforded pure preparations of truncated fetuin A without detectable contaminants. Low levels of fetuin A are strongly associated with significant increases in all-cause mortality of patients undergoing hemodialysis regimens[24], suggesting that the *in situ* enhancement of fetuin A bioavailability by e.g. PEG-ylation may improve outcomes in such patients. Additionally, covalent modification of

fetuin A enables the direct study of its proposed roles in hepatocyte invasion by *P. berghei*[26] and insulin sensitivity[38].

The milligram-scale synthesis of protein-PEG conjugates mediated by the sortases evolved in this study demonstrates the effectiveness of orthogonal transpeptidases in the rapid synthesis of complex biomolecules. The combination of two orthogonal, high-activity enzymes enabled the facile synthesis of ten distinct fluorophore-FGF-PEG conjugates, five of them at milligram scale in a way that is not easily achieved by other existing methods of bioconjugation. Given the growing use of bioconjugates as human therapeutics[39-41], we anticipate that this technique may prove useful in the rapid generation and testing of a wide variety of protein-small molecule and protein-polymer constructs.

Finally, our use of orthogonal eSrtA variants for the synthesis of peptide-conjugated surfaces from complex starting mixtures illustrates the potential utility of our evolved SrtA variants for novel materials syntheses. By enabling the specific and orthogonal conjugation of proteins and material surfaces, we anticipate that orthogonal evolved sortases will enable the construction of previously inaccessible materials containing multiple, homogenously immobilized proteins.

The relative infrequency of any given peptide 5-mer among within a typical proteome means that any given SrtA-derived transpeptidase is unlikely to react with more than a small number of targets. The successful demonstrations achieved in this study, coupled with the generality of our eSrtA reprogramming strategy, suggests that it should be possible to reprogram sortases to selectively target other proteins as well.

Methods

750-LAETG-FGF-LPESG-PEG Dual Labeling Protocol

SUMO-TEV Site-FGF-LPESG-His_6 conjugates were treated with 0.2eq eSrtA(4S-9), 1mM GGG-PEG and 10mM CaCl2 in TBS and incubated at room temperature at 500µL final volumes. These samples were then quenched by the addition of 100µM $_{H2N}$LPESGG peptide and 100µL of pre-equilibrated Ni-NTA resin slurry in TBS, then incubated on ice for 15 minutes. This mixture was then passed through a 0.2µm spin filter, diluted 1:10 into PBS + 10µM $_{H2N}$LPESGG peptide, and concentrated against a 10kDa MWCO spin concentrator to a final volume of 400µL. This process was repeated five times to afford the crude SUMO-TEV Site-FGF-LPESGGG-PEG conjugates.

These conjugates were then co-treated with 0.5eq TEV Protease, 0.2eq eSrtA(2A-9), 1mM 750-LAETG and 10mM CaCl2 in TBS for 1 hour, then subjected to an identical purification process. This crude sample was separated into >30kDa fractions and <30kDa fractions by a 30 kDa MWCO spin concentrator to provide the conjugates in good purity. Concentrations were determined by BCA assay

Plasma Labeling of Fetuin A

Normal human plasma was purchased from VWR (part number 89347-902), aliquotted to 1mL fractions and stored at -20°C. For all reactions, an aliquot was thawed at 37°C for 15 minutes, then vortexed to resuspend any coagulated material. To this sample was added 2 µL of 0.1M GGGK(Biotin) for analytical reactions. Higher concentrations of GGGK(Biotin) were avoided for analytical purposes, as they are known to cause increased background in downstream Western blotting. 10µL of 1M $CaCl_2$ was added in cases of calcium supplementation. Reactions were initiated by the addition of 10µL of 100µM eSrtA, eSrtA(2A-9) or eSrtA(4S-9) and incubated at room temperature for 2 hours. Reactions were quenched by 10:1 dilution into SDS-PAGE loading buffer, followed by 10 minute incubation at 95°C. These samples were then run

on 4-12% Bis-Tris PAGE gels, blotted to PVDF membrane using the iBlot2 dry blotting system, blocked with Pierce Superblock buffer for 1 hour followed by incubation with 1:500 dilutions of Abcam α-Fetuin A antibody (MM0273-6M23) in Superblock buffer with 0.1% Tween-20 for 1 hour. The blot was then washed 3 times with PBS + 0.1% Tween-20, then incubated again in 1:15,000 LiCor goat anti-mouse 680 + 1:15,000 Licor Streptavidin-800 in Superblock buffer with 0.1% Tween and 0.01% SDS added for 45 minutes. The blot was then washed 3 times with PBS + 0.1% Tween and visualized on an Odyssey IR imager.

Materials Functionalization

GGG-functionalized substrate was generated by incubating 100 μL, 2 μM of biotin-PEG (5K)-GGG in streptavidin coated 96 well microplates (Pierce) for 2 hour at RT, and washed with TBST buffer (20 mM Tris, 100 mM NaCl, pH 7.5 with 0.05% Tween 20) for three times. Then, GGG-well plates were reacted at RT with 100 μL of pools containing different enzymes (50 nM) and fluorophore-peptides (2.5 uM). For orthogonal specificity test, Alexa fluoro® 488–LAETG, Alexa fluoro® 647–LPESG or both were reacted with eSrt(2A-9), eSrt(4S-9), or both in the presence of 100 mM of $CaCl_2$ in 25 mM Tris, 500 mM NaCl, pH 7.5. After 2 hour, the well plates were washed with TBST for three times, and TBS buffer was added to each well. Then, the total fluorescent intensities were measured at 488 nm and 647 nm using Biotek Synergy NEO HTS Multi Mode microplate reader at Wyss Institute, Boston, MA. Experiments from three independents sets were averaged, and depicted in the graph after normalization.

Yeast Contamination Cleanup

Periodically, *S. cerevisiae* cultures would become contaminated with an unknown fungal growth, believed to originate from our laboratory HVAC system. In spite of repeated attempts to scrub the contaminant using antifungal agents or altered media compositions, we were unable to

prevent its reemergence and eventual takeover of library cultures. Thus, we chose a strategy of physical separation. Whenever contamination was observed, each outgrowth of library material was centrifuged at 400xg for 30 minutes in a spinning bucket rotor against a step gradient of 30%, 27.5% and 25% Ficoll-400PM in PBS. Under these conditions, *S. cerevisiae* pelleted efficiently while contaminating organisms were isolated in the lower-density layers of the Ficoll gradient.

Library Subcloning and Gene Isolation

Following selections, yeast were grown to saturation (OD ~1.5) in SCD –Trp –Ura dropout media + 100 U/mL Penicillin, 100 μg/mL Streptomycin, 100 μg/mL Kanamycin at 30°C, then lysed using a Zymo Research Zymoprep II kit according to manufacturer's instructions. The zymoprepped material was then either transformed directly into NEB One-Shot Chemically Competent Top10 cells according to manufacturer's instructions, or PCR-ed by external primers HR2.Fwd and HR2.Rev, gel purified and then either mutated directly for another round of selection or digested by BamHI and XhoI and ligated into pre-digested pET29B vector, then transformed into NEB One-Shot Chemically Competent NEBTurbo cells.

Chemical Mutagenesis Library Construction (rounds 1-3)

Libraries were synthesized as in Chen et al (2011)[11]. In short, genes were isolated from miniprepped yeast libraries by subcloning into Invitrogen chemically competent TOP10 cells, grown up in 25mL LB + 50 μg/mL carbenicillin, harvested by miniprepping and then mutagenized by PCR reactions containing 5μM 8-oxo-2'deoxyguanosine (8-oxo-dGTP), 5μM 6-(2-deoxy-b-D-ribofuranosyl)-3,4-dihydro-8H-pyrimido-[4,5-C][1,2]oxazin-7-one (dPTP), 200μM each dNTP, and 0.4 μM each of primers pCTCon2CTEV.HR2.F and pCTCon2CTEV.HR2.R. Reactions were thermocycled ten times and the mutagenized genes

were further amplified in PCR reactions without mutagenic dNTP analogs using the same primers. Gel-purified genes were combined with NheI/BamHI-digested pCTCon2CTev vectors in a 5:1 insert:backbone mass ratio and electroporated into ICY200 as described to yield the listed library sizes.

Site Saturation Mutagenesis Library Construction (rounds 4-6)

Genes were isolated from miniprepped yeast libraries by PCR, digested using restriction enzymes XhoI and BamHI, ligated into pre-digested pET29B vectors and then cloned into Life Technologies One Shot® Mach1 cells, grown overnight in liquid culture with 25 μg/mL Kanamycin and then harvested to afford the subcloned library. 100ng of this material was then subjected to PCR with either of two randomization primer pairs (round 4, 2A Library: 104F/104R, 168+182F/168R; round 4, 4S Library: 104+118F/104R, 182F/182R; round 5, 2A Library: 162+168F/162R, 182F/182R; round 5, 4S Library: 118+122F/118R, 182F/182R; round 6, 2A Library: 99+138F/99R, one of 160F/160R, 165F/165R, 189F/189R, 190F/190R or 196F/196R; round 6, 4S Library: 132F/132R, one of 160F/160R, 165F/165R, 189F/189R, 190F/190R or 196F/196R), then gel purified, treated with the NEBNext® End Repair Module according to manufacturers' instructions, blunt end ligated using NEB Quick Ligase according to manufacturers' instructions and then cloned into Life Technologies One Shot® Mach1 cells, grown overnight in liquid culture with 25 μg/mL Kanamycin and then harvested to afford the semi-random library.

This was then repeated for the other randomization primer set in a given pair, and the products pooled and subsequently mutagenized by using the Stratagene Mutazyme II DNA mutagenesis kit for 25 cycles of amplification using primers pCTCon2CTEV.HR2.F and pCTCon2CTEV.HR2.R. Reactions were then purified by spin column and combined with

NheI/BamHI-digested pCTCon2CTev vectors in a 5:1 insert:backbone mass ratio and electroporated into ICY200 as described to yield the listed library sizes.

Primer Sequences:

104F NNKgaagaaaatgaatcactagatgatcaaaatatttc

104R aaagcttacacctctatttaattgttcagatgttgc

168+182F

NNKctagatgaacaaaaaggtaaagataaacaattaacattaNNKacttgtgatgattacaatgaagagacaggcgtttg

168R ttctacagctgttggcttaacatttcttatacttg

104+118F NNKgaagaaaatgaatcactagatgatcaaaatatttcaattNNKggacacactttcattgaccgtccgaactatc

104R aaagcttacacctctatttaattgttcagatgttgc

182F NNKacttgtgatgattacaatgaagagacaggcgtttg

182R taatgttaattgtttatctttacctttttgttc

99+138F

gcaggacacactttcattgaccgtccgaactatcaatttacaaatcttaaagcagccaaaNNKggtagtatggtgtactttaaag ttggtaatg

99R

aattgaaatattttgatcatctagtgattcattttcttcatgaaagcttacaccMNNatttaattgttcagatgttgctggtcctggata tac

132F NNK cttaaagcagccaaaaaaggtagtatggtgtac

132R tgtaaattgatagttcggacggtcaatgaaagtg

160F NNK aagccaacagctgtagaagttctagatgaacaaaaag

160R atttcttatacttgtcattttatacttacgtg

165F NNK gtagaagttctagatgaacaaaaaggtaaag

165R tgttggcttaacatttcttatacttgtcattttatac

189F NNK gagacaggcgtttgggaaactcgtaaaatctttg

189R attgtaatcatcacaagtaattaatgttaattg

190F NNK acaggcgtttgggaaactcgtaaaatctttgtag

190R ttcattgtaatcatcacaagtaattaatgttaattg

196F NNK cgtaaaatctttgtagctacagaagtcaaactc

196R ttcccaaacgcctgtctcttcattgtaatcatc

Mutagenic PCR Library Construction (rounds 7-9)

Genes were isolated from miniprepped yeast libraries by PCR, gel purified, and subsequently mutagenized by using the Stratagene Mutazyme II DNA mutagenesis kit for 25 cycles of amplification using primers pCTCon2CTEV.HR2.F and pCTCon2CTEV.HR2.R. Reactions were then purified by spin column and combined with NheI/BamHI-digested pCTCon2CTev vectors in a 5:1 insert:backbone mass ratio and electroporated into ICY200 as described to yield the listed library sizes

Alexa$_{750}$-LAETG Synthesis

25 mg Alexa Fluor® 750 NHS Ester was dissolved in 45μL of 0.4M $_{H2N}$LAETGG peptide in DMSO and incubated at room temperature for 6 hours, at which point 2.5 μL DIPEA was added and incubated at room temperature overnight. Reactions were quenched by the addition of 450μL 1M Tris, pH 7.5, and were incubated on ice for 2 hours. This reaction was purified on a preparative Kromasil 100-5-C18 column (21.2×250 mm, Peeke Scientific) by reverse phase HPLC (flow rate: 9.5 mL/min; gradient: 10% to 70% acetonitrile with 0.1% TFA in 0.1% aqueous TFA gradient over 30 minutes; retention time 8 minutes) before pooling and

lyophilizing the collected fractions. The concentration of the peptide was determined by the known molar extinction coefficient of Alexa Fluor® 750, ε_{749nm} = 290,000 M^{-1} cm^{-1}

GGG-PEG Synthesis

100mg 10kDa PEG-NH2, 10kDa *bis*-PEG-NH2, 10kDa 4-arm-PEG-NH2 or 10kDa Biotin-PEG-NH2 was dissolved in 500μL dry dichloromethane, to which was added 250μL of a slurry composed of 164 mg Fmoc-Gly-Gly-Gly-COOH (BAChem), 132 mg of HATU and 56 mg of HOAt dissolved in 1mL dry DMF. This mixture was sonicated for 20 minutes before the addition of 35μL DIPEA, then sonicated an additional 20 minutes before incubation at room temperature for 16 hours. The mixture was quenched on ice by the addition of 100μL trifluoroacetic acid (TFA) then precipitated by addition to 10mL of cold diethyl ether and recrystallized twice from warm, absolute ethanol. This material was filtered, dried under reduced pressure, then taken up in 1 mL 20% Piperidine/DCM and incubated at room temperature for 30 minutes. This was quenched by the addition of 1mL TFA on ice, ethanol precipitated, and then recrystallized twice from warm, absolute ethanol.

FGF Expression and Purification

Codon-optimized FGF1 and FGF2 constructs were synthesized as gBlocks from Integrated DNA Technologies. These were cloned via restriction digestion and ligation into pET29 expression plasmids with similarly optimized SUMO-TEV Cleavage site and LPESG- linkers at their N- and C-termini, respectively. *E. coli* BL21(DE3) transformed with these plasmids were cultured at 37 °C in LB with 50 μg/mL kanamycin until OD_{600} = 0.5-0.8. IPTG was added to a final concentration of 0.4 mM and protein expression was induced for three hours at 30 °C. The cells were harvested by centrifugation and resuspended in lysis buffer (50 mM Tris pH 8.0, 300 mM NaCl supplemented with 1 mM $MgCl_2$, 2 units/mL DNAseI (NEB), 260 nM aprotinin, 1.2 μM

leupeptin, and 1 mM PMSF). Cells were lysed by sonication and the clarified supernatant was purified on Ni-NTA agarose following the manufacturer's instructions. Fractions that were >95% purity, as judged by SDS-PAGE, were consolidated and dialyzed against Tris-buffered saline (25 mM Tris pH 7.5, 150 mM NaCl). Protein concentration was calculated from BCA assay.

In Vitro SrtA Characterization

Assays to determine k_{cat} and $K_{m\ LPETG}$ were performed in 300 mM Tris pH 7.5, 150 mM NaCl, 5 mM $CaCl_2$, 5% v/v DMSO, and 9 mM Gly-Gly-Gly-COOH (GGG). The concentration of the LPETG peptide substrate ranged from 12.5 μM to 10 mM, and enzyme concentrations ranged from 25 nM to 1000 nM. Assays for determination of $K_{m\ GGG}$ were performed under the same conditions, except the LPETG peptide concentration was fixed at 1 mM, the enzyme concentration was fixed at 41.5 nM, and the concentration of GGG was varied from 0 μM to 100 mM, depending on the enzyme. Reactions were initiated with the addition of enzyme and incubated at 22.5 °C for 3 to 20 minutes before quenching with 0.2 volumes of 5 M HCl. Five to ten nmol of peptide from the quenched reactions were injected onto an analytical reverse-phase Eclipse XDB-C18 HPLC column (4.6×150 mm, 5 μm, Agilent Technologies) and chromatographed using a gradient of 10 to 65% acetonitrile with 0.1% TFA in 0.1% aqueous TFA over 13 minutes. Retention times under these conditions for the Abz-LPETGK(Dnp)-$CONH_2$ substrate, the released GKDnp peptide, and the Abz-LPETGGG-COOH product were 12.8, 10.4, and 9.1 min, respectively. To calculate the percent conversion, the ratio of the integrated areas of the GK(Dnp)- $CONH_2$ and Abz-LPETGK(Dnp)-$CONH_2$ peptide Abs_{355} peaks were compared directly. To determine k_{cat} and $K_{m,LPETG}$, reaction rates were fit to the Michaelis-Menten equation using Microsoft Excel using the Solver add-in. To determine $K_{m,GGG}$ and K_H,

reaction rates were fit to the modified Michaelis-Menten $v = \frac{[Enz]k_{cat}([GGG]+K_H)}{[GGG]+K_{m,GGG}}$, for which K_H is as defined when $K_H << K_{m,GGG}$.

Preparative Scale Biotinylation of Fetuin A

As in analytical labeling of Fetuin A, 1 mL of normal human plasma was supplemented with 10µL 1M $CaCl_2$, a boosted concentration of 10µL 0.1M GGGK(Biotin) and 10µL eSrtA(4S-9), then incubated at room temperature for 2 hours. 100µL of pre-equilibrated Ni-NTA resin slurry and 12.5µL 0.4M $_{H2N}$LPESGG peptide was then added to the mixture, the latter to act as a competitive inhibitor for thioester formation, and incubated at room temperature with shaking for 15 minutes. This was then filtered through a 0.2µm spin filter before dilution to 10mL final volume in PBS + 1mM EDTA + 100µM $_{H2N}$LPESGG, and concentrated against a 10kDa molecular weight cutoff spin concentrator for 20 minutes at 3500xg and a final volume of <1mL. This was repeated six times to an expected small molecule biotin concentration of <1nM. This was then incubated with 200µL of pre-equilibrated Invitrogen MyOne Streptavidin C1 Dynabeads with shaking for 30 minutes before magnetic separation and washing three times with PBS + 0.1% Tween-20. The beads were then resuspended in 100µL SDS-PAGE loading buffer with 100µM free biotin and incubated at 95°C for 15 minutes. A 15µL aliquot was then run on a 4-12% Bis-Tris PAGE gel, visualized by coomassie and excised with a clean razor. This sample was then subjected to proteolytic digestion and analyzed by microcapillary reverse-phase HPLC nano-electrospray tandem mass spectrometry (µLC/MS/MS) on a Thermo LTQ-Orbitrap mass spectrometer by the Harvard Mass Spectrometry and Proteomics Resource Laboratory, FAS Center for Systems Biology, Northwest Bldg Room B247, 52 Oxford St, Cambridge MA.

GGG-diblock Functionalization

GGG-functionalized amphiphilic diblock polypeptide (ADP) was used as a template for orthogonal reactivity test of the two evolved soratses in solution. A recombinant amphiphilic diblock polypeptide (ADP) derived from elastin-mimetic sequences, $[(VPGVG)(VPGEG)(VPGVG)(VPGEG)(VPGVG)]_{10}$ for hydrophilic N-block and $[(IPGVG)2VPGYG(IPGVG)2]_{15}$ for hydrophobic C-block, and prepared as previously reported (W Kim DOI: 10.1002/anie.201001356; doi: 10.1016/j.actbio.2012.04.011). GGG-functionalization of the ADP was achieved by conjugating Gly-Gly-Gly to N-terminal amine of a recombinant ADP via EDC-mediated carboxylate condensation. In a 0.6 mL Eppendorf tube, GGG-functionalized ADP (10 μM) was mixed with fluorophore-peptide (0.1 μM), evolved sortase (15 μM) and $CaCl_2$ (100 mM), then reacted for 1 hour at RT. Samples with different combinations of fluorophore-peptide conjugates (Alexa Fluor® 488-LAETG or Alexa Fluor® 647-LPESG) and evolved sortases (eSrtA(2A-9) or eSrtA(4S-9)) were prepared for comparison of their cross-reactivity. Then, 4.7 μL of 4X SDS-PAGE loading buffer was added to 14 μL of reaction mixture, and incubated at 95°C for 3 minutes, and then run on a 15 % Tris-HCl Precast gel (BioRad) at 150 V for 60 minutes. After electrophoresis, fluorescent images were taken first without any staining using GE Typhoon FLA 7000 Gel Scanner at Wyss Institute at resolution = 25 μm. Then, the gel was stained with coomasie blue to visualize protein bands containing GGG-diblock and scanned.

Enzyme Specificity Assay

Assays to determine eSrtA(2A) and eSrtA(4S) specificity were performed by preparing 10μM stocks of LAETG, LPETG, LSETG, LGETG, LVETG, LPEAG, LPESG, LPETG, LPEVG and LPEGG in 300mM Tris pH 7.5, 150mM NaCl, 5mM $CaCl_2$, 5% v/v DMSO, and 100 mM Gly-Gly-Gly-COOH (GGG). Reactions were performed by adding eSrtA(2A) to a final

concentration of 6.4, 64 or 640 nM, or eSrtA(4S) to a final concentration of 5.5, 55 or 550 nM and a final volume of 50µL, then incubating at 22.5 °C for 15 minutes. Reactions were quenched by the addition of 0.2 volumes of 5M HCl, then were injected onto an analytical reverse-phase Eclipse XDB-C18 HPLC column (4.6×150 mm, 5 µm, Agilent Technologies) and chromatographed using a gradient of 10 to 65% acetonitrile with 0.1% TFA in 0.1% aqueous TFA over 13 minutes. Retention times under these conditions for the Abz-LPETGK(Dnp)-$CONH_2$ substrate, the released GKDnp peptide, and the Abz-LPETGGG-COOH product were 12.8, 10.4, and 9.1 min, respectively. To calculate the percent conversion, the ratio of the integrated areas of the GK(Dnp)- $CONH_2$ and Abz-LPETGK(Dnp)-$CONH_2$ peptide Abs_{355} peaks were compared directly.

All other methods are as described in Chapter 2

References

1 Leader, B., Baca, Q. J. & Golan, D. E. Protein therapeutics: a summary and pharmacological classification. *Nat Rev Drug Discov* **7**, 21-39 (2008).

2 Jevševar, S., Kunstelj, M. & Porekar, V. G. PEGylation of therapeutic proteins. *Biotechnology Journal* **5**, 113-128, doi:10.1002/biot.200900218 (2010).

3 Fierz, B., Kilic, S., Hieb, A. R., Luger, K. & Muir, T. W. Stability of Nucleosomes Containing Homogenously Ubiquitylated H2A and H2B Prepared Using Semisynthesis. *Journal of the American Chemical Society* **134**, 19548-19551, doi:10.1021/ja308908p (2012).

4 Ito, T. *et al.* Highly Oriented Recombinant Glycosyltransferases: Site-Specific Immobilization of Unstable Membrane Proteins by Using Staphylococcus aureus Sortase A. *Biochemistry* **49**, 2604-2614, doi:10.1021/bi100094g (2010).

5 Ling, J. J., Policarpo, R. L., Rabideau, A. E., Liao, X. & Pentelute, B. L. Protein Thioester Synthesis Enabled by Sortase. *Journal of the American Chemical Society* **134**, 10749-10752, doi:10.1021/ja302354v (2012).

6 Witte, M. D. *et al.* Preparation of unnatural N-to-N and C-to-C protein fusions. *Proceedings of the National Academy of Sciences* **109**, 11993-11998 (2012).

7 Proft, T. Sortase-mediated protein ligation: an emerging biotechnology tool for protein modification and immobilisation. *Biotechnology letters* **32**, 1-10 (2010).

8 Pritz, S. *et al.* Synthesis of biologically active peptide nucleic acid-peptide conjugates by sortase-mediated ligation. *The Journal of organic chemistry* **72**, 3909-3912 (2007).

9 Antos, J. M., Miller, G. M., Grotenbreg, G. M. & Ploegh, H. L. Lipid Modification of Proteins through Sortase-Catalyzed Transpeptidation. *Journal of the American Chemical Society* **130**, 16338-16343, doi:10.1021/ja806779e (2008).

10 Chan, L. *et al.* Covalent attachment of proteins to solid supports and surfaces via sortase-mediated ligation. *PLoS one* **2**, e1164 (2007).

11 Chen, I., Dorr, B. M. & Liu, D. R. A general strategy for the evolution of bond-forming enzymes using yeast display. *Proceedings of the National Academy of Sciences*, doi:10.1073/pnas.1101046108 (2011).

12 Kruger, R. G. *et al.* Analysis of the Substrate Specificity of the Staphylococcus aureus Sortase Transpeptidase SrtA†. *Biochemistry* **43**, 1541-1551, doi:10.1021/bi035920j (2004).

13 Piotukh, K. *et al.* Directed Evolution of Sortase A Mutants with Altered Substrate Selectivity Profiles. *Journal of the American Chemical Society* **133**, 17536-17539, doi:10.1021/ja205630g (2011).

14 Antos, J. M. *et al.* Site-Specific N- and C-Terminal Labeling of a Single Polypeptide Using Sortases of Different Specificity. *Journal of the American Chemical Society* **131**, 10800-10801, doi:10.1021/ja902681k (2009).

15 Race, P. R. *et al.* Crystal Structure of Streptococcus pyogenes Sortase A: IMPLICATIONS FOR SORTASE MECHANISM. *Journal of Biological Chemistry* **284**, 6924-6933, doi:10.1074/jbc.M805406200 (2009).

16 Zong, Y., Bice, T. W., Ton-That, H., Schneewind, O. & Narayana, S. V. L. Crystal Structures of Staphylococcus aureus Sortase A and Its Substrate Complex. *Journal of Biological Chemistry* **279**, 31383-31389, doi:10.1074/jbc.M401374200 (2004).

17 Ilangovan, U., Ton-That, H., Iwahara, J., Schneewind, O. & Clubb, R. T. Structure of sortase, the transpeptidase that anchors proteins to the cell wall of Staphylococcus aureus. *Proceedings of the National Academy of Sciences* **98**, 6056-6061, doi:10.1073/pnas.101064198 (2001).

18 Suree, N. *et al.* The structure of the Staphylococcus aureus sortase-substrate complex reveals how the universally conserved LPXTG sorting signal is recognized. *Journal of Biological Chemistry* **284**, 24465-24477 (2009).

19 Kruger, R. G., Dostal, P. & McCafferty, D. G. Development of a high-performance liquid chromatography assay and revision of kinetic parameters for the Staphylococcus aureus sortase transpeptidase SrtA. *Analytical Biochemistry* **326**, 42-48, doi:http://dx.doi.org/10.1016/j.ab.2003.10.023 (2004).

20 Tanaka, T., Yamamoto, T., Tsukiji, S. & Nagamune, T. Site-Specific Protein Modification on Living Cells Catalyzed by Sortase. *ChemBioChem* **9**, 802-807, doi:10.1002/cbic.200700614 (2008).

21 Consortium, T. U. Activities at the Universal Protein Resource (UniProt). *Nucleic Acids Research* **42**, D191-D198, doi:10.1093/nar/gkt1140 (2014).

22 Nanjappa, V. *et al.* Plasma Proteome Database as a resource for proteomics research: 2014 update. *Nucleic Acids Research* **42**, D959-D965, doi:10.1093/nar/gkt1251 (2014).

23 Jahnen-Dechent, W., Heiss, A., Schäfer, C. & Ketteler, M. Fetuin-A Regulation of Calcified Matrix Metabolism. *Circulation Research* **108**, 1494-1509, doi:10.1161/circresaha.110.234260 (2011).

24 Ketteler, M. *et al.* Association of low fetuin-A (AHSG) concentrations in serum with cardiovascular mortality in patients on dialysis: a cross-sectional study. *The Lancet* **361**, 827-833 (2003).

25 Wang, A. Y.-M. *et al.* Associations of serum fetuin-A with malnutrition, inflammation, atherosclerosis and valvular calcification syndrome and outcome in peritoneal dialysis patients. *Nephrology Dialysis Transplantation* **20**, 1676-1685, doi:10.1093/ndt/gfh891 (2005).

26 Jethwaney, D. *et al.* Fetuin-A, a Hepatocyte-Specific Protein That Binds Plasmodium berghei Thrombospondin-Related Adhesive Protein: a Potential Role in Infectivity. *Infection and Immunity* **73**, 5883-5891, doi:10.1128/iai.73.9.5883-5891.2005 (2005).

27 Popp, M. W., Dougan, S. K., Chuang, T.-Y., Spooner, E. & Ploegh, H. L. Sortase-catalyzed transformations that improve the properties of cytokines. *Proceedings of the National Academy of Sciences* **108**, 3169-3174 (2011).

28 Xia, X., Babcock, J. P., Blaber, S. I., Harper, K. M. & Blaber, M. Pharmacokinetic Properties of 2nd-Generation Fibroblast Growth Factor-1 Mutants for Therapeutic Application. *PLoS one* **7**, e48210 (2012).

29 Yanagisawa-Miwa, A. *et al.* Salvage of infarcted myocardium by angiogenic action of basic fibroblast growth factor. *Science* **257**, 1401-1403 (1992).

30 Laham, R. J. *et al.* Transendocardial and transepicardial intramyocardial fibroblast growth factor-2 administration: myocardial and tissue distribution. *Drug metabolism and disposition* **33**, 1101-1107 (2005).

31 Jordan, S. W. & Chaikof, E. L. Novel thromboresistant materials. *Journal of vascular surgery* **45**, A104-A115 (2007).

32 de Mel, A., Jell, G., Stevens, M. M. & Seifalian, A. M. Biofunctionalization of biomaterials for accelerated in situ endothelialization: a review. *Biomacromolecules* **9**, 2969-2979 (2008).

33 Banerjee, I., Pangule, R. C. & Kane, R. S. Antifouling coatings: recent developments in the design of surfaces that prevent fouling by proteins, bacteria, and marine organisms. *Advanced Materials* **23**, 690-718 (2011).

34 Bentley, M. L., Lamb, E. C. & McCafferty, D. G. Mutagenesis studies of substrate recognition and catalysis in the sortase A transpeptidase from Staphylococcus aureus. *Journal of Biological Chemistry* **283**, 14762-14771 (2008).

35 Varadarajan, N., Rodriguez, S., Hwang, B.-Y., Georgiou, G. & Iverson, B. L. Highly active and selective endopeptidases with programmed substrate specificities. *Nat Chem Biol* **4**, 290-294, doi:http://www.nature.com/nchembio/journal/v4/n5/suppinfo/nchembio.80_S1.html (2008).

36 Yi, L. *et al.* Engineering of TEV protease variants by yeast ER sequestration screening (YESS) of combinatorial libraries. *Proceedings of the National Academy of Sciences* **110**, 7229-7234, doi:10.1073/pnas.1215994110 (2013).

37 Nie, Z. Fetuin: its enigmatic property of growth promotion. *American Journal of Physiology-Cell Physiology* **263**, C551-C562 (1992).

38 Pal, D. *et al.* Fetuin-A acts as an endogenous ligand of TLR4 to promote lipid-induced insulin resistance. *Nat Med* **18**, 1279-1285, doi:http://www.nature.com/nm/journal/v18/n8/abs/nm.2851.html#supplementary-information (2012).

39 Walsh, G. Biopharmaceutical benchmarks 2006. *Nat Biotech* **24**, 769-776 (2006).

40 Hughes, B. Antibody–drug conjugates for cancer: poised to deliver? *Nature Reviews Drug Discovery* **9**, 665-667 (2010).

41 Carter, P. J. Introduction to current and future protein therapeutics: a protein engineering perspective. *Experimental cell research* **317**, 1261-1269 (2011).